

Neural Circuit Dynamics and Ensemble Coding  
in the Locust and Fruit Fly Olfactory System

Thesis by

Vivek Jayaraman

In Partial Fulfillment of the Requirements for the

Degree of

Doctor of Philosophy

CALIFORNIA INSTITUTE OF TECHNOLOGY

Pasadena, California

2007

(Defended October 23, 2006)

© 2007

Vivek Jayaraman

All Rights Reserved

*Dedicated to:*

*CWC & SG,*

*Jo & KS,*

*Pax (think of this as yours too),*

*&*

*Pappa*

## ACKNOWLEDGEMENTS

I have much to thank my graduate advisor for. Gilles Laurent's obvious pleasure when doing electrophysiology, enthusiasm for taking on new and challenging experiments, and artistry at the rig did much to inspire even this computer-loving engineer to become a reasonably competent experimentalist. I did not come to Caltech thinking I would work on insects. I would like to thank Gilles for letting me discover the joys of working with simple systems in his lab. His insight and knowledge about how neurons and neural circuits work has been educational. Scientific discussions with him—including long sessions poring over data trying to make sense of what we saw and debating about how it all fit into the bigger picture—were a highlight of my intellectual life at Caltech. And finally, I appreciate the freedom and opportunities that I have had working in his lab. It has been a blast Gilles. Thanks for everything (including the memorable and genre-redefining limericks).

I appreciate the unhesitating support and generous advice I have received from my committee members: Erin Schuman (thanks, also, for my first lab rotation at Caltech), Michael Dickinson, Erik Winfree, Mark Konishi, and Christof Koch. I am also grateful to the Sloan-Swartz Center for Theoretical Neurobiology at Caltech for two years of financial support.

Much of my work at Caltech has been done in fruitful collaborations with very capable colleagues, and for that I would like to thank my experimental collaborators Mark Stopfer (chapter 2) and Bede Broome (chapter 3).

As much as anything else, what has made this experience unforgettable for me is the camaraderie I have found in the Laurent lab. It was wonderful to come in each morning to work (and play) with so many smart, talented, knowledgeable, thoughtful, generous and fun people. I would like to specially thank: Glenn Turner, whose depth of knowledge, thoroughness and openness to scientific viewpoints different from his own I will always admire, for his generosity, sound counsel, countless pieces of experimental advice, good humor, soccer, badminton and the bubble that I hope never quite bursts; Stijn Cassenaer, whose mastery of the experimental craft I will never cease to be amazed by, for his advice, tennis, food (carrot cake in particular), shoes, poor taste in music, movies, and many other things besides; Mark Stopfer, collaborating with whom was an absolute delight and whose patience, care and artistry when doing experiments was inspiring, for his willingness to educate a green rotation student on the subtleties of locust olfaction and Snood; Rachel Wilson, for introducing someone with unsteady hands to the challenging fruit fly preparation, for numerous interesting discussions/debates, and for the most memorable moment of *Gladiators 2002*; Anusha Narayan, whose boldness taking on unfamiliar and daunting experimental challenges was awe inspiring, for numerous interesting conversations, scientific and otherwise, and for her editing skills, dubious wordplay, and delightful Mexican sauce; Ofer Mazor, for many engaging scientific discussions, for trying to get me hooked on the masochistic sport that is cycling, and for serving the best escargot in town; Maria Papadopoulou, for the clever ideas and experimental skills that made

working and TAing with her so enjoyable, and for her generosity, good cheer and for sharing the best pancake I have never eaten; Benjamin Rubin, whose love for discussing science (and bscience) and Zen-like calm made sharing an office with him a great experience, for his valuable and generous input on all kinds of technical matters, Joshua Tree, and his attempts to get me into rock climbing; Roni Jortner, whose starring role in a wide variety of entertaining stories will remain a treasured memory, for introducing me to a lot of great work in less fashionable model systems, for his big heart and for sharing his rig with me in the early days; Cindy Chiu, for being so much fun to share an office and a rig with (thanks, in particular, for all the ergonomic improvements!), and for her roles in Star Wars and Cats; and Markus Meister, whose clarity of scientific thought, creativity and approach to problem solving I respect enormously, for the many helpful discussions, tennis and the short-term (hopefully renewable) lease of office space.

Thanks also to Laurent Moreaux, for unforgettable quotes and for introducing me to two-photon microscopy in his own unique way; Bede Broome, for his remarkable patience when dealing with a colleague who perhaps had a slight tendency to do things at the last minute; Javier Perez-Orive, for interesting discussions, and for his impressively consistent and utterly useless ratings scale; Mala Murthy, for her useful input on the fly project; Jonathan Young, for his consideration, generosity and good humor when sharing the two-photon; Mikko Vähäsöyrinki, for the many stimulating technical discussions that I hope will continue; and Misha Rabinovich, Ramon Huerta, Thomas Nowotny, Valentin Zhigulin, Kai Shen, and other members, visitors and rotation students of the Laurent lab, for useful and interesting discussions.

My scientific life at Caltech was made much richer by informal conversations over coffee/tea and lunch with many people. I am particularly grateful to W. Bryan Smith—his intelligence, curiosity and experimental derring-do were inspiring—and to Anne Hergarden and Jasper Simon, for VJAM and many enjoyable scientific and nonscientific gatherings. Thanks also to Ulrik Beierholm, Kerstin Preuschoff, Rebecca Schulman and the other members of the CNS class of 2001: it was great to kick it all off with you guys.

I have had a bit of a journey before coming to neuroscience, and my interactions with many teachers and peers have shaped me as an engineer and scientist. This list is therefore doomed to be incomplete. But, I would particularly like to thank the following people: Amitabha Gupta, P. G. Poonacha, K. Sudhakar, Rajiv Kumar, Mayuresh Patil, Somnath Mani and Ravi Kanda (all IIT Bombay); Wei Shyy, H. S. Udaykumar, Ganesh Shenoy (University of Florida); Larry Abbott, Eve Marder, James Pustejovsky, Sen Song (Brandeis University); and Ricardo Paxson (The MathWorks Inc.).

On a more personal note, I would like to thank my family: Amma, for her incredible patience when teaching a kid whose attention was unequally divided between the ball he was kicking around and whatever course material he was supposed to be absorbing; Pappa, for setting an inspirational example in so many ways; Shobha, for her untiring efforts to get me educational books, meccano sets and the like when I was growing up, and for

eventually giving up and getting me the games/sporting equipment/comics that I actually wanted; and Jo, for more than I can ever express here.

As for my best friend, partner in life, sounding board, and most significant other, Malathi: thank you for countless things, but—perhaps most relevant to this thesis—thanks for steering me towards one of the two best decisions of my life. I'm glad I came to Caltech.

## ABSTRACT

Raw sensory information is usually processed and reformatted by an organism's brain to carry out tasks like identification, discrimination, tracking and storage. The work presented in this dissertation focuses on the processing strategies of neural circuits in the early olfactory system in two insects, the locust and the fruit fly.

Projection neurons (PNs) in the antennal lobe (AL) respond to an odor presented to the locust's antennae by firing in slow information-carrying temporal patterns, consistent across trials. Their downstream targets, the Kenyon cells (KCs) of the mushroom body (MB), receive input from large ensembles of transiently synchronous PNs at a time. The information arrives in slices of time corresponding to cycles of oscillatory activity originating in the AL.

In the first part of the thesis, ensemble-level analysis techniques are used to understand how the AL-MB system deals with the problem of identifying odors across different concentrations. Individual PN odor responses can vary dramatically with concentration, but invariant patterns in PN ensemble responses are shown to allow odor identity to be extracted across a wide range of intensities by the KCs. Second, the sensitivity of the early olfactory system to stimulus history is examined. The PN ensemble and the KCs are found capable of tracking an odor in most conditions where it is pulsed or overlapping with another, but they occasionally fail (are masked) or reach intermediate states distinct from those seen for the odors presented alone or in a static mixture.

The last part of the thesis focuses on the development of new recording techniques in the fruit fly, an organism with well-studied genetics and behavior. Genetically expressed fluorescent sensors of calcium offer the best available option to study ensemble activity in the fly. Here, simultaneous electrophysiology and two-photon imaging are used to estimate the correlation between G-CaMP, a popular genetically expressible calcium sensor, and electrical activity in PNs. The sensor is found to have poor temporal resolution and to miss

significant spiking activity. More generally, this combination of electrophysiology and imaging enables explorations of functional connectivity and calibrated imaging of ensemble activity in the fruit fly.

## TABLE OF CONTENTS

Acknowledgements .....	iii
Abstract .....	vii
Table of Contents.....	ix
Chapter 1: Introduction.....	1
Neural representations .....	1
Insect olfactory systems .....	3
Circuit dynamics and ensemble coding in the locust olfactory system .....	6
Imaging ensemble activity .....	11
Outline of specific aims.....	13
Bibliography .....	16
Chapter 2: Intensity versus Identity Coding in an Olfactory System .....	26
Chapter 3: Encoding and Decoding of Overlapping Odor Sequences .....	66
Chapter 4: Simultaneous Electrophysiology and Two-photon Imaging in the Intact Adult Fruit Fly .....	114
Chapter 5: Concluding Remarks .....	140
Ensemble coding in the locust olfactory system .....	140
Simultaneous electrophysiology and imaging of fruit fly neurons .....	144
Bibliography .....	147

## *Chapter 1*

### **INTRODUCTION**

An organism's survival and success depends in large part on its ability to monitor changes in its environment and modify its behavior accordingly. For creatures with a nervous system, this involves transducing raw sensory information into electrical signals that are then processed internally, leading eventually to a behavioral response. The kind of processing that is performed depends on the specific problems that the organism must solve. For example, organisms living in fast-changing environments have time constraints on sensory processing—decisions about whether to approach or avoid something may need to be made rapidly. A major goal of sensory neuroscience is to understand the sort of neural processing involved in tasks such as identification, discrimination, tracking and aspects of learning and memory: what are the neural representations and computational strategies underlying these capabilities?

#### **1.1 Neural representations**

Sensory information needs to be converted from its “raw” format (e.g., photons, molecules, pressure), into a format that neurons in the brain can use for efficient internal computations. The basic unit of neural communication in most nervous systems is an action potential, or spike. However, exactly how neurons transmit information with spikes is a matter of spirited debate (Rieke et al., 1997; Bair, 1999; Shadlen and Movshon, 1999). Is information encoded in the “rate” of spiking as measured by the average number of spikes over a stretch of time (commonly called a “rate code”), or is it perhaps in the precise timing of spikes (a type of “temporal code”)? One issue that complicates definitions is that there is usually information in the timing of spikes if they are evoked by a time-varying stimulus. The most satisfying definition then is that a true temporal code is one where there is

information in the timing of a spiking response on a time scale that is longer than that of the stimulus itself (Dayan and Abbott, 2001).

A related coding issue is whether information is represented in a distributed population of neurons or in a small percentage of neurons (distributed codes versus sparse codes). An “ensemble code” or “population code” is one where information is carried not just in the firing of individual neurons, but in the patterns of firing of one neuron relative to that in the other. The different neurons can act synergistically, redundantly or independently, and the nature of the interneuronal correlations determines whether the population code provides an added benefit in information-carrying capacity or not (Pouget et al., 2000; Schneidman et al., 2003; Averbek et al., 2006).

In reality, the brain does not just uniformly use one or the other strategy, and there is a problem beyond definitions and encoding schemes. There may well be information for the ideal observer carried in rate and timing of spikes, in single neurons or over a population of neurons, but the critical question is how this information is read out by the neurons that actually do the decoding—the most efficient encoding scheme may not actually be the one used by the nervous system because of other constraints. Depending on the decoding scheme and the nature of the correlations between different neurons, there can be more or less information in the responses in any of these cases (Averbek et al., 2006). It is also important to note that it is not easy to measure the level of correlations within a population of neurons, and that correlations measured between pairs of neurons do not easily scale up to meaningful measures at the population level. In addition, such problems are usually under-constrained —many different encoding and decoding strategies can be consistent with the limited sample of neural data collected by an experimenter. One key to progress in such issues is to record from as many neurons as possible and to understand the decoding strategy employed by the system. This is not often possible and is far easier to achieve in smaller, simpler systems, such as the brains of insects. Principles of circuit function extracted from simpler systems can then be tested on or applied to larger and more complex brains as well.

The work described in Chapters 2 and 3 of this thesis discusses studies of neural coding in the locust olfactory system, a system that has been intensively studied over the past decade (Laurent and Davidowitz, 1994; Laurent, 1996; Laurent, 2002; Perez-Orive et al., 2002). Chapter 4 focuses on the olfactory system of the fruit fly, *Drosophila melanogaster*, an organism which, despite its long history as a stalwart of behavioral genetics (Benzer, 1967; Konopka and Benzer, 1971), is in its infancy as a model system for systems neuroscience .

## **1.2 Insect olfactory systems**

Insects are the most successful animal (metazoan) inhabitants of our planet and account for the majority of recorded species (May, 1988). A large part of their success must surely come from their remarkable sensory systems that allow them to cope with a variety of environmental conditions. Of all sensory systems, olfaction is considered the oldest—even bacteria have basic chemosensory capabilities. There are notable similarities between olfactory circuits across phyla, and insect olfactory circuits are structurally and functionally analogous to mammalian ones (Strausfeld and Hildebrand, 1999). This makes studying olfaction in insects all the more relevant to understand olfaction in general.

### 1.2.1 Anatomy: Olfactory receptor neurons

The major olfactory organs of insects are the antennae and the maxillary and labial palps. Olfactory signals are transduced by olfactory receptor neurons (ORNs)—also called olfactory sensory neurons (OSNs)—that are located in hair-like cuticular structures called sensilla that are distributed over the surface of the olfactory organs. Odorant molecules are thought to enter small (10–25 nm diameter) pores in the sensilla and bind to odorant receptors (ORs) on the outer segments of OSN dendrites. Information about an odor is first encoded across combinations of ORs (Buck and Axel, 1991; de Bruyne et al., 2001; Hallem and Carlson, 2006). Different odorants interact with different subsets of ORs, and the activity of individual OSNs is determined by the OR they express (de Bruyne et al., 2001; Hallem et al., 2004). Thus, a combinatorial activation of subsets of OSNs is the first odor-related electrical input to the brain.

In flies, most of the ~1300 OSNs express two types of OR genes: Or83b, a broadly expressed receptor of unknown function and one receptor from within a family of ~60 selectively expressed receptors (Clyne et al., 1999; Vosshall et al., 1999). The OSNs project axons to a structure called the antennal lobe (AL), where they terminate in discrete regions of neuropil called glomeruli. In both insects and mammals, the axons of OSNs expressing the same ORs converge to the same glomeruli in the olfactory bulb or antennal lobe (Buck and Axel, 1991; Mombaerts, 1996; Gao et al., 2000; Vosshall, 2000). Here they contact two populations of cells, the excitatory projection neurons (PNs) and local neurons (LNs), the majority of which are known to be inhibitory.

### 1.2.2 Anatomy: Antennal lobe

In fruit flies, the ~43 glomeruli are identifiable (Laissue et al., 1999) and stereotyped across animals (Vosshall et al., 1999; Gao et al., 2000). In locusts, OSN axons innervate glomeruli of the ipsilateral AL (Chapman, 1998), but in flies ~80% of OSN axons bifurcate to corresponding glomeruli on both sides of the brain (Stocker et al., 1983; Stocker et al., 1990; Vosshall et al., 1999; Gao et al., 2000). There are two types of neurons in the AL, the cholinergic PNs (Yasuyama et al., 2003) and the GABAergic LNs (Leitch and Laurent, 1996; Hansson and Anton, 2000; Python and Stocker, 2002; Wilson and Laurent, 2005). In flies as in most studied insects (honeybees, moths, cockroaches), the PNs, which are the sole output of the AL, extend dendrites to a single glomerulus (Stocker, 1994), while in locusts, PNs are multiglomerular (Masson and Mustaparta, 1990; Farivar, 2005). In all known species, PN axons project ipsilaterally to the calyx of the mushroom body (MB) and to the lateral horn (LH) region (Ernst et al., 1977; Oleskevich, 1999; Marin et al., 2002; Wong et al., 2002; Yasuyama et al., 2003; Tanaka et al., 2004). Inhibitory local interneurons (LNs) in both flies and locusts arborize in many different glomeruli within the AL (MacLeod and Laurent, 1996; Wilson and Laurent, 2005). LNs fire action potentials in some insect species, including flies (Wilson and Laurent, 2005), but do not in others, such as the locust, where they respond to odors with graded potentials and calcium spikes (Laurent and Davidowitz, 1994; Leitch and Laurent, 1996). This becomes relevant when

interpreting extracellular recordings, because, in locusts, all spikes recorded from the AL can be unambiguously attributed to PNs.

Although the only somata in the AL are thought to be those belonging to PNs and LNs, there are also, in the AL neuropil, the projections of a few neurons. These neurons, which appear to be aminergic are thought to be modulatory in their function (Hansson and Anton, 2000). The best known of these neurons are the VUMmx1 in the honeybee (Hammer, 1993), and a similar octopaminergic neuron in the locust (Braunig, 1997).

### 1.2.3 Anatomy: Mushroom body

The MB is required for learning and memory in many insects (Quinn et al., 1974; Heisenberg et al., 1985; Menzel, 1987; Davis, 1993). The neurons intrinsic to this important structure of the insect brain are the Kenyon cells (KCs). Their small cell bodies are packed tightly above a cup-shaped neuropilar region of the MB, the calyx, and the dendrites of each KC extend into a small fraction of the calyx (Zhu et al., 2003; Farivar, 2005). In the locust, the calyx is divided into two parts: the main part is considered olfactory and the accessory part gustatory. PN axons innervate large parts of the main calyx in the locust (Farivar, 2005). In flies however, the span of PN axons is much more restricted suggesting that the connectivity patterns are different (Marin et al., 2002; Wong et al., 2002; Tanaka et al., 2004). The MB has been primarily associated with olfactory learning, but KCs are thought to receive input from other sensory modalities as well. This is well demonstrated in the honeybee (Strausfeld, 2002).

In both locusts and *Drosophila*, there are many more KCs than PNs: ~2300 in flies and ~50,000 in locusts. Thus, the early olfactory circuit features convergence (OSNs onto a smaller number of PNs) and then divergence (PNs to tenfold or more KCs). The precise connectivity of PNs to KCs has not yet been worked out, but there are suggestions that it is dense in locusts—with almost  $50\% \pm 13$  of the PNs in an AL appearing to connect to any given KC (Jortner et al., 2007)—and relatively sparse in flies (Zhu et al., 2003; Tanaka et al., 2004).

The next stages of this pathway are in the MB lobes. KC axons leave the calyx in a dense tract known as the pedunculus. There is evidence in the locust for reciprocal synaptic connection in this axon bundle (Leitch and Laurent, 1996; Watson and Schurmann, 2002). After they pass through the pedunculus, KC axons bifurcate and enter one or more regions called the  $\alpha$ , and  $\beta$  lobes (and  $\gamma$ ,  $\alpha'$ , and  $\beta'$  lobes in *Drosophila* (Strausfeld et al., 2003)) where they make synapses with MB extrinsic neurons. The MB-extrinsic neurons are known to have odor responses and their morphology has been studied to some extent as well (MacLeod et al., 1998; Farivar, 2005), but their precise connectivity to the KCs and their role in the circuit is less well understood.

### 1.2.3 Anatomy: Lateral protocerebrum

Not much is known about this region of the insect brain. In the locust, a subpopulation of ~60 GABA-ergic cells—lateral horn inhibitory (LHI) neurons—that appear to get convergent input from large numbers of PNs and send axonal projections to the MB has been identified. In the fly, PN projections to the LH appear to be stereotyped and regionally restricted (Tanaka et al., 2004). It has been suggested that the LH plays a role in the processing of innate rather than learned responses to odor (Heimbeck et al., 2001; Kido and Ito, 2002).

## 1.3 Circuit dynamics and ensemble coding in the locust olfactory system

Oscillations are a prominent feature of brain dynamics across phyla. They are typically seen in the summated activity of populations of neurons, and were first reported in human electroencephalogram (EEG) recordings, by Hans Berger in 1929 (Buzsaki and Draguhn, 2004), and in the local field potential (LFP) recorded in hedgehog brains by Adrian (Adrian, 1942). Oscillations have been theorized to be involved in numerous phenomena including attention (Fries et al., 2000), binding of different parts of a whole percept (Singer, 1995; Fries et al., 2000; Engel et al., 2001), memory (Pesaran et al., 2002; Sederberg et al., 2006), information transfer between brain regions (Siapas and Wilson, 1998), signal amplification (Steriade and Timofeev, 2003) and gating of sensory input during sleep (Steriade et al., 1993). Oscillations are also common in olfactory systems from

invertebrates to mammals (Adrian, 1942; Freeman, 1959; Gelperin and Tank, 1990; Laurent and Naraghi, 1994) and their possible function in olfactory perception has received considerable attention (Stopfer et al., 1997; Teyke, 1999; Brody and Hopfield, 2003; Gelperin, 2006; Schaefer et al., 2006).

Some studies have correlated the presence or absence of oscillations with behavioral events (Abeles, 1993; Vaadia et al., 1995; Stopfer et al., 1997), but it has been hard to show how this link might be achieved. One approach towards addressing this problem is to understand the role oscillations can play at the circuit level. Compelling experimental evidence for the significance of oscillations in circuit function has come from the locust olfactory system (Perez-Orive et al., 2002). The locust has also been a valuable model system for the study of circuit dynamics and neural coding in general and is discussed in some detail below.

### 1.3.1 Fast and slow dynamics in the antennal lobe

Perhaps the most important circuit-level feature of the antennal lobe is the recurrent connectivity between excitatory PNs and inhibitory LNs. The interplay between the PNs and LNs gives rise to AL dynamics at two time scales (Bazhenov et al., 2001a; Bazhenov et al., 2001b). First, PNs respond to odors with slow temporal spike patterns that last over a second and outlast the odor stimulus (Laurent et al., 1996). The patterns include both excitatory and inhibitory epochs. Second, PNs transiently synchronize with each other during an odor presentation (Wehr and Laurent, 1996). This transient synchrony gives rise to ~20Hz oscillations seen in the LFP—the consequence of summated synaptic output of the PNs measured in the MB (Laurent and Davidowitz, 1994; MacLeod and Laurent, 1996; MacLeod et al., 1998). These odor-evoked oscillations are also visible in the subthreshold activity of PNs, LNs and the recipients of PN output in the MB, the KCs (Laurent and Naraghi, 1994; Perez-Orive et al., 2002). Mechanistically, GABA-A conductances in the LNs (Bazhenov et al., 2001b) are thought to underlie the oscillations, which can be abolished by the application of picrotoxin, a Cl<sup>-</sup>-channel blocker.

### 1.3.2 Ensemble coding and population dynamics in the AL

The combination of slow temporal patterning and transient synchrony seen during odor responses has important consequences for the format of PN output that is sent to the next layer of the olfactory circuit. The PN population output can be thought of as being formatted in sequences of oscillation cycle-width high-dimensional state vectors, with each dimension being the number of spikes fired by one PN in a particular cycle (Laurent, 2002). These ~840-dimensional (one for each PN in the AL) vectors are updated based on which PNs fire together in a given cycle. The vectors exist in the space of all possible combinations of PN-ensemble firing patterns (PN phase space). An individual odor response produces a progression of ensemble states and, therefore, a trajectory in PN phase space. The evolution of a particular odor trajectory depends on the specific combinations of transiently synchronous PNs produced, and the rate of evolution of the trajectory is thus affected by both the slow and fast dynamics of individual PN responses. In response to sustained exposure to an odor, the slow-temporal patterning only lasts for ~2 seconds, after which the PN ensemble reaches a fixed point, with individual PNs either stably active or silent until the odor is switched off, at which point there is further patterning before a return to near-baseline levels of activity (Mazor and Laurent, 2005). The correlation width (the time on either side of a given cycle during which PN ensemble vectors are still significantly correlated) is on the order of 100 ms early in the response period and can be many hundreds of ms in the later stages of the response (Stopfer et al., 2003). Interestingly, the greatest distance between trajectories of different odors and the highest success in classifying the odors correctly is reached early in the transient phases of the response rather than at the fixed points (Stopfer et al., 2003; Mazor and Laurent, 2005).

During a typical odor response (for a 1s long stimulus), ~ 55% of PNs are active at some point during the response period (Mazor and Laurent, 2005). In a given cycle however, only up to 10% of PNs fire reliably (across trials). Another 30% of PNs fire during any given cycle, but the identity of those PNs is variable across trials even for the same odor. The remaining 60% of PNs are reliably silent during a given cycle. In each cycle, 55% of the spikes come from a “reliable” PN, with the remaining number coming from the pool of

unreliably firing PNs (Mazor and Laurent, 2005). Thus, the ensemble vector that represents the state of the PN population at a given cycle includes a changing cast of unreliably firing PNs. This becomes relevant for how the PN vectors are decoded, which is discussed in the next section.

### 1.3.3 Decoding PN ensemble activity: Sparse coding in the KCs

MB KC firing patterns are very different from those of their input PNs. KCs have almost zero baseline firing rates, respond to ~1–10% of odors with only ~2 spikes per response (Perez-Orive et al., 2002). Thus, in contrast to the broad tuning and dense representation in the PNs, KCs have very sparse odor representations and respond with very few spikes.

Sparse coding refers to an encoding and representational scheme that uses only a small number of narrowly tuned cells. This coding strategy is found in many other systems (Hahnloser et al., 2002; Olshausen and Field, 2004; Leonardo, 2005; Quian Quiroga et al., 2005; Rinberg et al., 2006). Neurons such as KCs that have the additional characteristic of also responding with very few spikes can be very hard to detect in extracellular recordings, and such cells may thus be vastly underrepresented in the literature. There are important reasons for neurons that are involved in associative memory, which is the role KCs are thought to play, to be sparse coders (Marr, 1969; Kanerva, 1988; Fiete et al., 2004; Olshausen and Field, 2004). Sparseness ensures a reduced probability of overlap and potential interference between memories, i.e., forming a new association does not affect an existing one. Also, the number of synapses that need to be modified in creating an association is smaller. The sparse strategy is also an energy efficient one, particularly when accompanied by almost binary spiking neurons. Finally, sparse codes tend to facilitate synthetic representations which lack detail of the constituent parts, which is in fact how odors are perceived (multicomponent mixtures that excite a wide array of receptors are nonetheless perceived as a single synthetic odor, e.g., coffee). Sparse coding is limiting in terms of capacity, but this disadvantage is offset by the large number of KCs in the MB.

#### 1.3.4 Mechanisms of sparsening

How do sparse responses arise? In KCs, there is experimental support for a combination of contributory mechanisms (Perez-Orive et al., 2002). First, each KC appears to be connected to ~50% of PNs in the AL (Jortner et al., 2007). This high number and the large space of different PN combinations that it allows implies that there are a large number of patterns that KCs could potentially encode (Jortner et al., 2007), i.e., associations can presumably be formed for a very wide range of possible odors. Such convergence (many PNs–one KC) and divergence (one PN–many KCs) would lead to a lot of KC firing unless the KC's threshold were appropriately high, which appears to be the case. Second, intrinsic properties of KCs contribute to their action as coincidence detectors (König et al., 1996), allowing them to fire even with high thresholds. Voltage-dependent conductances serve to sharpen excitatory postsynaptic potentials (EPSPs) when the KCs are depolarized. Thus, a PN spike that arrives synchronously with others can contribute disproportionately towards the KC reaching threshold. Third, KCs receive odor-evoked feedforward inhibition from the LHI neurons. These GABA-ergic neurons which respond non-specifically to odors appear to have extensive axonal arborizations in the MB. Lastly, KCs receive excitatory and inhibitory inputs at specific times that are clocked by the odor-evoked oscillations. PNs tend to fire preferentially during the rising phase of each cycle. LHIs, which receive their input from PNs, tend to fire with a delay and during the falling phase of the cycle. Thus, in each cycle during an odor response, a KC receives excitatory input from the set of PNs it is connected to that happen to be active during that cycle. Immediately after this, the KC receives non-specific inhibitory input from the LHIs that resets its membrane potential limiting integration of EPSPs across oscillation cycles. This narrowing of a KC's integration window means that the KC only has the opportunity to fire during a small part of each cycle, and then only if it gets the appropriately synchronous input from the PNs it is connected to. KC firing phases reflect the strong effect of this oscillatory input. KCs are strongly phase-locked with the LFP and tend to fire in the period between the arrival of PN and LHI input. The importance of this well-timed inhibitory input has been tested pharmacologically. Blocking inhibition in the MB led to a significant increase in the

breadth of tuning of KCs (i.e., a decrease in their sparseness), and a disruption of KC phase-locking to the LFP (Perez-Orive et al., 2002).

In summary, oscillatory patterning, feedforward inhibition, convergent and divergent PN-KC connectivity, and nonlinear intrinsic properties of the KCs all appear to be important to making the KCs sparse coders. During an odor response each KC can be thought of as matching its connectivity matrix (the PNs it is connected to) with the entire ensemble PN state vector at every oscillation cycle. If there is significant overlap (i.e., sufficient numbers of its input PNs fire synchronously near the top of a given cycle), the KC reaches threshold and fire. If this does not happen, the KC's membrane potential is reset by periodic inhibition from the LHI neurons and it must wait until the next cycle to make a new decision as to whether to fire. With only ~55% of spikes during a given odor-evoked oscillation cycle coming from reliable PNs however, the threshold must be reached with the help of spikes from the unreliable PNs, i.e., although these PNs are individually unreliable, some variable subset of them fire reliably during each cycle for a reliable KC response. Whether this unusual design facilitates robustness to noise or confers some other advantage is an open question.

#### **1.4 Imaging ensemble activity**

Electrical recordings can provide the most direct measurement of neural activity. However, performing electrical recordings from large populations of neurons presents several challenges (Buzsaki, 2004). Extracellular recordings typically pick up the activity of anonymous neurons—with the identity and spatial location of the neurons inferred through other means (such as triangulation, matching to firing profile recorded intracellularly, or processing of the tissue to establish electrode path). The insertion of even the smallest available electrodes into a region of the brain can cause some tissue damage (Csicsvari et al., 2003). Because spikes from multiple neurons are recorded on a single probe (and spikes from a single neuron are typically recorded on multiple probes), they must be assigned to individual neurons by posthoc analysis of recorded waveforms, i.e., spike-sorting and clustering. Even the best of the available algorithms can misclassify synchronous spikes

(from multiple cells) and need a minimum number of spikes in order to produce reliable results. Thus, there is a built-in bias against synchronous spikes and neurons whose spikes evoke smaller extracellular currents, or those that spike infrequently (e.g., KCs) are likely to be underrepresented (if it doesn't spike loudly enough, it's not there). One solution to many of these problems, albeit one with problems of its own, is optical recording. The most common approach is to load cells in the region of interest with synthetic dyes that change their optical properties when the voltage changes (Cohen and Salzberg, 1978; Cohen et al., 1978; Taylor et al., 2003; Grinvald and Hildesheim, 2004) or when dye molecules bind to particular ions, such as calcium (Grynkiewicz et al., 1985; Tank et al., 1988; Svoboda et al., 1997; Stosiek et al., 2003). The changes in resulting fluorescence are monitored using an image-sensing device, such as a photomultiplier tube (PMT) or charge-coupled device (CCD) camera, and a microscope. Calcium-based dyes that are loaded extracellularly and then taken up by neurons have—to date—provided the best combination of spatial and temporal resolution with minimal deleterious effects on the neurons being imaged (Stosiek et al., 2003; Ohki et al., 2005; Sullivan et al., 2005; Ohki et al., 2006). The problems with extracellular dyes have been their inconsistent loading and their inability to resolve single spikes when the overall level of activity is high. Nonetheless, this is an area of significant recent progress and already has much to offer.

#### 1.4.2 Imaging with genetically expressed sensors in *Drosophila*

Although imaging with synthetic dyes can be very informative, the availability of genetics opens up the possibility for alternative imaging approaches in *Drosophila* that may prove more fruitful in the long term (Miesenbock and Kevrekidis, 2005). Using sensors based on biological proteins (Chalfie et al., 1994) rather than synthetic dyes, makes it possible to genetically express them in living systems. By making the sensor's expression depend on cell-specific promoters, it is then possible to target them to identified subpopulations of neurons in the fly brain (Fiala et al., 2002; Ng et al., 2002; Wang et al., 2003). While this is clearly a powerful method, biological sensors of neural activity do not yet provide the temporal resolution of their synthetic counterparts (Pologruto et al., 2004; Reiff et al., 2005). In addition, the relationship between the optical signal and neural activity is likely to

be variable depending on the level of expression and cell type. Thus, although their use is attractive, signals from such genetically expressed sensors need to be interpreted with caution.

### **1.5 Outline of specific aims**

The focus of this thesis is on ensemble coding in the locust and fruit fly. The emphasis in the locust work is on the analysis of ensemble neural data; in the fruit fly it is on the development of an experimental technique that could enable ensemble coding work in the future.

The work presented in Chapters 2 and 3 builds on a large body of previous research that has elucidated the roles of different elements of the locust olfactory system and described some of the rules governing their interactions (Laurent and Davidowitz, 1994; MacLeod and Laurent, 1996; Wehr and Laurent, 1996; MacLeod et al., 1998; Perez-Orive et al., 2002). This work has led to a fairly detailed understanding of the mechanisms that underlie the integration of ensemble PN input by KCs in the MB. In the chapters to follow, this knowledge forms the basis for the interpretation of PN data in a way that is more relevant to the actual neural decoders. Thus, PN data are analyzed at an ensemble level and at time scales that correspond to those of odor-evoked LFP oscillations.

Chapter 2 investigates the issue of intensity-invariant identification of odors. Locust PNs (and mammalian mitral cells (Harrison and Scott, 1986)) change their response patterns to the same odor if the odor is presented at a different concentration. These changes can sometimes be as dramatic as those seen when the odor itself is changed. This represents a possible confound for the system—how can the identity of an odor be preserved across concentrations if PN responses vary with concentration? The apparent conundrum is, however, resolved when the PN data are examined at the population level and in LFP oscillation-cycle-width time slices, much as the KCs receive their PN input. A nonlinear dimensionality technique, locally linear embedding (LLE) (Roweis and Saul, 2000), is employed—for the first time with neural data—to visualize the dynamics of an ensemble of

110 PNs in 3D. LLE is used in combination with more quantitative linear analyses to show that there is sufficient information at the level of the PN ensemble for successful decoding of odor identity by subsequent layers. Recordings from the downstream decoders of PNs, the KCs, match predictions based on PN ensemble analysis, lending support to the current model of PN encoding and KC decoding. The work in Chapter 2 was published as Stopfer\*, Jayaraman\* and Laurent in *Neuron* (Stopfer et al., 2003).

Chapter 3 uses a novel olfactory stimulus paradigm, of temporally overlapping and offset two-odor sequences to examine the sensitivity of the olfactory system to initial conditions (stimulus history). This paradigm also allows us to test our understanding of encoding and decoding in the AL-MB circuit: analysis of PN ensemble responses during switching and overlaps allows us to make specific predictions about KC responses. PN activity vectors track odor changes fairly accurately, but there are interesting exceptions. For example, PN ensemble responses to an odor can be partially “masked” if that odor is preceded by another. Masking prevents the PN ensemble trajectories from traveling through regions of PN phase space that correspond to times of maximal KC firing probability. One would predict that KCs tuned to the second odor would show decreased responses in such cases. A different example is of response trajectories for some sequences that travel through regions of PN phase space not occupied by either the individual odors or their static binary mixture. Such trajectories suggest that KCs tuned to that region of PN phase space might fire uniquely during these sequences but not when presented with either odor alone. KCs with these types of responses were found, suggesting that KCs indeed have short time windows in which to integrate their ensemble PN input. The work in this chapter was published as Broome\*, Jayaraman\* and Laurent in *Neuron* (Broome et al., 2006).

The locust is an excellent system for electrophysiological experiments. The fruit fly, on the other hand, has historically presented problems to physiologists seeking to record from neurons in its brain, but comes with a wide array of genetic tools (Brand and Perrimon, 1993; Kitamoto, 2002; Nitabach et al., 2002) and has been the subject of a large number of behavioral experiments (Quinn et al., 1974; Frye and Dickinson, 2001; Tang and Guo,

2001). Recent research has made possible both imaging (Fiala et al., 2002; Ng et al., 2002; Wang et al., 2003) and electrophysiology (Wilson et al., 2004) in the fly brain. These technical developments have opened the way to making the fly a suitable model system for systems neuroscience, but one with additional advantages. One of the key prerequisites for this to become a reality is the ability to record from many fly neurons at the same time. This is currently possible with imaging of genetically expressible fluorescent sensors, but these signals can be hard to interpret. The work discussed in Chapter 4 focuses on developing experimental techniques that make the calibration of imaging signals possible. A two-photon laser scanning microscope is used to monitor the signal from a calcium sensor (G-CaMP) that is genetically expressed in subsets of identified neurons. Simultaneous electrophysiological recordings from these neurons allow a quantitative relationship between the two types of signals to be extracted. The analysis shows that although G-CaMP is a sensor that does not appear to affect the cell's functioning in any way, it has a low threshold and is unable to detect signals below a certain firing rate. Thus the signal has to be interpreted with some caution when issues of neural coding are being considered. This work is in preparation for publication.

## BIBLIOGRAPHY

- Abeles, M., Bergman, H., Margalit, E., and Vaadia, E. (1993). Spatiotemporal firing patterns in the frontal cortex of behaving monkeys. *J Neurophysiol* 70, 1629-1638.
- Adrian, E. (1942). Olfactory reactions in the brain of a hedgehog. *J Physiol (Lond)* 100, 459-473.
- Averbeck, B. B., Latham, P. E., and Pouget, A. (2006). Neural correlations, population coding and computation. *Nature Reviews Neuroscience* 7, 358-366.
- Bair, W. (1999). Spike timing in the mammalian visual system. *Curr Opin Neurobiol* 9, 447-453.
- Bazhenov, M., Stopfer, M., Rabinovich, M., Abarbanel, H. D., Sejnowski, T. J., and Laurent, G. (2001a). Model of cellular and network mechanisms for odor-evoked temporal patterning in the locust antennal lobe. *Neuron* 30, 569-581.
- Bazhenov, M., Stopfer, M., Rabinovich, M., Huerta, R., Abarbanel, H. D., Sejnowski, T. J., and Laurent, G. (2001b). Model of transient oscillatory synchronization in the locust antennal lobe. *Neuron* 30, 553-567.
- Benzer, S. (1967). Behavioral mutants of *Drosophila* isolated by countercurrent distribution. *Proc Natl Acad Sci USA* 58, 1112-1119.
- Brand, A. H., and Perrimon, N. (1993). Targeted gene expression as a means of altering cell fates and generating dominant phenotypes. *Development* 118, 401-415.
- Braunig, P. (1997). The peripheral branching pattern of identified dorsal unpaired median (DUM) neurones of the locust. *Cell Tissue Res* 290, 641-654.
- Brody, C. D., and Hopfield, J. J. (2003). Simple networks for spike-timing-based computation, with application to olfactory processing. *Neuron* 37, 843-852.
- Broome, B. M., Jayaraman, V., and Laurent, G. (2006). Encoding and decoding of overlapping odor sequences. *Neuron* 51, 461-482.
- Buck, L. B., and Axel, R. (1991). A novel multigene family may encode odorant receptors: a molecular basis for odor recognition. *Cell* 65, 175-187.
- Buzsaki, G. (2004). Large-scale recording of neuronal ensembles. *Nat Neurosci* 7, 446-451.

- Buzsaki, G., and Draguhn, A. (2004). Neuronal oscillations in cortical networks. *Science* 304, 1926-1929.
- Chalfie, M., Tu, Y., Euskirchen, G., Ward, W. W., and Prasher, D. C. (1994). Green fluorescent protein as a marker for gene expression. *Science* 263, 802-805.
- Chapman, R. (1998). *The Insects: Structure and Function*, 4th edn (Cambridge, Cambridge University Press).
- Clyne, P. J., Warr, C. G., Freeman, M. R. L. D., Kim, J., and Carlson, J. R. (1999). A novel family of divergent seven-transmembrane proteins: Candidate odorant receptors in *Drosophila*. *Neuron* 22, 327-338.
- Cohen, L. B., and Salzberg, B. M. (1978). Optical measurement of membrane potential. *Rev Physiol Biochem Pharmacol* 83, 35-88.
- Cohen, L. B., Salzberg, B. M., and Grinvald, A. (1978). Optical methods for monitoring neuron activity. *Annu Rev Neurosci* 1, 171-182.
- Csicsvari, J., Henze, D. A., Jamieson, B., Harris, K. D., Sirota, A., Bartho, P., Wise, K. D., and Buzsaki, G. (2003). Massively parallel recording of unit and local field potentials with silicon-based electrodes. *J Neurophysiol* 90, 1314-1323.
- Davis, R. L. (1993). Mushroom bodies and *Drosophila* learning. *Neuron* 11, 1-14.
- Dayan, P., and Abbott, L. (2001). *Theoretical Neuroscience: Computational and mathematical modeling of neural systems* (Cambridge, MIT Press).
- de Bruyne, M., Foster, K., and Carlson, J. R. (2001). Odor coding in the *Drosophila* antenna. *Neuron* 30, 537-552.
- Engel, A. K., Fries, P., and Singer, W. (2001). Dynamic predictions: oscillations and synchrony in top-down processing. *Nat Rev Neurosci* 2, 704-716.
- Ernst, K., Boeckh, J., and Boeckh, V. (1977). A neuroanatomical study on the organization of the central antennal pathways in insects. *Cell Tissue Res* 176, 285-308.
- Farivar, S. S. (2005) *Cytoarchitecture of the locust olfactory system*, California Institute of Technology, Pasadena.
- Fiala, A., Spall, T., Diegelmann, S., Eisermann, B., Sachse, S., Devaud, J. M., Buchner, E., and Galizia, C. G. (2002). Genetically expressed cameleon in *Drosophila melanogaster* is used to visualize olfactory information in projection neurons. *Curr Biol* 12, 1877-1884.

- Fiete, I. R., Hahnloser, R. H., Fee, M. S., and Seung, H. S. (2004). Temporal sparseness of the premotor drive is important for rapid learning in a neural network model of birdsong. *J Neurophysiol* 92, 2274-2282.
- Freeman, W. J. (1959). Distribution in time and space of prepyriform electrical activity. *J Neurophysiol* 22, 644-665.
- Fries, P., Reynolds, J. H., Rorie, A. E., and Desimone, R. (2000). Modulation of oscillatory neuronal synchronization by selective visual attention. *Science* 291, 1560-1563.
- Frye, M. A., and Dickinson, M. H. (2001). Fly flight. A model for the neural control of complex behavior. *Neuron* 32, 385-388.
- Gao, Q., Yuan, B., and Chess, A. (2000). Convergent projections of *Drosophila* olfactory neurons to specific glomeruli in the antennal lobe. *Nat Neurosci* 3, 780-785.
- Gelperin, A. (2006). Olfactory computations and network oscillation. *J Neurosci* 26, 1663-1668.
- Gelperin, A., and Tank, D. (1990). Odour-modulated collective network oscillations of olfactory interneurons in a terrestrial mollusc. *Nature* 345, 437-440.
- Grinvald, A., and Hildesheim, R. (2004). VSFI: a new era in functional imaging of cortical dynamics. *Nat Rev Neurosci* 5, 874-885.
- Grynkiewicz, G., Poenie, M., and Tsien, R. Y. (1985). A new generation of Ca<sup>2+</sup> indicators with greatly improved fluorescence properties. *J Biol Chem* 260, 3440-3450.
- Hahnloser, R. H., Kozhevnikov, A. A., and Fee, M. S. (2002). An ultra-sparse code underlies the generation of neural sequences in a songbird. *Nature* 419, 65-70.
- Hallem, E. A., and Carlson, J. R. (2006). Coding of odors by a receptor repertoire. *Cell* 125, 143-160.
- Hallem, E. A., Ho, M. G., and Carlson, J. R. (2004). The molecular basis of odor coding in the *Drosophila* antenna. *Cell* 117, 965-979.
- Hammer, M. (1993). An identified neuron mediates the unconditioned stimulus in associative olfactory learning in honeybees. *Nature* 366, 59-63.
- Hansson, B. S., and Anton, S. (2000). Function and morphology of the antennal lobe: new developments. *Annu Rev Entomol* 45, 203-231.

- Harrison, T. A., and Scott, J. W. (1986). Olfactory bulb responses to odor stimulation: analysis of response pattern and intensity relationships. *J Neurophysiol* 56, 1571-1589.
- Heimbeck, G., Bugnon, V., Gendre, N., Keller, A., and Stocker, R. F. (2001). A central neural circuit for experience-independent olfactory and courtship behavior in *Drosophila melanogaster*. *Proc Natl Acad Sci U S A* 98, 15336-15341.
- Heisenberg, M., Borst, A., Wagner, S., and Byers, D. (1985). *Drosophila* mushroom body mutants are deficient in olfactory learning. *J Neurogenet* 2, 1-30.
- Jortner, R., Farivar, S., Laurent, G. (2007). A simple connectivity scheme for sparse coding in an olfactory system. *J. Neurosci* 27, 1659-1669.
- Kanerva, P. (1988). *Sparse Distributed Memory* (Cambridge, MA, MIT Press).
- Kido, A., and Ito, K. (2002). Mushroom bodies are not required for courtship behavior by normal and sexually mosaic *Drosophila*. *J Neurobiol* 52, 302-311.
- Kitamoto, T. (2002). Conditional disruption of synaptic transmission induces male-male courtship behavior in *Drosophila*. *Proc Natl Acad Sci U S A* 99, 13232-13237.
- König, P., Engel, A. K., and Singer, W. (1996). Integrator of coincidence detector? The role of the cortical neuron revisited. *Trends Neurosci* 19, 130-137.
- Konopka, R. J., and Benzer, S. (1971). Clock Mutants of *Drosophila-Melanogaster*. *Proceedings of the National Academy of Sciences of the United States of America* 68, 2112-2116.
- Laissue, P. P., Reiter, C., Hiesinger, P. R., Halter, S., Fischbach, K. F., and Stocker, R. F. (1999). Three-dimensional reconstruction of the antennal lobe in *Drosophila melanogaster*. *J Comp Neurol* 405, 543-552.
- Laurent, G. (1996). Dynamical representation of odors by oscillating and evolving neural assemblies. *Trends Neurosci* 19, 489-496.
- Laurent, G. (2002). Olfactory network dynamics and the coding of multidimensional signals. *Nat Rev Neurosci* 3, 884-895.
- Laurent, G., and Davidowitz, H. (1994). Encoding of olfactory information with oscillating neural assemblies. *Science* 265, 1872-1875.
- Laurent, G., and Naraghi, M. (1994). Odorant-induced oscillations in the mushroom bodies of the locust. *J Neurosci* 14, 2993-3004.

- Laurent, G., Wehr, M., and Davidowitz, H. (1996). Temporal representations of odors in an olfactory network. *J Neurosci* *16*, 3837-3847.
- Leitch, B., and Laurent, G. (1996). GABAergic synapses in the antennal lobe and mushroom body of the locust olfactory system. *J Comp Neurol* *372*, 487-514.
- Leonardo, A. (2005). Degenerate coding in neural systems. *J Comp Physiol A Neuroethol Sens Neural Behav Physiol* *191*, 995-1010.
- MacLeod, K., Backer, A., and Laurent, G. (1998). Who reads temporal information contained across synchronized and oscillatory spike trains? *Nature* *395*, 693-698.
- MacLeod, K., and Laurent, G. (1996). Distinct mechanisms for synchronization and temporal patterning of odor-encoding neural assemblies. *Science* *274*, 976-979.
- Marin, E. C., Jefferis, G. S., Komiyama, T., Zhu, H., and Luo, L. (2002). Representation of the glomerular olfactory map in the *Drosophila* brain. *Cell* *109*, 243-255.
- Marr, D. (1969). A theory of cerebellar cortex. *J Physiol* *202*, 437-470.
- Masson, C., and Mustaparta, H. (1990). Chemical information processing in the olfactory system of insects. *Physiol Rev* *70*, 199-245.
- May, R. M. (1988). How Many Species Are There on Earth. *Science* *241*, 1441-1449.
- Mazor, O., and Laurent, G. (2005). Transient Dynamics versus Fixed Points in Odor Representations by Locust Antennal Lobe Projection Neurons. *Neuron* *48*, 661-673.
- Menzel, R., U. Müller (1987). Memory traces in honeybees. In *Neurobiology and behavior of honeybees*, R. Menzel, A. Mercer, ed. (Berlin, Springer), pp. 310-325.
- Miesenbock, G., and Kevrekidis, I. G. (2005). Optical imaging and control of genetically designated neurons in functioning circuits. *Annu Rev Neurosci* *28*, 533-563.
- Mombaerts, P. (1996). Targeting olfaction. *Curr Opin Neurobiol* *6*, 481-486.
- Ng, M., Roorda, R. D., Lima, S. Q., Zemelman, B. V., Morcillo, P., and Miesenbock, G. (2002). Transmission of olfactory information between three populations of neurons in the antennal lobe of the fly. *Neuron* *36*, 463-474.
- Nitabach, M. N., Blau, J., and Holmes, T. C. (2002). Electrical silencing of *Drosophila* pacemaker neurons stops the free-running circadian clock. *Cell* *109*, 485-495.

- Ohki, K., Chung, S., Ch'ng, Y. H., Kara, P., and Reid, R. C. (2005). Functional imaging with cellular resolution reveals precise micro-architecture in visual cortex. *Nature* 433, 597-603.
- Ohki, K., Chung, S., Kara, P., Hubener, M., Bonhoeffer, T., and Reid, R. C. (2006). Highly ordered arrangement of single neurons in orientation pinwheels. *Nature* 442, 925-928.
- Oleskevich, S. (1999). Cholinergic synaptic transmission in insect mushroom bodies in vitro. *J Neurophysiol* 82, 1091-1096.
- Olshausen, B. A., and Field, D. J. (2004). Sparse coding of sensory inputs. *Curr Opin Neurobiol* 14, 481-487.
- Perez-Orive, J., Mazor, O., Turner, G. C., Cassenaer, S., Wilson, R. I., and Laurent, G. (2002). Oscillations and sparsening of odor representations in the mushroom body. *Science* 297, 359-365.
- Pesaran, B., Pezaris, J. S., Sahani, M., Mitra, P. P., and Andersen, R. A. (2002). Temporal structure in neuronal activity during working memory in macaque parietal cortex. *Nat Neurosci* 5, 805-811.
- Pologruto, T. A., Yasuda, R., and Svoboda, K. (2004). Monitoring neural activity and [Ca<sup>2+</sup>] with genetically encoded Ca<sup>2+</sup> indicators. *J Neurosci* 24, 9572-9579.
- Pouget, A., Dayan, P., and Zemel, R. (2000). Information processing with population codes. *Nat Rev Neurosci* 1, 125-132.
- Python, F., and Stocker, R. F. (2002). Immunoreactivity against choline acetyltransferase, gamma-aminobutyric acid, histamine, octopamine, and serotonin in the larval chemosensory system of *Drosophila melanogaster*. *J Comp Neurol* 453, 157-167.
- Quian Quiroga, R., Reddy, L., Kreiman, G., Koch, C., and Fried, I. (2005). Invariant visual representation by single-neurons in the human brain. *Nature In Press*.
- Quinn, W. G., Harris, W. A., and Benzer, S. (1974). Conditioned behavior in *Drosophila melanogaster*. *Proc Natl Acad Sci U S A* 71, 708-712.
- Reiff, D. F., Ihring, A., Guerrero, G., Isacoff, E. Y., Joesch, M., Nakai, J., and Borst, A. (2005). In vivo performance of genetically encoded indicators of neural activity in flies. *J Neurosci* 25, 4766-4778.

- Rieke, F., Warland, D., de Ruyter van Steneninck, R., and Bialek, W. (1997). *Spikes* (Cambridge, MIT Press).
- Rinberg, D., Koulakov, A., and Gelperin, A. (2006). Sparse odor coding in awake behaving mice. *J Neurosci* *26*, 8857-8865.
- Roweis, S. T., and Saul, L. K. (2000). Nonlinear dimensionality reduction by locally linear embedding. *Science* *290*, 2323-2326.
- Schaefer, A. T., Angelo, K., Spors, H., and Margrie, T. W. (2006). Neuronal oscillations enhance stimulus discrimination by ensuring action potential precision. *PLoS Biol* *4*, e163.
- Schneidman, E., Bialek, W., and Berry, M. J. (2003). Synergy, redundancy, and independence in population codes. *Journal of Neuroscience* *23*, 11539-11553.
- Sederberg, P. B., Schulze-Bonhage, A., Madsen, J. R., Bromfield, E. B., McCarthy, D. C., Brandt, A., Tully, M. S., and Kahana, M. J. (2006). Hippocampal and Neocortical Gamma Oscillations Predict Memory Formation in Humans. *Cereb Cortex*.
- Shadlen, M. N., and Movshon, J. A. (1999). Synchrony unbound: A critical evaluation of the temporal binding hypothesis. *Neuron* *24*, 67-77.
- Siapas, A. G., and Wilson, M. A. (1998). Coordinated interactions between hippocampal ripples and cortical spindles during slow-wave sleep. *Neuron* *21*, 1123-1128.
- Singer, W., and Gray, C. (1995). Visual feature integration and the temporal correlation hypothesis. *Annu Rev Neurosci* *18*, 555-586.
- Steriade, M., McCormick, D. A., and Sejnowski, T. J. (1993). Thalamocortical oscillations in the sleeping and aroused brain. *Science* *262*, 679-685.
- Steriade, M., and Timofeev, I. (2003). Neuronal plasticity in thalamocortical networks during sleep and waking oscillations. *Neuron* *37*, 563-576.
- Stocker, R. F. (1994). The organization of the chemosensory system in *Drosophila melanogaster*: a review. *Cell Tissue Res* *275*, 3-26.
- Stocker, R. F., Lienhard, M. C., Borst, A., and Fischbach, K. F. (1990). Neuronal architecture of the antennal lobe in *Drosophila melanogaster*. *Cell Tissue Res* *262*, 9-34.

- Stocker, R. F., Singh, R. N., Schorderet, M., and Siddiqi, O. (1983). Projection patterns of different types of antennal sensilla in the antennal glomeruli of *Drosophila melanogaster*. *Cell Tissue Res* 232, 237-248.
- Stopfer, M., Bhagavan, S., Smith, B. H., and Laurent, G. (1997). Impaired odour discrimination on desynchronization of odour-encoding neural assemblies. *Nature* 390, 70-74.
- Stopfer, M., Jayaraman, V., and Laurent, G. (2003). Intensity versus identity coding in an olfactory system. *Neuron* 39, 991-1004.
- Stosiek, C., Garaschuk, O., Holthoff, K., and Konnerth, A. (2003). In vivo two-photon calcium imaging of neuronal networks. *Proc Natl Acad Sci U S A* 100, 7319-7324.
- Strausfeld, N. J. (2002). Organization of the honey bee mushroom body: representation of the calyx within the vertical and gamma lobes. *J Comp Neurol* 450, 4-33.
- Strausfeld, N. J., and Hildebrand, J. G. (1999). Olfactory systems: common design, uncommon origins? *Curr Opin Neurobiol* 9, 634-639.
- Strausfeld, N. J., Sinakevitch, I., and Vilinsky, I. (2003). The mushroom bodies of *Drosophila melanogaster*: an immunocytological and golgi study of Kenyon cell organization in the calyces and lobes. *Microsc Res Tech* 62, 151-169.
- Sullivan, M. R., Nimmerjahn, A., Sarkisov, D. V., Helmchen, F., and Wang, S. S. (2005). In vivo calcium imaging of circuit activity in cerebellar cortex. *J Neurophysiol* 94, 1636-1644.
- Svoboda, K., Denk, W., Kleinfeld, D., and Tank, D. W. (1997). In vivo dendritic calcium dynamics in neocortical pyramidal neurons. *Nature* 385, 161-165.
- Tanaka, N. K., Awasaki, T., Shimada, T., and Ito, K. (2004). Integration of chemosensory pathways in the *Drosophila* second-order olfactory centers. *Curr Biol* 14, 449-457.
- Tang, S., and Guo, A. (2001). Choice behavior of *Drosophila* facing contradictory visual cues. *Science* 294, 1543-1547.
- Tank, D. W., Sugimori, M., Connor, J. A., and Llinas, R. R. (1988). Spatially resolved calcium dynamics of mammalian Purkinje cells in cerebellar slice. *Science* 242, 773-777.

- Taylor, A. L., Cottrell, G. W., Kleinfeld, D., and Kristan, W. B., Jr. (2003). Imaging reveals synaptic targets of a swim-terminating neuron in the leech CNS. *J Neurosci* 23, 11402-11410.
- Teyke, T., and Gelperin, A. (1999). Olfactory oscillations augment odor discrimination, not odor identification in *Limax* CNS. *NeuroReport* 10, 1-8.
- Vaadia, E., Haalman, I., Abeles, M., Bergman, H., Prut, Y., Slovin, H., and Aertsen, A. (1995). Dynamics of neuronal interactions in monkey cortex in relation to behavioural events. *Nature* 373, 515-518.
- Vosshall, L. B. (2000). Olfaction in *Drosophila*. *Curr Opin Neurobiol* 10, 498-503.
- Vosshall, L. B., Amrein, H., Morozov, P. S., Rzhetsky, A., and Axel, R. (1999). A spatial map of olfactory receptor expression in the *Drosophila* antenna. *Cell* 96, 725-736.
- Wang, J. W., Wong, A. M., Flores, J., Vosshall, L. B., and Axel, R. (2003). Two-photon calcium imaging reveals an odor-evoked map of activity in the fly brain. *Cell* 112, 271-282.
- Watson, A. H., and Schurmann, F. W. (2002). Synaptic structure, distribution, and circuitry in the central nervous system of the locust and related insects. *Microsc Res Tech* 56, 210-226.
- Wehr, M., and Laurent, G. (1996). Odor encoding by temporal sequences of firing in oscillating neural assemblies. *Nature* 384, 162-166.
- Wilson, R. I., and Laurent, G. (2005). Role of GABAergic inhibition in shaping odor-evoked spatiotemporal patterns in the *Drosophila* antennal lobe. *J Neurosci* 25, 9069-9079.
- Wilson, R. I., Turner, G. C., and Laurent, G. (2004). Transformation of olfactory representations in the *Drosophila* antennal lobe. *Science* 303, 366-370.
- Wong, A. M., Wang, J. W., and Axel, R. (2002). Spatial representation of the glomerular map in the *Drosophila* protocerebrum. *Cell* 109, 229-241.
- Yasuyama, K., Meinertzhagen, I. A., and Schurmann, F. W. (2003). Synaptic connections of cholinergic antennal lobe relay neurons innervating the lateral horn neuropile in the brain of *Drosophila melanogaster*. *Journal of Comparative Neurology* 466, 299-315.

Zhu, S., Chiang, A. S., and Lee, T. (2003). Development of the *Drosophila* mushroom bodies: elaboration, remodeling and spatial organization of dendrites in the calyx. *Development* *130*, 2603-2610.

*Chapter 2***INTENSITY VERSUS IDENTITY CODING IN AN  
OLFACTORY SYSTEM****Acknowledgements**

Mark Stopfer and I contributed equally to the work in this chapter. Mark performed all the experiments, the spike sorting for PN and KC tetrode recordings, and the statistical analysis for Figures 1, 2E and Supplementary Figure S4 of the manuscript. I performed all the other analyses (Figures 3-6; Supplementary Figures S1-3, S5 and S6).

## Summary

We examined the encoding and decoding of odor identity and intensity by neurons in the antennal lobe and the mushroom body, the first and second relays, respectively, of the locust olfactory system. Changes in odorant concentration led to changes in the firing patterns of individual antennal lobe projection neurons (PNs), similar to those caused by changes in odor identity, thus potentially confounding representations for identity and concentration. However, when these time-varying responses were examined across many PNs, concentration-specific patterns clustered by odor identity, resolving the apparent confound. This is explained by the fact that, across the PN population, representations changed in a relatively continuous manner over a range of concentrations of each odorant. The PNs' targets in the mushroom body—Kenyon cells (KCs)—had sparse identity-specific responses with diverse degrees of concentration invariance. The tuning of KCs to identity and concentration and the patterning of their responses are consistent with piecewise decoding of their PN inputs over oscillation-cycle length epochs.

## Introduction

Sensory pathways typically segment objects in the environment into simpler features (*e.g.*, shape, location, motion). Among those, intensity is of great functional importance. Encoding intensity, however, is not a simple matter, for it often interferes with the encoding of other stimulus attributes: in color vision, a photoreceptor's response to dim light at the receptor's optimal wavelength may not differ much from its response to a bright light at a non-optimal wavelength; this confound can be resolved by population coding using a few broadly tuned and overlapping channels (Rodiek, 1998). We examine here the encoding of odor intensity and its relationship to the encoding of odor identity. We have proposed that, in the olfactory systems of insects and fish, odor identity is encoded by spatiotemporal activity patterns (Friedrich and Laurent, 2001; Laurent, 2002; Laurent et al., 1996; Wehr and Laurent, 1996) across dynamic assemblies of principal neurons (mitral

cells, MCs in vertebrates; PNs in insects) in the first olfactory relay (olfactory bulb, OB, or antennal lobe, AL). Each odor representation can be thought of as a high-dimensional vector of principal neuron states (*e.g.*, instantaneous firing rates) evolving over the duration of the stimulus in a stimulus-specific manner (Laurent et al., 2001). This model, however, has not yet been extended to the context of intensity coding. This is essential, because recordings from amphibians and mammals indicate that MC temporal response patterns change as odor concentration is varied (Kauer and Moulton, 1974; Meredith, 1986; Wellis et al., 1989), raising the possibility that spatiotemporal codes for concentration and identity are confounded. In addition, imaging results indicate that higher odor concentrations increase glomerular response intensity and recruit additional glomeruli (Ng et al., 2002; Wang et al., 2003; Cinelli et al., 1995; Friedrich and Korsching, 1997; Joerges et al., 1997; Meister and Bonhoeffer, 2001; Rubin and Katz, 1999; Stewart et al., 1979), consistent with the observation that MC responses change both quantitatively and qualitatively with odor concentration (Kauer and Moulton, 1974; Meredith, 1986; Wellis et al., 1989). How then are odors represented such that they can be identified over many concentrations, as behavioral experiments in humans, rodents and insects indicate (Engen and Pfaffmann, 1959; Pelz et al., 1997; Slotnick and Ptak, 1977)? Are there, for example, some invariant features in the responses of principal neurons that allow accurate odor classification across concentrations? We examined this issue in the locust olfactory system by recording the activity of neurons in the AL and of Kenyon cells (KCs), the PNs' targets in the mushroom bodies, a structure known to participate in olfactory memory (Heisenberg et al., 1985; Heisenberg, 2003). Stimuli consisted of common odorants at dilutions spanning several orders of magnitude (see Experimental Procedures).

## **Results**

### **Oscillations and phase-coding of intensity**

Hopfield (Hopfield, 1995) has proposed an intensity-encoding scheme based on the phase of firing of principal cells relative to a global periodic signal. Because olfactory systems, including the locust AL (Laurent and Naraghi, 1994), display coherent oscillatory behavior in response to odors (Adrian, 1942; Freeman, 1978; Gray and Skinner, 1988) and because, in locusts, PN firing phase contains no information about odor identity (Laurent et al.,

1996), we set out to evaluate the effect of odor concentration on AL oscillatory synchronization and on the firing phase of PNs. First, extracellular local field potential (LFP) recordings (n=38, see Experimental Procedures) were made from the mushroom body, the target of the AL PNs (Fig 1A). Oscillatory potentials (20-30Hz) were evoked when odorants were applied to the antenna, revealing coordinated, periodic PN activity, as previously described (Laurent et al., 1996; Wehr and Laurent, 1996). The oscillatory frequency remained constant (mean=20.8Hz,  $f(3,198)=0.67$ , ns; not shown), but oscillatory power increased significantly with concentration (Fig 1A), suggesting tighter PN synchrony, increased global PN activity, or both (Laurent, 2002). Second, intracellular recordings were made from AL local neurons (LNs) (n=35, Fig 1B, see Experimental Procedures), the inhibitory neurons responsible for PN oscillatory synchronization (MacLeod and Laurent, 1996). LN intracellular potentials also revealed an increase in oscillatory power with odor concentration (Fig 1B). This suggests that the greater PN synchrony at high odor concentrations is due, at least in part, to stronger activation and periodic modulation of LNs. Third, extracellular (n=47, see Experimental Procedures) recordings were made from PNs, simultaneously with LFP recordings.

We found that the mean phase of PN spikes during odor responses was unchanged by stimulus concentration (Fig 1C); similar results were obtained with intracellular recordings. Thus, while global oscillatory power in the AL output increases with concentration, PN firing phase with respect to the ensemble response (LFP) appears not to be a coding variable in this system, at least within this range of concentrations.

### **PN temporal patterning and concentration**

Intracellular recordings from PNs (n=39) showed that the slow temporal patterns evoked by odors (Laurent and Davidowitz, 1994) changed substantially, and sometimes abruptly, with concentration. Figure 2A shows the responses of one PN to four concentrations of cherry odor.

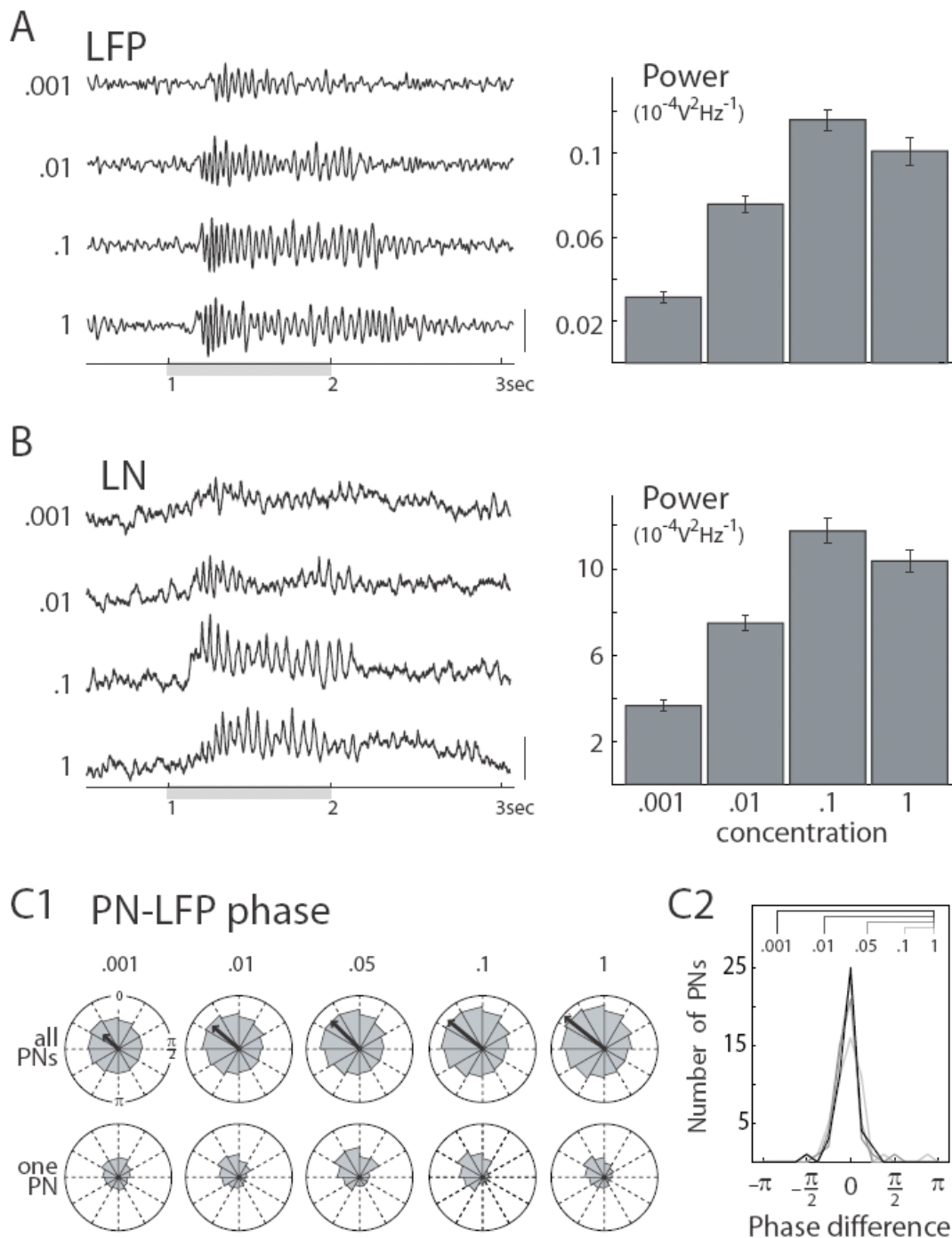


**Figure 1.** Network oscillations and PN phase preference over odor concentrations. **(A)** Higher odor concentrations elicit greater oscillatory power in the local field potential (LFP) (see also Bäcker, 2002). LFP power measured over 1-sec beginning with response onset. Left: examples of responses to hexanol from one experiment. Gray bar (here and throughout) indicates odor presentation. For display only, LFP was band-pass filtered, 5-55Hz. Scale bar: 0.5mV. Right: mean  $\pm$  sem response power from 38 experiments, ANOVA:  $f(3,175)=8$ ,  $p < 0.0001$ . LFP power slightly decreased at the highest concentration. The duration of the oscillatory response of the LFP also

increased with odor concentration; ANOVA:  $f(3,175)=21.2$ ,  $p<0.0001$ . **(B)** LN oscillatory power also increased with concentration. Left: intracellular responses of an LN to cherry; low-pass filtered, 3kHz. Scale bar: 8mV. Right: mean  $\pm$  sem responses from 35 experiments, ANOVA:  $f(3,162)=9.5$ ,  $p < 0.0001$ . **(C1)** PN spike phase preference (with respect to the LFP) is independent of odor concentration. Top, all PNs: polar histograms (0 rad = peak of LFP cycle) show phase preference of 47 PNs responding to 3 odorants (octanol, hexanol, and geraniol); Phase preference (arrow angle) was not significantly different across concentrations (cell-wise ANOVA:  $f(4,299)=.8$ , ns) (see also Bäcker, 2002)); vector strength (arrow length) increased with concentration. Bottom, one PN: phase preferences of a single PN for responses to octanol; this PN spiked vigorously during the period of LFP oscillation for all concentrations. Phase preference did not change with concentration (spike-wise ANOVA:  $f(4,2773)=2.1$ , ns). **(C2)** None of the 47 PNs examined showed a change in phase preference with odor concentration. For each PN, the preferred phase obtained with the highest concentration was subtracted from the phase obtained with the other 4 concentrations; all within-cell phase differences are plotted in the histogram. Within all PNs and across all concentration steps, an ANOVA detected no overall effect of concentration [ $F(3,184)=0.68$ ,  $p=.56$ ]. Phase differences are all distributed normally around 0 (confirmed by individual unpaired T-tests).

At 0.001, this PN fired with a sustained train of action potentials followed by a long hyperpolarization. At 0.01, the excitatory segment of its response to that odor was slightly lengthened and the hyperpolarization reduced, indicating some continuity in response tuning across concentrations. At 0.1, however, the response changed substantially, now consisting of an early period of hyperpolarization followed by a train of action potentials. As the concentration was increased again, the PN's response profile changed little. This example indicates that the responses of PNs to odors are determined by competing excitatory and inhibitory inputs, whose timing and relative influence change, sometimes unpredictably, with stimulus concentration. We then carried out extracellular tetrode recordings from multiple PNs ( $n=110$  cells in 15 experiments, odors adjusted to equalize vapor pressure, see Experimental Procedures).

The changes in response patterns over odors and concentrations varied greatly across PNs; we could find no simple rule that, if applied to each PN, would allow us to predict the evolution of its responses across odor concentrations. Figure 2B shows the responses of 14 simultaneously recorded PNs to 5 concentrations of the 3 odorants and Fig 2C shows the consistency of these responses over 15 trials with four PNs selected from the 14 in Fig 2B.

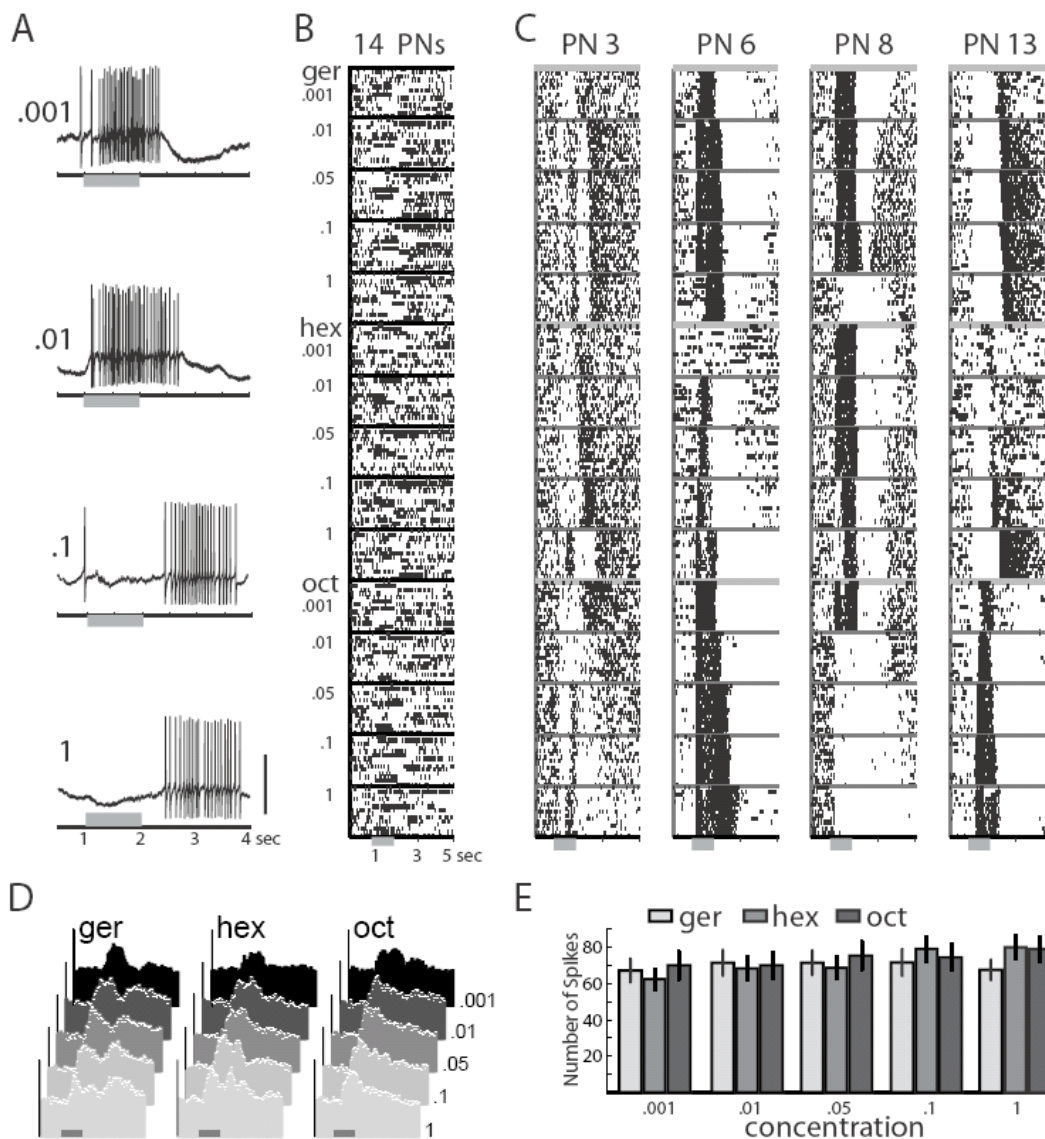


**Figure 2.** PN responses to odorant and concentrations. (A) Examples of responses to cherry from one experiment. Intracellular recordings of a single PN reveal concentration-specific interplay of excitation and inhibition, leading to temporal patterns that are consistent from trial to trial (see (C)). Odor pulse: 1sec; Scale bar: 35mV. (B) Ensemble view: spike time raster of simultaneous “tetrode” recordings from 14 PNs firing in response to 5 concentrations each of 3 odorants: geraniol (ger), hexanol, (hex) and octanol (oct). Only the 10th trial (of 15 for each odor-concentration pair) is shown; within the horizontal separator lines each row is a different PN. Odorants delivered in a randomized sequence. (C) Selected PNs from (B). Within separator lines each row is a different trial (from top to bottom). (D) Summed PN response profiles change moderately with odorant and concentration. 110 PNs (15 experiments), 15 trials per condition, 100ms bins. (E) Mean response intensity is constant across odors and concentrations. Pooled responses of 110 PNs; mean response rates measured over 1, 2, 3, or 4 sec from stimulus onset (1 sec shown) for all three odors and five concentrations; in all combinations, odor identity or concentration had no effect on mean response rates (2-way ANOVA for data shown:  $f_{\text{concentration}}(4,1635)=.92$ , ns;  $f_{\text{odor}}(2,1635)=.40$ , ns;  $f_{\text{interaction}}(8,1635)=.39$ , ns).

Responses differed greatly across odorants (*e.g.*, PN6, 0.001Ger and 0.001Hex) but changed also with concentration (*e.g.*, PN13). With some PN-odor combinations, spiking responses occurred earlier as the concentration was increased (*e.g.*, PN13-Oct). For others, the converse was true (*e.g.*, PN8 Hex). As observed with intracellular recordings, the changes from one response pattern to another could be abrupt as odor concentration was changed (*e.g.*, PN8, 0.1- to 1.0 Ger), but such discontinuities were not observed for the same concentration step in all PNs recorded simultaneously (*e.g.*, PN 13; 0.1- to 1 Ger). This suggests that not all local AL interactions change for a given concentration step. Hence, odor identity and concentration appeared to be confounded in the response patterns of individual projection cells.

### **PN mean firing rates and concentration**

We next examined mean PN response firing rates. In some PN-odor combinations, mean firing rates increased with concentration (*e.g.*, PN13, Ger and Hex, Fig 2C). In others, firing rates were highest at the lowest concentrations (*e.g.*, PN8-Oct, Fig 2C). The responses of 110 PNs (15 trials each) were pooled (Fig 2D), and mean response rates were measured over several intervals (1, 2, 3, or 4 sec from stimulus onset) for all three odors and five concentrations; in all combinations, neither odor identity nor concentration had any effect on mean response rates (2-way ANOVAs, Fig 2E). This indicates that, while total afferent input to the AL increased with concentration (see Experimental Procedures; Joerges et al., 1997; de Bruyne et al., 2001), the summed output of the AL varied little over these concentrations. Hence, if stimulus concentration is represented downstream from the AL, we predict that it should require decoding the patterning of the AL output rather than its integrated intensity (see Fig 2E). In addition, this result suggests that the increase in LFP power with concentration (Fig 1A) results mainly from tighter synchronization of PNs (their preferred firing phase indeed sharpens with concentration; see vector strength, Fig 1C), itself related to (possibly as a cause and a consequence of) increased efficacy of inhibition (Fig 1B). The total AL output is thus adaptively regulated over input intensities.

### **Spatiotemporal population patterns**

We sought to examine response patterns across the PN population, first, from groups of PNs recorded simultaneously (*e.g.*, Fig 3A, left bracket, the same 14 PNs as shown in Fig 2B), and second, to better assess the ensemble response of the AL, from 110 PNs pooled from 15 experiments (Fig 3A, full set). In each experiment, the animal was given 15 trials each of 5 concentrations of the same 3 odorants, in random order (225 trials per experiment). Of these 3 odorants, 2 were structurally similar (hexanol and octanol) and both were dissimilar from the third (geraniol, a terpene). For each experiment, spikes were binned using two methods: (1) because PN output is decoded by Kenyon cells (KCs) over individual LFP oscillation cycles (Perez-Orive et al., 2002), we binned the spikes by LFP oscillation cycle (50ms per cycle on average, see Experimental Procedures); (2) we measured spike counts in consecutive 50ms bins independent of LFP cycle boundaries. Each trial was represented as a high-dimensional vector of spike counts; each vector had  $k=n*m$  dimensions, where  $n$  is the number of PNs considered (up to 110), and  $m$  the number of time bins (*e.g.*,  $m = 20$  for 50ms bins over a 1s response period). Each vector thus represented the spatiotemporal pattern defined by the responses of  $n$  PNs over time in a single trial. We then analyzed the similarities between the vectors representing all trials; because first trial responses differ greatly from the others (Laurent and Naraghi, 1994; Stopfer and Laurent, 1999), they were excluded, giving us 14 trials\*5 concentrations\*3 odors=210 vectors. We will first examine the results obtained with groups of PNs recorded in single experiments, and later consider results from the composite set of 110 PNs.

We applied Principal Component Analysis (PCA) (see Experimental Procedures; (Turk and Pentland, 1991; Jolliffe, 1986)), a linear dimensionality reduction method, on the sets of simultaneously recorded PNs. The reduced data revealed odor- and concentration-specific structures in the spatiotemporal patterns that were not seen in individual PN responses. Visualizing the results using, for illustration purposes, the first 3 principal components (see Experimental Procedures), we found that the response patterns elicited by each odor formed distinct clusters. An unsupervised hierarchical clustering algorithm applied to the first 8 principal components (see Supplemental Figure S1) of these data (see Experimental Procedures) confirmed the existence of this structure and revealed further substructure in

the response patterns (Fig 3B2). Responses clustered by concentration (with some mixing among close concentrations), and concentration groups then clustered by odor, with a couple of exceptions (asterisks) for one very high and one very low concentration (Fig 3B2). We assessed the clustering using simple classification algorithms (tests A and B, see Experimental Procedures) based on the first 8 principal components and Euclidian distances. For the experiment shown, we could classify individual responses as belonging to the correct concentration group with >90% success (test A, see Experimental Procedures), and individual concentration subclusters as belonging to the correct odor group with >90% success, even after all trials with the tested concentration had been excluded from the template set (test B, see Experimental Procedures). These results were qualitatively similar across all experiments with comparable numbers of PNs, but we found tighter clustering and greater classification success for experiments with larger numbers of simultaneously recorded PNs. For sets of simultaneously recorded PNs, the results, while qualitatively similar for both binning methods, were quantitatively better (by up to 10%) when spikes were binned with respect to the simultaneously recorded LFP cycles (data not shown).

The locust has over 800 PNs per antennal lobe, from which we can presently record, at best, 25 simultaneously. In an effort to better approximate the response of the entire antennal lobe, we next analyzed odor response profiles from 110 PNs pooled from 15 tetrode experiments (*e.g.*, composite raster in Fig 3A; see Discussion). Spike counts were measured in consecutive 50 ms bins to produce population vectors (110 PNs \* 20 bins = 2200 dimensions for 1-s patterns).

When we applied PCA to this dataset, the reduced data once again revealed odor- and concentration-specific structures in the spatiotemporal patterns. Using 3 PCs for visualization, we found not only that the response patterns elicited by each odor formed distinct clusters (Fig 3C1), but that each odor cluster contained within it smaller subclusters of response patterns evoked by the different concentrations. Hierarchical clustering using 8 PCs (see Experimental Procedures) showed that responses now clustered nearly perfectly

by concentration (Fig 3C2), and concentration groups clustered by odor, with the same two exceptions (asterisks).

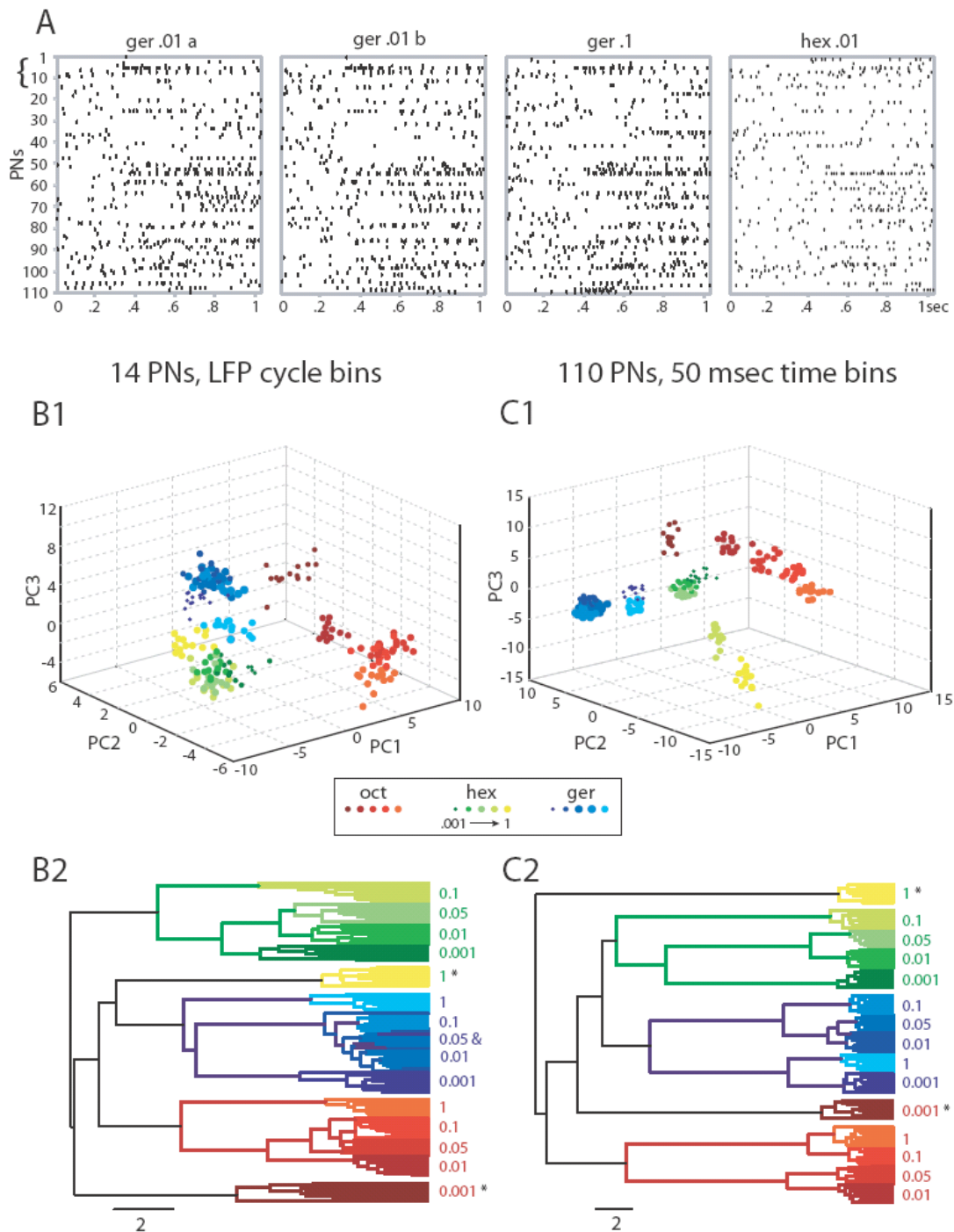


**Figure 3.** PN ensemble spatiotemporal patterns cluster by odorant and concentration. (A) Representative ensemble responses, (shown as raster plots, each row is a different PN), to two odorants, presented at two concentrations, throughout the time shown. The first 14 PNs (bracket at left) were recorded simultaneously in one experiment (see 3B). The rest were obtained in 14 other

experiments. Repeated presentations of ger .01 (a and b) elicited very similar ensemble responses; a different concentration (ger .1) elicited a somewhat different response; a different odorant (hex .01) elicited a very different response. **(B1)** Spatiotemporal responses from 14 simultaneously recorded PNs (bracket at left in 3A) to 5 concentrations of 3 odors projected onto space of first three principle components (PC1-3). Spike counts were measured in bins defined by the simultaneously-recorded LFP oscillation cycle. Each dot represents an ensemble response such as shown in 3A. The distribution of variance is discussed in Experimental Procedures. **(B2)** Hierarchical clustering of the reduced data (8PCs) shows that individual trials cluster by concentration; concentration groups then cluster by odor. Stars (\*) identify the two exceptions. **(C1)** Same analysis as in 3B1, but using all 110 PNs (pooled from 15 animals). Spike counts for individual PNs were measured in 50ms bins. **(C2)** Same as in 3B2, with set of 110 PNs from 3C1.

We could classify individual responses as belonging to the correct concentration group with 100% success (test A), and individual concentration subclusters as belonging to the correct odor group with >90% success (test B). In conclusion, odors appear to evoke distributed spatiotemporal patterns in which many neurons contribute to encoding both concentration and identity; the firing of the PN population analyzed over individual PNs and over time (with oscillation-cycle length resolution) can be used by an observer to identify both concentration and identity.

### **Analysis and visualization of the spatiotemporal patterns**

Recent results indicate that, during an odor presentation, PN output is decoded by KCs over individual LFP oscillation cycles at a rate of 20-30Hz (Perez-Orive et al., 2002). In a given KC, these periodic epochs of integration each seem to be independent of the preceding ones, owing to a periodic inhibitory reset of KCs after each oscillation cycle (Perez-Orive et al., 2002). From this we infer that quantifying the response of a PN over the entire duration of a stimulus (*e.g.*, by integrating its total discharge or by quantifying its patterned response over a long time, as in Fig 3) is probably not a functionally relevant approach. The PNs' output should rather be interpreted from the perspective of their targets, *i.e.*, piecewise. The following analysis attempts to identify, from PN population patterns analyzed over oscillation-cycle lengths, the features that might differentially encode odor concentration and identity.

We examined the PN population output as time series of 110-D vectors (110-PN dataset in Fig 3), sampled in consecutive 50ms "time slices". To track the evolution of the different

odor responses, we calculated average Euclidean distances (in 110-D space) between time-matched vectors, *i.e.*, one slice at a time (Fig 4A). The PN assembly responded fairly consistently over repeated trials with the same odor and concentration (blue, Fig 4A). When the concentration alone was changed, however, the patterns diverged, evident as increased average distances between corresponding time slices (black, Fig 4A). When the odor itself was changed, the ensemble responses diverged even further (red, Fig 4A). Because the patterns of PN activation changed over time, we also examined, for each response, differences between slice-vectors measured at different times.

A matrix of Euclidian distances (calculated as in Fig. 4B-D) showed that distances between vectors were small (dark blue) during the baseline period but were larger between baseline and slices 400-500 ms after stimulus onset (light green and yellow) (Fig 4E-G). Note, however, that the distances between neighboring time slices after the response had started (flanking the diagonal, box, Fig 4E) were small when comparing trials in the same odor-concentration series. This indicates that the sets of firing PNs are updated incrementally over the duration of each response. In addition, distances between time-matched and neighboring slices across nearby concentrations of a same odor (Fig 4F) were smaller than those across different odors at the same concentration (Fig 4G). This suggests a greater overlap between the sets of firing PNs during the response to different concentrations of an odor than between PN sets activated by different odors. We also carried out a similar analysis using correlations rather than distances (Fig 4H-J). Matrices showing significant ( $p < 0.001$ ) correlations between time slice vectors also showed the same trends (Fig 4H-J).

Our goal thus became to visualize, in just a few dimensions, an approximation of the trajectories defined by the evolving responses of the 110 PNs to each odor and concentration.

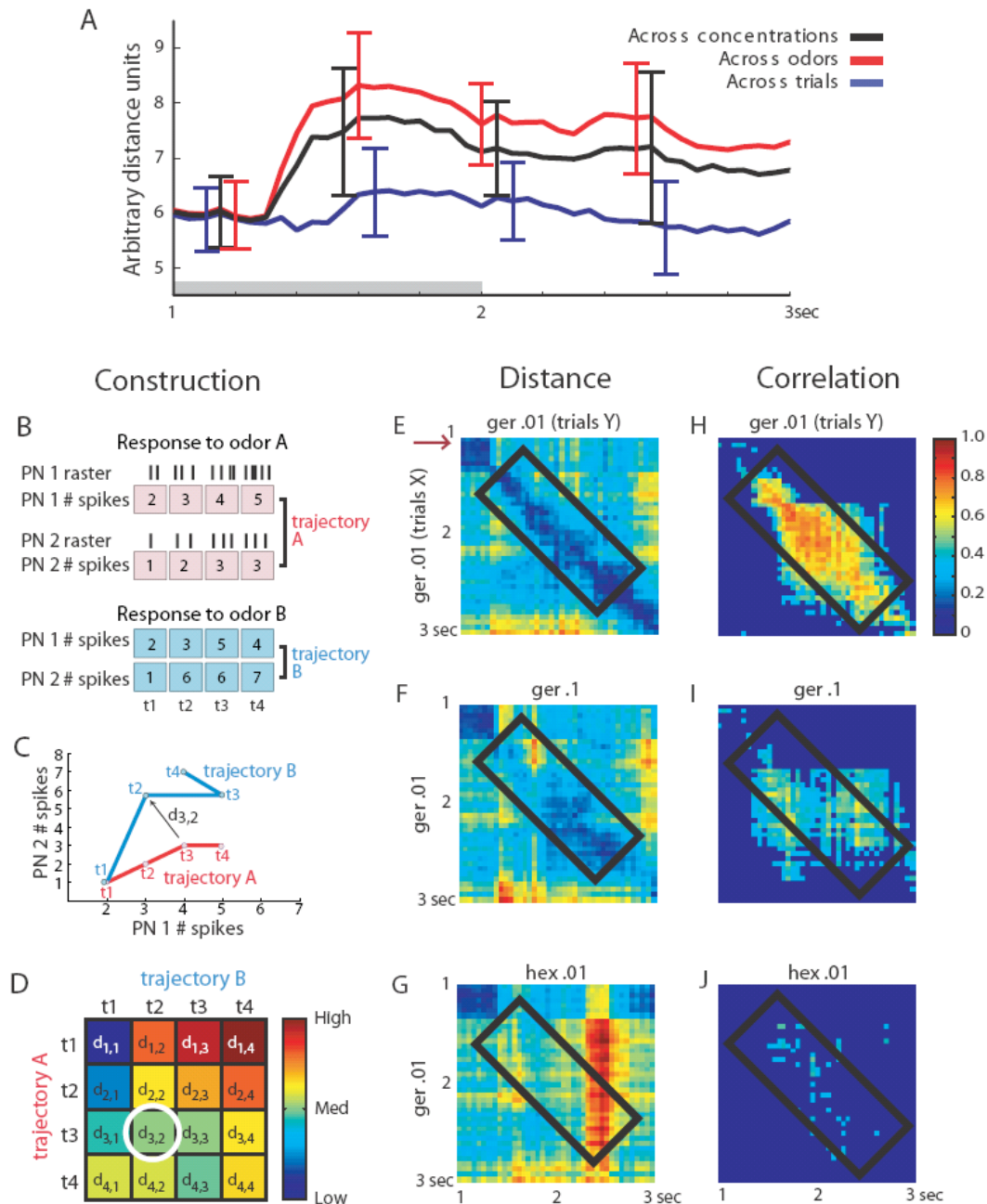


**Figure 4.** Quantifying differences among response patterns as they evolve over time. (A) Average Euclidean distances ( $\pm$ SD) calculated for each 50-ms time slice, across 110-PN vectors. Across trials: same odor-concentration pair; Across concentrations: same odor; Across odors: same concentration. (B-D) Procedure to construct trajectories from individual spike trains (artificial data). (B) Spike counts for individual PNs are measured in bins of given width over the time of the response. When stacked together across PNs, this produces a series of time-slice vectors, each of a dimension equal to the number of PNs included. These vectors, when linked in sequence, produce trajectories that represent the evolution of the PNs' states in the high-dimensional space of PN spike counts. (C) The two trajectories corresponding to example in (B). Euclidean distance between different trajectories can then be measured between any two high-dimensional time slices (in this two-dimensional example,  $d_{3,2}$  is the distance of the time slice of trajectory A at time  $t_3$  to the time

slice of trajectory B at time  $t_2$ ). **(D)** Matrix of Euclidean distances, calculated as in 4C. Each pixel  $d_{i,j}$  represents the color-coded distance between the time slice  $i$  of trajectory A and time slice  $j$  of trajectory B. Diagonal represents the distance between time-matched time slices of trajectories, and each row represents the distance from a particular time slice of trajectory A to all others of trajectory B. **(E-G)** Real data: Distance matrices calculated from 110 PN dataset in Figure 3c, bin width: 50ms, averaged over three trials. Of all possible matrix permutations, only three examples are given. **(E)** Distance matrix calculated as in 4C, between 110-d vectors taken from different sets of trials of 0.01X geraniol stimulation. Stimulation onset: 1s; PN response onset is  $\sim 300$ ms later, owing mainly to delays in odor propagation and olfactory transduction. The first row (arrow) shows distances from a time slice in the baseline period to the subsequent time slices. Distance is initially minimal (dark blue) until  $\sim 300$  ms after stimulus onset, when the system begins to respond. Blue pixels around diagonal (black box) show that distances between nearby time slices across trials are low even when the ensemble response has moved away from baseline, indicating that PN ensemble response changes gradually from one time slice to the next. **(F)** Distances between responses to two concentrations of the same odorant, 0.01X geraniol and 0.1X geraniol. Increase in distance from baseline state after 400 ms is greater than in 4E (first row: yellow and orange pixels). However, time-matched time slices are still somewhat similar to each other across responses to different-concentration stimuli (blue and green pixels around diagonal, box). **(G)** Distances between the responses to different odorants, 0.01X geraniol and 0.01X hexanol. Distance at baseline is minimal; the increase in distance after the system begins to respond (first row) is comparable to those in 4E and 4F, indicating that they are all at roughly comparable distances to baseline during the period of the response. A significant difference is observed around the diagonal: yellow and red pixels (box) indicate that the responses to the two different odors at the same concentration are very different from each other. **(H-J)** normalized correlation matrices matching the Euclidean distance matrices (4E-G). All correlations shown are significant ( $p < 0.001$ ).

Locally Linear Embedding (LLE) (Roweis and Saul, 2000), an unsupervised nonlinear dimensionality reduction technique well-suited to uncovering low-dimensional structure present in high-dimensional data (see Experimental Procedures; Seung and Lee, 2000), was used to visualize (here in 3 dimensions, Fig 5A) the successive time points representing the states of the 110 PNs in response to multiple concentrations of the three odors.

When connected in temporal order (Fig 5B), these points formed closed and stimulus-specific trajectories away from the initial resting state upon stimulus onset and back to rest some time after the stimulus ended. In agreement with the Euclidean distance measurements, the trajectories representing responses to different concentrations of an odor remained close to one another (forming odor-specific manifolds), but far from those of other odors. The trajectories and manifolds appeared connected only at rest. We also applied LLE to a dataset obtained with just one odor (*e.g.*, hexanol, Fig 5C). This embedding suggested that odor-evoked patterns move progressively further away from the

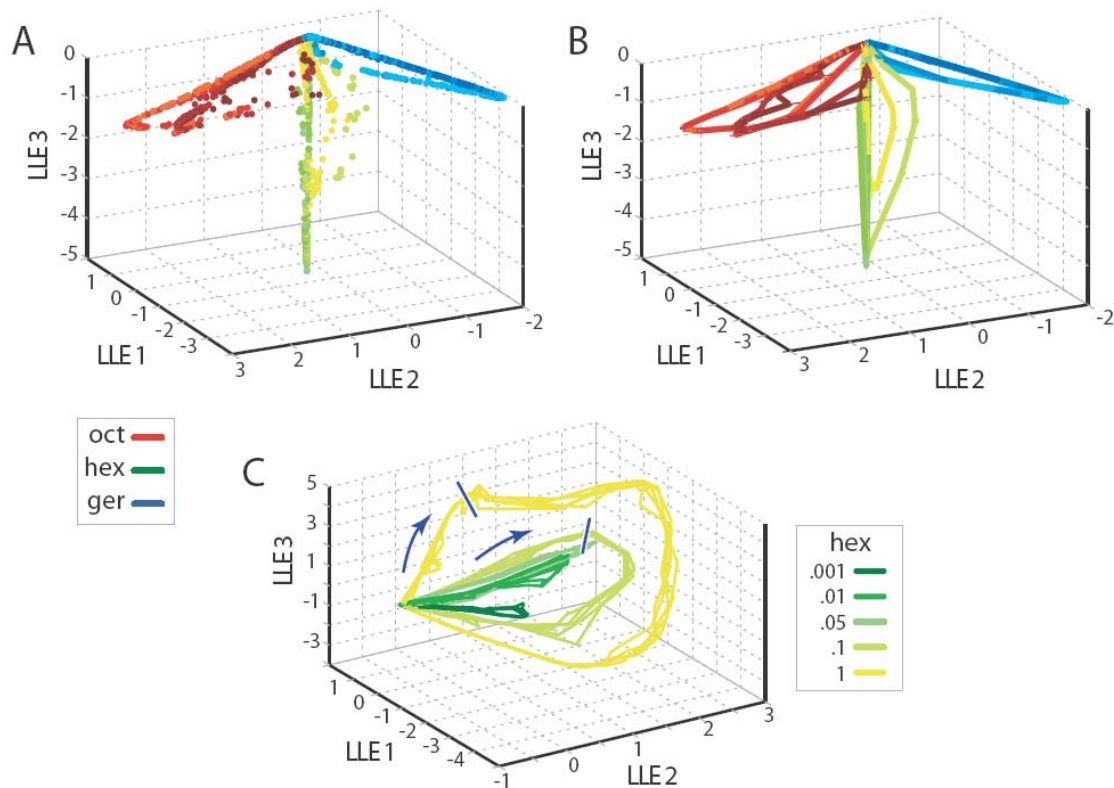


**Figure 5.** (A) Time-slice points calculated from 110-PN responses to 4 concentrations (.01X, 0.05X, 0.1X, 1X) of 3 odors, projected onto three dimensions using locally linear embedding. Shown are 60 time-slice points per trajectory (6 seconds total, beginning 1 sec before stimulus onset, 100 msec bins, averaged over 3 trials). (B) Time-slice points in (A) were connected in sequence to visualize trajectories. Initially in a resting state (origin of the coordinate system), the system responds with stimulus-specific trajectories. The trajectories in response to different concentrations of the same odor remain on the same (odor-specific) manifold. Five-trial averages for each odor-concentration pair; lines at vertices indicate S.D. (C) Trajectories corresponding to responses to 5 concentrations of hexanol, projected onto three dimensions using LLE. Arrows: direction of motion; blue lines: time of stimulus offset, shown for two concentrations. Five trajectories (each an average of 3 trials, 15 trials per odor-concentration pair) for each concentration are shown. These overlapping trajectories are separate from those of other concentrations.

resting state (baseline) as the concentration is increased. Trajectories representing higher concentrations appeared to take longer to return to the rest state. The antennal lobe network can thus be described as a dynamical system that responds to stimuli by moving away from

its baseline state, in what can be visualized as concentration-specific trajectories on odor-specific manifolds. These manifolds exist because of concentration-invariant features (similarities in the sets of transiently co-activated PNs) in the odor-evoked PN ensemble activity patterns. These features, which appear only with multiPN data and can be most clearly seen in this compressed representation (Fig 5B-C), resolve the apparent confounding of identity and concentration in single PN data (Fig 2A-C).

### **Decoding cycle by cycle**

Given that KCs assess the state of PNs cycle by cycle during a response (Perez-Orive et al., 2002), we wanted to estimate the information content of the PN assembly for individual cycles at successive times along the trajectories. We used PCA to reduce the dimensionality of individual 50-ms slices, one slice at a time. We found that, at certain times during odor presentation, responses once again clustered by odor identity (*e.g.*, see Fig 6A, showing the first 3 PCs). Hierarchical clustering using 8 principal components (Fig 6B), showed that responses clustered in concentration groups, with some exceptions (primarily mixing among responses to nearby concentrations of the same odor), and that concentration groups clustered by odor (again, with some exceptions, see asterisks). Individual time-slice reconstructions of odor responses using 8 principal components (Fig 6C, see also Supplemental Figure S2) revealed subsets of PNs that preferentially contributed to particular features of the representation (identity, concentration); these subsets, however, changed over time (*e.g.*,  $t_1=1.5s$  and  $t_2=2.25s$ , Fig 6C). Classification of responses into odor groups was 90% successful for many time slices all through the response (Fig 6D) with errors in some of the lowest and highest concentration groups.

Classification into concentration subclusters was only slightly less successful on average (tests A and B, see Experimental Procedures). The evolution towards peak classification success occurred very rapidly (200-300ms) (inset, Fig 6D), and there appeared to be sufficient information for both identity and concentration to be decoded by an observer over single cycles well into the response. Classification success using only subsets of the 110 PNs (100 random samples of 5,10...100 PNs each) is shown in Fig 6E (see Experimental Procedures). Whereas the distribution of success rates was broad for all PN

subset sizes, a few random PN combinations (top points of each distribution, *e.g.*, green box, Fig 6E) reached success rates between 75 and 90% for subsets containing as few as 10 PNs. Hence, enough information about stimulus identity and concentration (in the range tested) can be found by an observer in small PN subsets, provided the right PNs are considered.

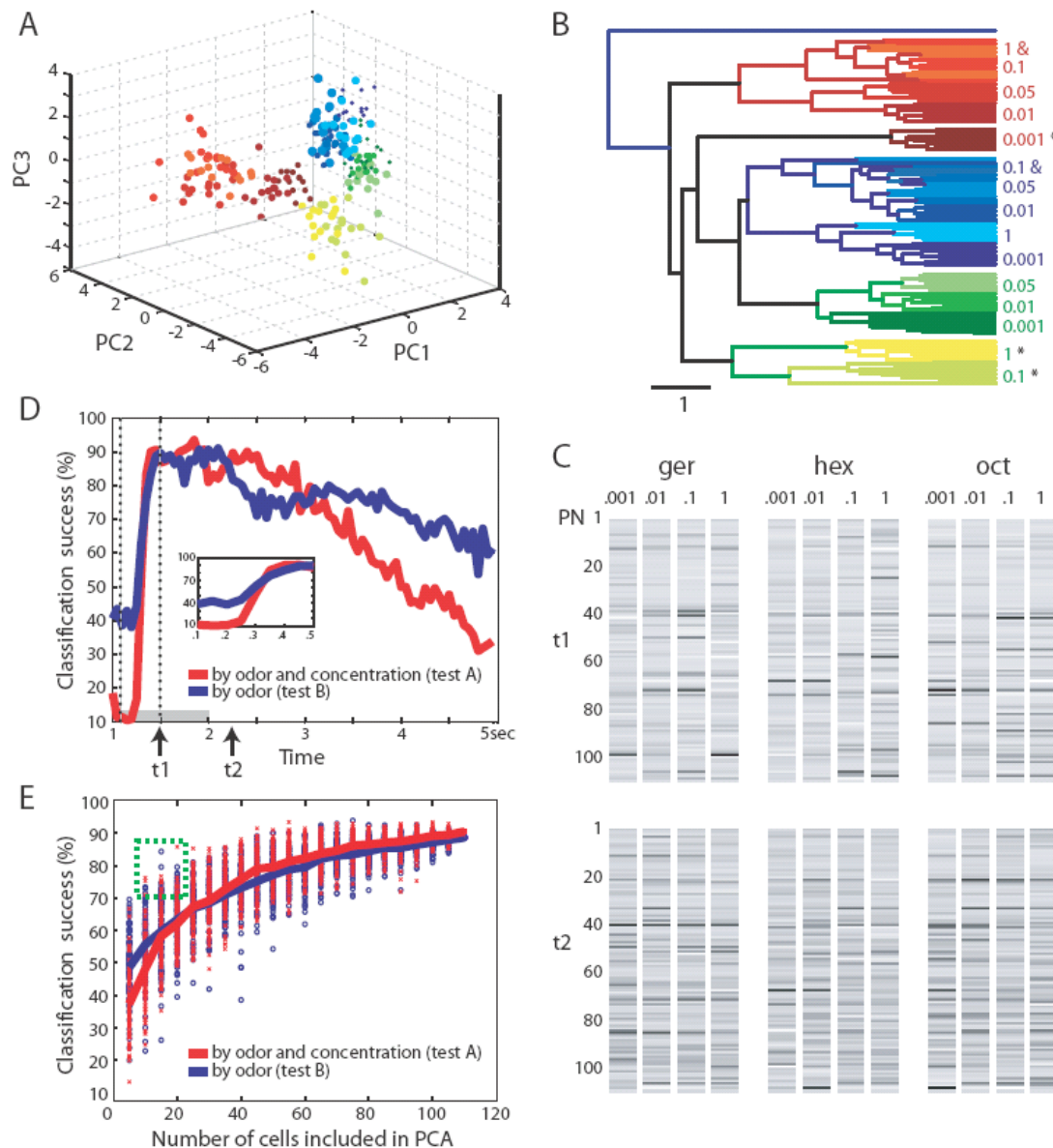


**Figure 6.** Classification by single cycle-length time slices. (A) Points from the 50ms time slice 0.5 seconds after stimulus onset; 110 PN set projected onto space of first three principal components. Points cluster by odor and concentration. (B) Hierarchical clustering shows that points from the time slice in (A) largely cluster by concentration; concentration groups then cluster by odor, with

some exceptions (indicated by \*s). (C) Reconstructions of PN activity states in two time slices ( $t_1 = 0.5\text{s}$ ;  $t_2 = 1.25\text{s}$  after stimulus onsets; see (D)) using 8 PCs, show significant positive contributors (darker pixels indicate higher spike counts) for different odors and concentrations. The set of PNs active in response to a particular odor-concentration pair (column) changes over time ( $t_1$  and  $t_2$  rows), although vectors from either time slice can be classified successfully by both odor and concentration, (arrows in (D)). (D) Classification success with single (50 ms) time slices stays high well into the response. Inset: evolution towards peak classification performance is attained within 200-300ms after the response begins. (E) Classification success as a function of the number of PNs included in the time slice. Small numbers of PNs sufficed for good classification only for a few PN combinations (top points in each distribution, outlined in green box for the 10-20 PN range).

### **Concentration tuning and invariance of KCs**

We estimate that 50,000 KCs each receive inputs from 10-20 on average of the 830 AL PNs (Perez-Orive et al., 2002), but the structure of this connectivity matrix is so far unknown. If each KC is connected to a subset of PNs that, for the appropriate stimulus, is co-activated within the same cycle or cycles, that KC's responses should reflect the variations (across odors and concentrations) of co-activity of the PNs connected to it. That is, some KCs might respond to a narrow concentration range of one odor while others would be relatively indifferent to concentration (invariant), reflecting the combined sensitivities of their presynaptic PNs. Further, if KCs decode PN output over LFP-cycle-length epochs, we would predict that KC responses should occur at cell- and stimulus-specific times during each response.

We recorded from many KCs simultaneously (total of 133 KCs in 17 experiments) while stimulating the animal with different odors and concentrations. KC responses were brief and rare (Perez-Orive et al., 2002) but when found, displayed the predicted kinds of specificity (Fig 7A). Some KCs (~30%, *e.g.*, KC6) responded selectively to specific concentrations of particular odors, others (~15%, *e.g.*, KC1) to one odor across a contiguous range of concentrations, and a few in less specific ways still. Also, the timing of KC responses relative to the stimulus onset differed across KCs and stimuli (Fig 7B), consistent with the finding that decoding of the PNs' output occurs both piecewise (Perez-Orive et al., 2002) and throughout the stimulus duration (Fig 7C).

These results indicate that odors are represented in the mushroom body by identity-selective sets of KCs, containing cells with different degrees of concentration invariance.

The observed degrees of selectivity (to odor identity and concentration) are consistent with the amount of information present in a small proportion of randomly chosen assemblies of 10-20 PNs (Fig 6E).

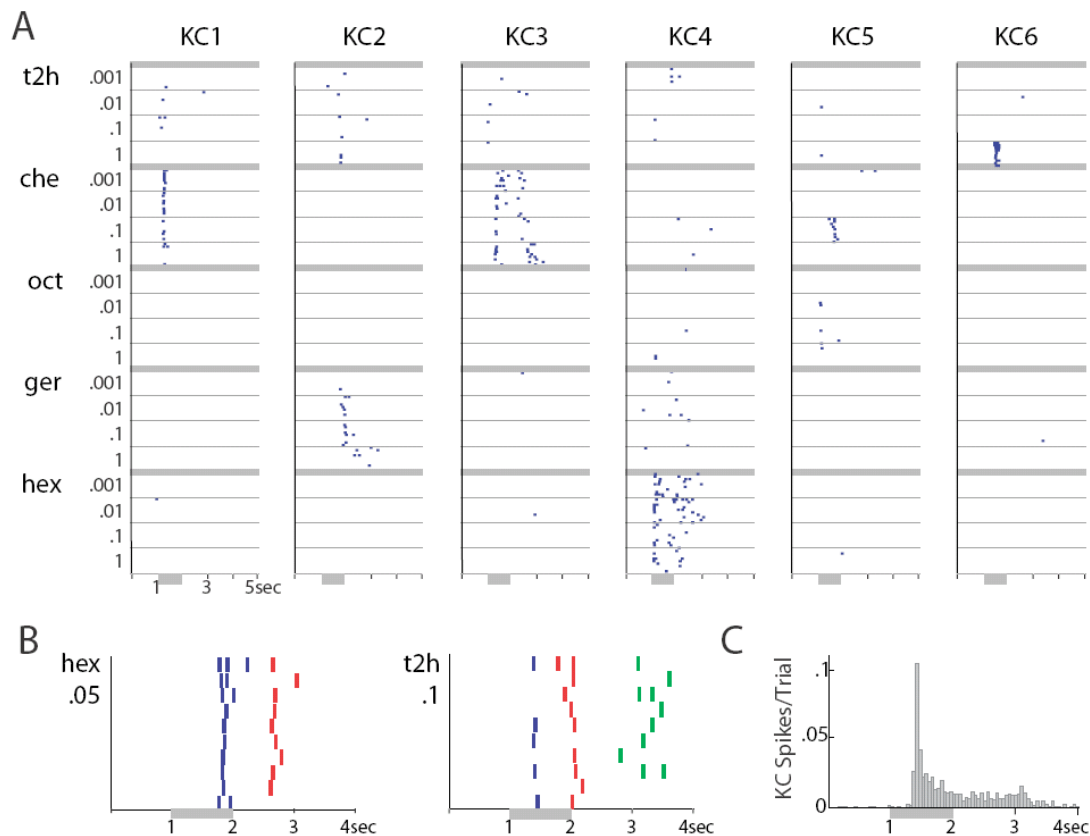


**Figure 7.** KCs respond to specific odors or specific concentrations of odors. **(A)** Rasters show examples of KC response specificity. KCs 1-4 responded reliably to a range of concentrations of an odor; KCs 5-6 responded to only one tested concentration of one odor. KCs 1,3,4,5 were recorded simultaneously in one preparation; KCs 2,6 were recorded simultaneously in a different preparation. t2h: trans-2-hexanal; che: cherry. **(B)** KCs fired at different, favored times after odor onset. Left: superimposed rasters of two simultaneously-recorded KCs (red, blue rasters), both responding to .05 hexanol. Right: from a different experiment, three simultaneously-recorded KCs (blue, red, green rasters), all responding to .1 trans-2-hexanal. **(C)** Histogram of response times for all KCs with stimulus-specific responses.

## Discussion

### Pooling: technical considerations

PNs recorded in several animals were pooled for some of our analyses (Figures 3C, 4, 5, and 6). Is this pooling strategy well-founded? We will assume that the set of pooled PNs approximates a large sample from a single locust if the following conditions are met: (1)

Different locusts should have sets of similarly tuned PNs. While this condition has not been resolved for locust, morphological studies in *Drosophila* suggest PNs in that species are indeed identifiable across animals (Wong et al., 2002; Marin et al., 2002). This interindividual morphological identifiability in *Drosophila* is paralleled by physiological properties and odor tuning (Wilson, R.I. and Laurent, G., unpublished observations). The great majority of presently known neurons in locusts are also identifiable from animal to animal (Burrows, 1996). In the absence of evidence to the contrary, we assume that PN populations are very similar across individual locusts. (2) The pooled set should not contain many “duplicate” PNs (i.e., the same PN from different animals represented more than once). Two lines of evidence suggest that the presence of duplicates in our set is unlikely. First, a probabilistic analysis based upon the number of PNs in one locust (~830), the number of PNs sampled per experiment (2—14) and condition (1) above, shows that the probability of repeatedly sampling many PNs across experiments is very small (see probability distribution in Supplementary figure S3). Second, the 110 PNs in the pooled set had distinct responses tunings when assessed on the three odors tested (see fig. 6C). While we cannot be certain that the pooled set is identical to a large sampling of PNs in a single individual, all available data suggest that conditions (1) and (2) above are met.

### **Gain control and absence of phase encoding**

Imaging data indicates that the total afferent input to the AL (and OB) increases with odor concentration (Ng et al., 2002; Wang et al., 2003; Cinelli et al., 1995; Friedrich and Korsching, 1997; Joerges et al., 1997; Meister and Bonhoeffer, 2001; Rubin and Katz, 1999; Stewart et al., 1979); yet, the total AL output, integrated across PNs and time, does not change significantly over a 1,000-fold increase in odor concentration. This indicates the existence of adaptive gain control within the AL, consistent with the observed increased modulation of LNs over concentrations. This apparent involvement of LNs in controlling PN output is also consistent with the increased synchronization of PNs with odor concentration. Whereas oscillatory synchronization is relevant for behavioral discrimination (Stopfer et al., 1997) and for decoding by KCs (Perez-Orive et al., 2002) and their downstream neurons (MacLeod et al., 1998), there is so far no experimental evidence for a phase code (with respect to the LFP) for concentration (see Hopfield, 1995). Other

investigators suggest that response latencies with respect to the slower respiration cycles (rodent olfactory bulb: Spors and Grinvald, 2002; Margrie and Schaefer, 2003; Cang and Isaacson, 2003) could be used as features in odor concentration coding; in the insect, odor sampling is not coupled to respiration. In conclusion, as in other systems, AL circuits adapt their mean output to dramatically compress input levels (Wachowiak et al., 2002); unlike other systems, however, AL circuits reflect—and transmit information about—input intensity through variations in the spatiotemporal patterning of their output, that are decoded by downstream neurons.

### **Concentration clusters within identity super-clusters**

As observed in other animals (Kauer and Moulton, 1974; Meredith, 1986; Wellis et al., 1989), the patterned responses of single AL principal neurons depend both on odor identity and concentration. Thus, steps in concentration of one odor can evoke single-PN response pattern changes indistinguishable from changes caused by a change in odor identity. Information about both odor identity and concentration, however, can easily be separated when odor representations are considered as evolving instantaneous vectors of activity across many PNs (i.e. sets of transiently coactive PNs), an analysis consistent with the known properties of their targets, the KCs (Perez-Orive et al., 2002). The activation patterns across the PN population are such that the abstract “coding space” can be thought of as divided into regions representing odor identities, each consisting of ordered subregions representing odor concentrations. The representation of an odor at very low or very high concentrations occasionally differed significantly from the others within its cluster. We predict that perceptual discontinuities should occur at these transitions; this needs to be tested behaviorally.

### **Differences between concentration and identity patterning**

These data extend our proposed spatiotemporal models for odor representations (Laurent, 2002; Laurent et al., 2001; Rabinovich et al., 2001) and for temporal decorrelation (Friedrich and Laurent, 2001; Laurent, 2002). Odor representations can be described as sequences of odor- and concentration-specific PN activity patterns, or trajectories. Trajectories representing different concentrations—within the range examined—of the

same odor lie next to one another, implying that they share common elements (that is, PNs and times of co-activation). These families of trajectories define low-dimensional structures (manifolds) (Fig 5B-C). How can this population view be reconciled with the results of single PN recordings (Fig 2 A-C) that indicate discontinuities?

When the concentration of an odor was changed, individual PN response patterns to an odor could change suddenly and drastically with certain concentration steps (Fig 2). These changes, however, did not occur at the same concentration steps across all PNs. Hence, trajectories (*i.e.*, the high-dimensional state of the PN assembly over time) corresponding to different concentrations of an odor remained close to one another (because most changes in PN responses were relatively small when seen over the population). Each family of such nearby trajectories thus defines an odor manifold. Manifolds represent the degree of concentration invariance across the PN population responses for particular odors; they reflect the relative continuity in PN population responses across concentrations of an odorant, something that is not apparent in the responses of individual PNs, which often show discontinuities (see fig 2C).

By contrast, when the identity of an odor was changed, a greater proportion of PNs changed their responses significantly, explaining the larger distances between resulting odor trajectories, and thus defining distinct manifolds. The key difference, therefore, between individual PN response patterns evoked by odor identity and by concentration, appears to be not the extent of the pattern change per PN, but rather the probability that such significant changes will co-occur across many PNs for a given change in the stimulus. For a 10- to 1000-fold change in concentration, this probability is low. For a change in identity, it is generally high.

### **PN patterning is consistent with KC selectivity**

The selectivity of the postsynaptic KCs to odor intensity could be explained by their connectivity to particular sets of PNs. A KC connected to PNs that are largely coactive (during a given oscillation cycle) across many concentrations should be concentration invariant within that range. By contrast, a KC connected to PNs that are not coactive across

concentrations should be more selective. We found KCs of all concentration specificities, suggesting a diversity of PN-KC connection patterns. Given 830 PNs, 50,000 KCs and an estimated fan-out of 1PN:600KCs in locust (Perez-Orive et al., 2002), there exists an enormous number of possible connectivity matrices between the two populations. This connectivity has yet to be characterized.

Each KC integrates PN output cycle by cycle (50ms mean cycle duration) and over 10-20 PNs on average (Perez-Orive et al., 2002). Many individual 50 ms-time slices across the 110 PNs were sufficient to discriminate between odors and concentrations in our sample. If the number of PNs was reduced, however, discrimination became possible only with some PN subsets (Fig 6E), consistent with the observed rarity of KC responses (Perez-Orive et al., 2002).

Maximum distances between representations were, on average, reached within 200-300 ms of PN response onset. At response onset, LFP oscillation frequency is generally around 30Hz (Laurent and Davidowitz, 1994; Laurent and Naraghi, 1994), indicating that maximum divergence between representations can be reached within 5-10 oscillation cycles or steps of AL processing, a process apparently faster than that described for zebrafish (Friedrich and Laurent, 2001). The processes internal to the AL that generate this divergence must therefore be tuned to be both dynamically unstable—to allow this fast divergence (e.g., Rabinovich et al., 2001)—and yet well controlled—to enable the representations of different concentrations of one odor to diverge less than those of different odors. How this remarkable equilibrium is achieved remains to be understood.

## **Experimental Procedures**

### **Odorants**

For experiments with intracellular recording, odorants (monomolecular, including 1-hexanol, 1-heptanol, cis-3-hexen-1-ol, trans-2-hexen-1-ol, hexanal, 2-heptanone, 1-octanol, and geraniol (Sigma) and 3-pentanone, (Aldrich); and blends: mint and cherry, (LorAnn Oils), neat, or serially diluted in mineral oil (J.T. Baker) to yield stimuli at 0.001, 0.01, 0.1, or 1x of full strength, were applied to small strips of filter paper and placed in cartridges in

series with separate pipettes (1-cm diameter). Puffs of desiccated and filtered air (1-sec, 20s-1) carried the contents of the cartridges' headspace past the antenna (distance 1-cm). A large vacuum funnel behind the antenna maintained a steady flow of background air, and quickly removed the odorants. For experiments with tetrodes, octanol, hexanol, and geraniol were mineral-oil-dilution-standardized by vapor pressure in accordance with Raoult's Law and then serially diluted in mineral oil to yield strengths 0.001, 0.01, 0.05, 0.1, or 1x that of the standard. To the experimenter, the highest concentration smelled sharp and distinct; the lowest was too weak to be detected. KCs were typically tested with a larger set of odors, to increase chances of detectable responses. 20ml of each odorant was placed into a glass vial (60 ml). The headspace content was carried by puffs of desiccated and filtered air (0.3l/min, 1-sec, 20s-1) into a teflon tube (1-cm diameter) to mix with a constant stream of air (0.3l/min) directed to the antenna (distance 1-cm). A large vacuum funnel behind the antenna removed odorants.

### **Electrophysiology**

Results were obtained from 54 male and female locusts (*Schistocerca americana*) raised in a crowded colony. Young adults were immobilized with one antenna intact and fixed in place. The brain was exposed, desheathed, and bathed in locust saline, as previously described (Laurent and Naraghi, 1994; Stopfer and Laurent, 1999). LFPs were recorded either using saline-filled blunt glass micropipettes (tip,  $\sim 10\mu\text{m}$ ,  $\sim 10\text{M}\Omega$ ), amplified with a d.c. amplifier (NPI, Adams-List), or using custom wire tetrodes, amplified with a custom d.c. amplifier.

Intracellular recordings from antennal lobe neurons were made using 0.5M potassium acetate-filled sharp glass micropipettes ( $\sim 150\text{ M}\Omega$ , Sutter P87 horizontal puller) and amplified with a separate d.c. amplifier (Axon Instruments). Intracellular data were acquired using NBM116L hardware and LabVIEW (National Instruments).

Tetrode data with PNs were acquired using silicon probes from the Center for Neural Communication Technology (Drake et al., 1988); KC data were acquired using custom twisted wire tetrodes (Perez-Orive et al., 2002). PN and KC spikes were sorted offline

using an algorithm (Pouzat et al., 2002) implemented in Igor (WaveMetrics Inc.). Because LNs do not produce sodium action potentials (Laurent and Davidowitz, 1994), all spikes in the AL were unambiguously attributed to PNs. KC somata are clustered in a layer containing no other cell type. All spikes recorded in this cluster of 50,000 somata were thus unambiguously assigned to KCs. Results were analyzed with MATLAB (The MathWorks Inc.) software. Only the records from unambiguously separated clusters (see quantitative criteria in Pouzat et al., 2002) were kept and analyzed (PNs and KCs). Samples can be seen in Supplemental figure S4.

### **Data analysis**

Statistical comparisons were made by unpaired T-tests and 1- and 2-way analysis of variance with significance level set at  $p < 0.05$ . LFP and LN power was estimated by integrating a 15-Hz band centered on each preparation's peak odor response frequency. Power spectra were calculated from unfiltered records.

Principal component analysis (PCA) was performed using functions from MATLAB's Statistics Toolbox (The MathWorks Inc.). Observation of the "elbow" of the scree plot and the "broken stick rule" (Jolliffe, 1986), led us to retain the first 8 principal components (PCs) for further analysis; we used the first 3 PCs for display purposes. In general, for the  $k$ -dimensional vectors representing single trials ( $k = n \text{ PNs} * m \text{ bins}$ ;  $m = 20$  for Fig 3,  $m = 1$  for Fig 6), the variance captured by the first few PCs was low (24% and 30% for 3 and 8 PCs respectively in Fig 3B; 8% and 33% respectively in Fig 3C; 31% and 51% respectively in Fig 6). The remaining variance was evenly distributed among the remaining components, each contributing about 1% or less. When we performed the same analysis with data averaged across same-condition trials (thereby reducing the variation among vectors corresponding to the same concentration and odor pairs), the amount of variance accounted for by individual components greatly increased. For 3-trial averages (across trials of the same concentration and odor), the first 3 and 8 PCs (analyses similar to those in Fig 3C) captured 33% and 55% of the variance respectively; with 4-trial averages, these numbers were 37% and 62% respectively. In both cases, the clustering of vectors within concentration clusters and the clustering of concentration clusters within odor super-

clusters was tighter, and the classification success was greater than with single trial responses. Thus, the large variance unaccounted for by the first few PCs in the single trial analyses is due to (small but widespread in dimension) variation across trials, and is unrelated to differences in the concentration or the identity of the stimulus presented.

Hierarchical clustering shown was performed using 8 PCs and average linkage. Results were similar for nearest and complete linkages. The *k-means* method was also used for confirmation of clustering, and showed similar results.

Two simple tests were used for classification, both based on Euclidean distances of individual points from group centroids (means of the remaining points in a group). In test A, points were individually classified as belonging to 1 of 15 (5 concentrations of 3 odors) groups. Test A measures mainly trial-to-trial reliability. In test B, all points belonging to a particular concentration of an odor were taken out, so as not to bias the location of group centroids, and were then each classified as individually belonging to 1 of 3 (odor) groups. Test B measures similarity between concentration subclusters within an odor group. Results with other classification procedures such as linear discriminant analysis produced similar results. Classification results were also robust to the number of PCs used (from 3 upwards).

To bin PN spike times by oscillation cycle, cycles were identified using successive peaks of the bandpass-filtered LFP (10-30Hz). Spike counts were then computed for each so defined cycle (bin). This analysis was performed only for those experiments in which high quality LFP recordings could be obtained.

Distance and correlation matrices were computed by measuring pairwise distances and cross-correlations between all time slices (from stimulus onset to 1 second after the end of stimulus) across concentrations and odors. The distance and correlation matrices shown are for 50 ms time slice widths averaged over 3 trials. The t-statistic was used to assess statistical significance for the correlation matrices (only statistically significant correlations with  $p < 0.001$  are shown).

For nonlinear dimensionality reduction with Locally Linear Embedding (Roweis and Saul, 2000), we used code from Sam Roweis (<http://www.cs.toronto.edu/~roweis/lle/>), with Gerard Sleijpen's code for the JDQR eigensolver (<http://www.math.uu.nl/people/vorst/JDQR.html>). In the figures shown for nonlinear dimensionality reduction with LLE, we used as input, 110-D time slices, each 100 ms wide and averaged over 3 trials. Results obtained with slice widths of 50 ms are included as Supplemental Data (see Figure S5). For a particular choice of embedding dimension, LLE requires only one user-specified parameter (K), the number of nearest neighbors to consider in the reconstructions of individual high-dimensional points. We chose values for K such that distances to the K nearest neighbors were, for all points, small (see Supplemental Figure S6). The results we obtained were qualitatively similar (i.e., concentration trajectories localized within odor manifolds) with a wide range of K values (8 to 25).

For the analysis of classification success using subsets of PNs, 5 to 100 PNs (in increments of 5) were randomly selected (100 combinations per number of PNs) from the pool of 110 PNs, and PCA was performed on each selection.

### **Acknowledgements**

This work was supported by grants from the National Institute for Deafness and Communication Disorders, the National Science Foundation (BITS Program), the Keck and McKnight Foundations to GL. MS received support from the Burroughs Wellcome Fund. VJ was supported by the Sloan-Swartz Center for Theoretical Neurobiology at Caltech. We are grateful to Pietro Perona, Marzia Polito, Sam Roweis, Erik Winfree, Rainer Friedrich and the Laurent lab for helpful discussions throughout the course of this work and for comments on the manuscript, to Ofer Mazor, Stijn Cassenaer and Javier Perez-Orive for suggestions with the extracellular probe recordings, and to Sachiko Murase for vapor pressure calculations. Multichannel silicon probes were kindly provided by the University of Michigan Center for Neural Communication Technology, sponsored by NIH NCRR grant P41RR09754.

## BIBLIOGRAPHY

- Adrian, E. (1942). Olfactory reactions in the brain of the hedgehog. *J. Physiol. (Lond)* *100*, 459-473.
- Bäcker, A. (2002) Pattern recognition in the olfactory system of the locust: priming, gain control and coding issues, Ph. D., California Institute of Technology.
- Burrows, M. (1996). *The Neurobiology of an Insect Brain* (New York: Oxford University Press).
- Cang, J. and Isaacson, J. S. (2003). *In vivo* whole-cell recording of odor-evoked synaptic transmission in the rat olfactory bulb. *J. Neurosci.* *23*, 4108-4116.
- Cinelli, A., Hamilton, K. A., and Kauer, J. S. (1995). Salamander olfactory bulb neuronal activity observed by video rate, voltage-sensitive dye imaging. III. Spatial and temporal properties of responses evoked by odorant stimulation. *J. Neurophysiol.* *73*, 2053-2071.
- de Bruyne, M., Foster, K., Carlson, J. R. (2001). Odor coding in the *Drosophila* antenna. *Neuron* *30*, 537-52.
- Drake, K. L., Wise, K. D., Farraye, J., Anderson, D. J., and Bement, S. L. (1988). Performance of planar multisite microprobes in recording extra-cellular single-unit intracortical activity. *IEEE Trans. on Biomed. Engineer.* *35*, 719-732.
- Engen, T., and Pfaffmann, C. (1959). Absolute judgements of odor intensity. *J. Exp. Psychol.* *58*, 23-26.
- Freeman, W. J. (1978). Spatial properties of an EEG event in the olfactory bulb and cortex. *Electroencephalogr. Clin. Neurophysiol.* *44*, 586-605.
- Friedrich, R. W., and Korsching, S. I. (1997). Combinatorial and chemotopic odorant coding in the zebrafish olfactory bulb visualized by optical imaging. *Neuron* *18*, 737-752.
- Friedrich, R. W., and Laurent, G. (2001). Dynamic optimization of odor representations by slow temporal patterning of mitral cell activity. *Science* *291*, 889-894.
- Gray, C. M., and Skinner, J. E. (1988). Centrifugal regulation of neuronal activity in the olfactory bulb of the waking rabbit as revealed by reversible cryogenic blockade. *Exp. Brain Res.* *69*, 378-386.

- Heisenberg, M., Borst, A., Wagner, S., and Byers, D. (1985). *Drosophila* mushroom body mutants are deficient in olfactory learning. *J. Neurogenet.* 2, 1-30.
- Heisenberg, M. (2003). Mushroom body memoir: from maps to models. *Nat. Rev. Neurosci.* 4, 266-275.
- Hopfield, J. J. (1995). Pattern recognition computation using action potential timing for stimulus representation. *Nature* 376, 33-36.
- Joerges, J., Kuttner, A., Galizia, C. G., and Menzel, R. (1997). Representations of odours and odour mixtures visualized in the honeybee brain. *Nature* 387, 285-288.
- Jolliffe, I. T. (1986). *Principal Component Analysis* (New York: Springer-Verlag).
- Kauer, J. S., and Moulton, D. G. (1974). Responses of olfactory bulb neurones to odour stimulation of small nasal areas in the salamander. *J. Physiol.* 243, 717-737.
- Laurent, G. (2002). Olfactory network dynamics and the coding of multidimensional signals. *Nat. Rev. Neurosci.* 3, 884-895.
- Laurent, G., and Davidowitz, H. (1994). Encoding of olfactory information with oscillating neural assemblies. *Science* 265, 1872-1875.
- Laurent, G., and Naraghi, M. (1994). Odorant-induced oscillations in the mushroom bodies of the locust. *J. Neurosci.* 14, 2993-3004.
- Laurent, G., Stopfer, M., Friedrich, R. W., Rabinovich, M. I., Volkovskii, A., and Abarbanel, H. D. (2001). Odor encoding as an active, dynamical process: experiments, computation, and theory. *Annu. Rev. Neurosci.* 24, 263-297.
- Laurent, G., Wehr, M., and Davidowitz, H. (1996). Odour encoding by temporal sequences of firing in oscillating neural assemblies. *J. Neurosci.* 16, 3837-3847.
- MacLeod, K., Bäcker, A., and Laurent, G. (1998). Who reads temporal information contained across synchronized and oscillatory spike trains? *Nature* 395, 693-698.
- MacLeod, K., and Laurent, G. (1996). Distinct mechanisms for synchronization and temporal patterning of odor-encoding neural assemblies. *Science* 274, 976-979.
- Margrie T. W., and Schaefer A. T. (2003). Theta oscillation coupled spike latencies yield computational vigour in a mammalian sensory system. *J Physiol.* 546, 363-74.
- Marin E. C., Jefferis G. S., Komiyama T., Zhu H., Luo L. (2002). Representation of the glomerular olfactory map in the *Drosophila* brain. *Cell* 109, 243-255.

- Meister, M., and Bonhoeffer, T. (2001). Tuning and topography in an odor map on the rat olfactory bulb. *J. Neurosci.* *21*, 1351-1360.
- Meredith, M. (1986). Patterned response to odor in mammalian olfactory bulb: the influence of intensity. *J. Neurophysiol.* *56*, 572-597.
- Ng, M., Roorda, R. D., Lima, S. Q., Zemelman, B. V., Morcillo, P., Miesenbock, G. (2002). Transmission of olfactory information between three populations of neurons in the antennal lobe of the fly. *Neuron* *36*, 463-474.
- Pelz, C., Gerber, B., and Menzel, R. (1997). Odorant intensity as a determinant for olfactory conditioning in honeybees: roles in discrimination, overshadowing and memory consolidation. *J. Exp. Biol.* *200* (4), 837-847.
- Perez-Orive, J., Mazor, O., Turner, G. C., Cassenaer, S., Wilson, R. I., and Laurent, G. (2002). Oscillations and sparsening of odor representations in the mushroom body. *Science* *297*, 359-365.
- Pouzat, C., Mazor, O. and Laurent, G. (2002) Using noise signature to optimize spike-sorting and to assess neuronal classification quality. *J. Neurosci. Meth.* *122*, 43-57.
- Rabinovich, M., Volkovskii, A., Lecanda, P., Huerta, R., Abarbanel, H. D., and Laurent, G. (2001). Dynamical encoding by networks of competing neuron groups: Winnerless competition. *Phys. Rev. Lett.* *87*, 068102.
- Rodiek, R. W. (1998). *The First Steps in Seeing* (Sunderland, MA: Sinauer Associates, Inc.).
- Roweis, S. T., and Saul, L. K. (2000). Nonlinear dimensionality reduction by locally linear embedding. *Science* *290*, 2323-2326.
- Rubin, B. D., and Katz, L. C. (1999). Optical imaging of odorant representations in the mammalian olfactory bulb. *Neuron* *23*, 499-511.
- Spors H. and Grinvald A. (2002). Spatio-temporal dynamics of odor representations in the mammalian olfactory bulb. *Neuron* *34*, 301-15.
- Seung, H. S., and Lee, D. D. (2000). The manifold ways of perception. *Science* *290*, 2268-2269.
- Slotnick, B. M., and Ptak, J. E. (1977). Olfactory intensity-difference thresholds in rats and humans. *Physiol. Behav.* *19*, 795-802.

- Stewart, W. B., Kauer, J. S., and Shepherd, G. M. (1979). Functional organization of rat olfactory bulb analysed by the 2-deoxyglucose method. *J. Comp. Neurol.* *185*, 715-734.
- Stopfer, M., Bhagavan, S., Smith, B. H., and Laurent, G. (1997). Impaired odour discrimination on desynchronization of odour-encoding neural assemblies. *Nature* *390*, 70-74.
- Stopfer, M., and Laurent, G. (1999). Short-term memory in olfactory network dynamics. *Nature* *402*, 664-668.
- Turk, M., and Pentland, A. (1991). Eigenfaces for recognition. *J. Cog. Neurosci.* *3*, 71-86.
- Wachowiak, M., Cohen, L. B., and Zochowski, M. R. (2002). Distributed and concentration-invariant spatial representations of odorants by receptor neuron input to the turtle olfactory bulb. *J. Neurophysiol.* *87*, 1035-1045.
- Wang, J. W., Wong, A. M., Flores, J., Vosshall, L. B., Axel, R. (2003). Two-photon calcium imaging reveals an odor-evoked map of activity in the fly brain. *Cell* *112*, 271-282.
- Wehr, M., and Laurent, G. (1996). Odour encoding by temporal sequences of firing in oscillating neural assemblies. *Nature* *384*, 162-166.
- Wellis, D. P., Scott, J. W., and Harrison, T. A. (1989). Discrimination among odorants by single neurons of the rat olfactory bulb. *J. Neurophysiol.* *61*, 1161-1177.
- Wong, A.M., Wang, J. W., Axel, R. (2002). Spatial representation of the glomerular map in the *Drosophila* protocerebrum. *Cell* *109*, 229-241.

## Supplementary information

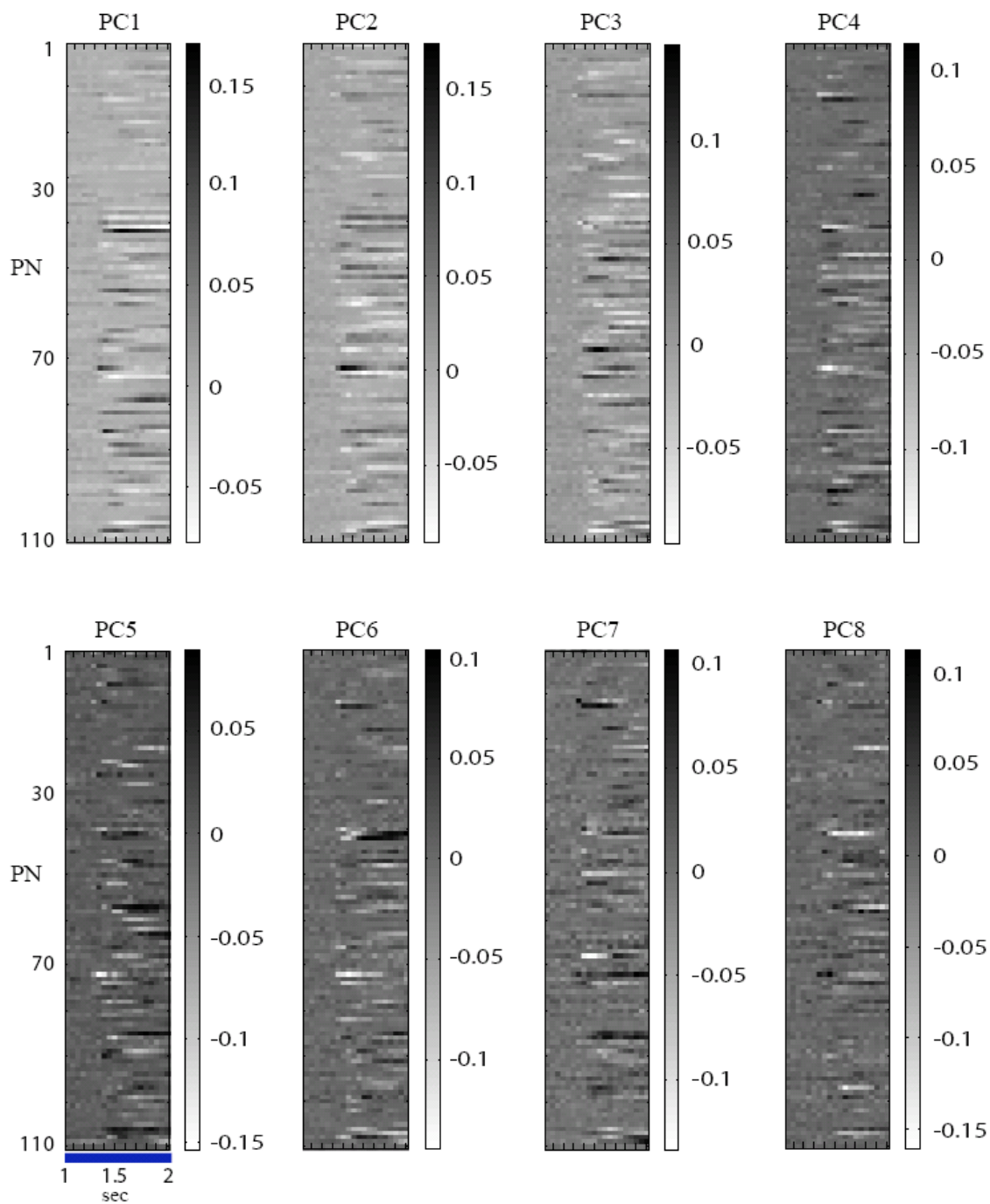


**Figure S1.** The first 8 principal components from the analysis described in Figure 3C. The PCs show contributions from numerous cells across several time slices.

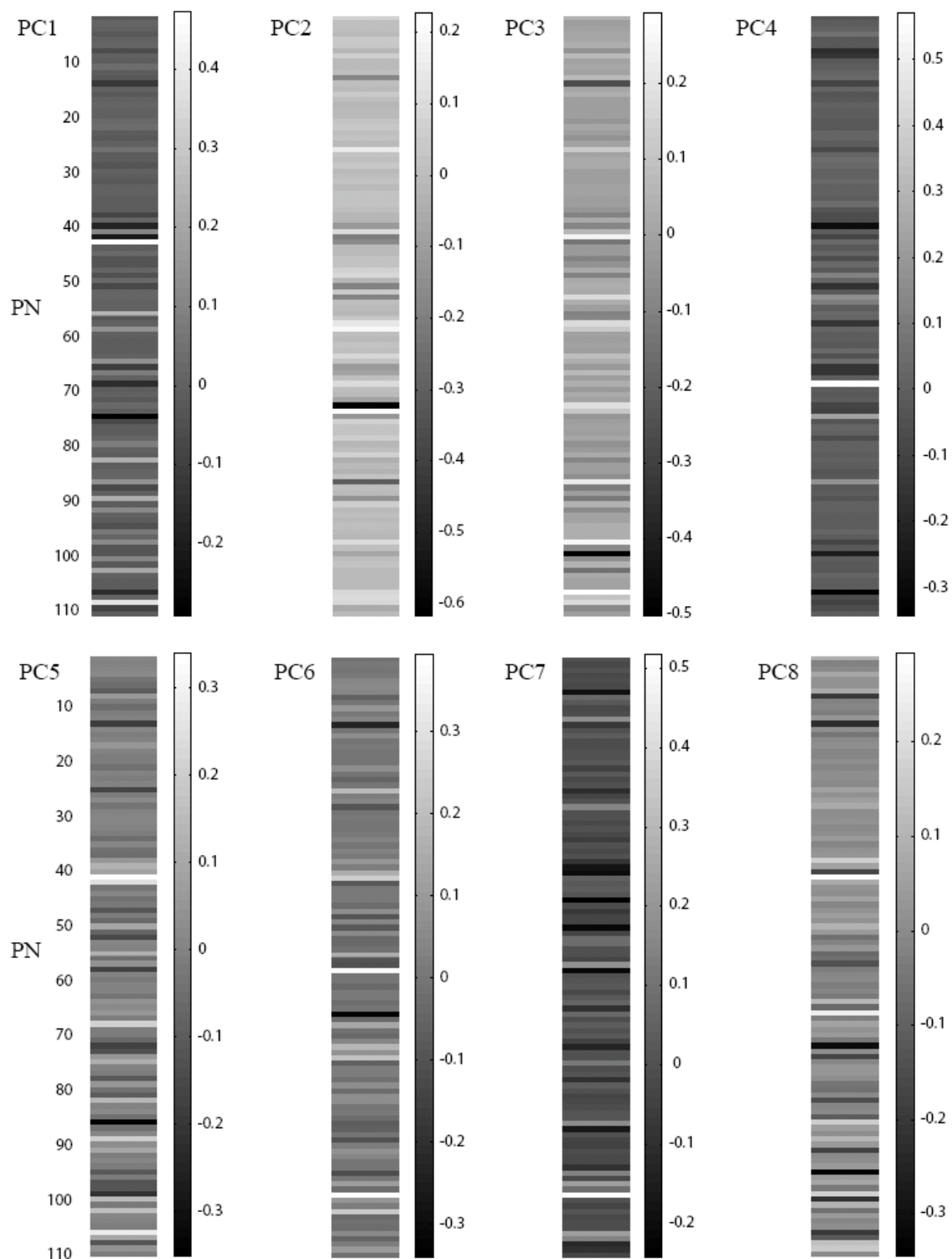


**Figure S2.** The first 8 principal components from the time slice PC analysis illustrated in Figure 6. The PCs show both positive and negative (inhibitory) contributions coming from numerous cells.

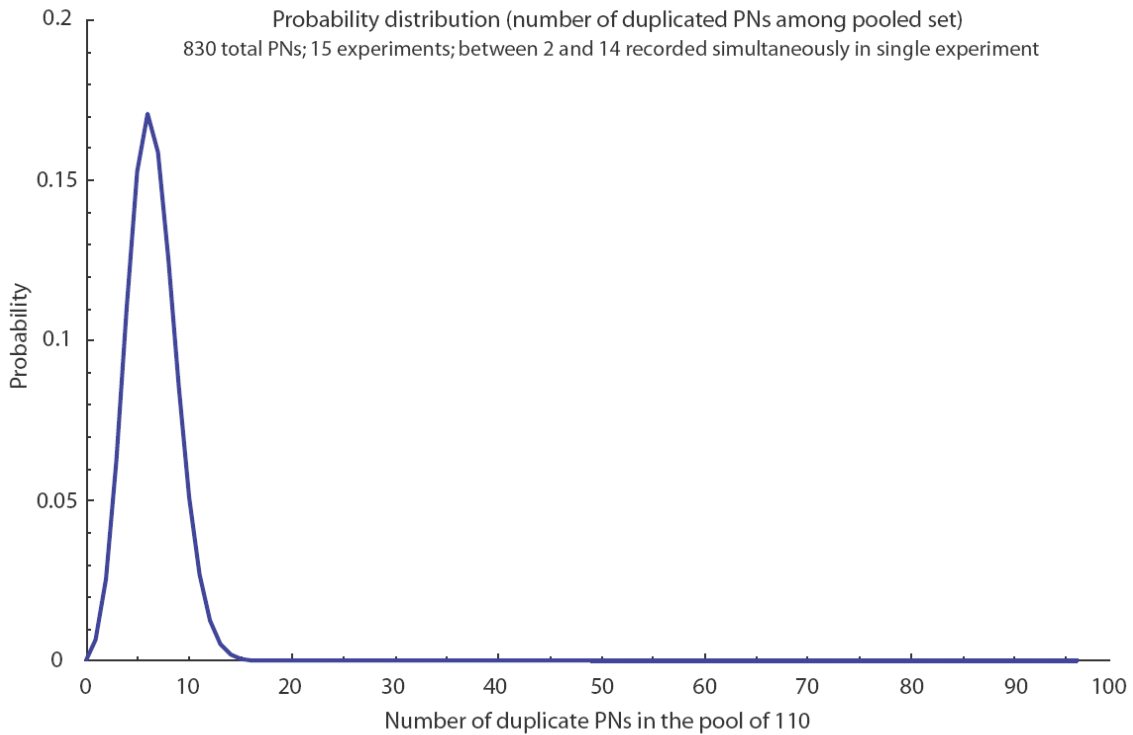


**Figure S3.** There are about 830 PNs in the locust antennal lobe, from which we sampled up to 14 PNs in a single experiment. If PNs in the locust are identifiable, as has been suggested for *Drosophila*, and shown for other types of neurons in the locust, we may have recorded from the same cell multiple times in different experiments. Since we pool cells recorded in different experiments (and animals) for some of our analyses, it becomes important to estimate how many duplicates we might have in the pooled set. The analysis below allows us to estimate these numbers for a pooled set of 110 neurons from 15 different animals. We assume that, in each experiment, cells are sampled randomly from the total of 830 PNs

**Notation:**

$N_{AL}$  = total number of PNs in an antennal lobe

$N_{ex}$  = number of experiments

$n(i)$  = number of PNs recorded in the  $i^{th}$  experiment

$n_{mx}$  = maximum number of PNs recorded simultaneously in an experiment (this is also the minimum number of different PNs guaranteed to be in the pooled set)  
=  $\max(n(i))$

$P_{dup}(k)$  = probability of getting exactly  $k$  duplicated PNs in the pooled set

$P(k)$  = probability of getting exactly  $k$  different PNs in the pooled set

$P_p(k)$  = probability of getting a particular set of  $k$  different PNs

$$P_{dup}(k) = 1 - (\text{probability of getting exactly } k \text{ different PNs in the pooled set}) \\ = 1 - P(k)$$

$$P(k) = (\text{number of ways of choosing } k \text{ out of } N_{AL}) \times \\ (\text{probability of getting a particular set of } k \text{ different PNs})$$

$$\Rightarrow P(k) = \binom{N_{AL}}{k} \times P_p(k),$$

$$\Rightarrow P(k) = \frac{N_{AL}!}{(N_{AL}-k)! k!} \times P_p(k), \text{ where,}$$

$$P_p(k) = (\text{Prob. of choosing PNs from within a particular subset of } k \text{ different PNs}) - \\ (\text{Prob. of choosing PNs from subsets of } s < k \text{ PNs in this particular subset})$$

$$\Rightarrow P_p(k) = \prod_{i=1}^{N_{ex}} \prod_{j=1}^{n(i)} \frac{(k-j)}{\binom{N_{AL}-j}{k}} - \sum_{s=n_{mx}}^{k-1} \binom{k}{s} \times P_p(s)$$

In our case:  $N_{AL} = 830$ ;  $N_{ex} = 15$ ;  $n_{mx} = 14$ ;  $n(i)$  is obtained from the actual number of cells recorded from in the 15 different experiments, i.e., 4, 10, 6, 5, 5, 14, 2, 4, 5, 10, 7, 11, 9, 4, and 14 (110 cells total, when pooled together). Shown in this figure is the distribution of probabilities  $P_{dup}(k)$  for all possible values of  $k$ . We conclude that the expected probability of finding duplicates in our sample of 110 PNs is not 0, but that the number of expected duplicates is very small.

Our experimental results indicate that there were no duplicates across our pooled set of 110 PNs. This could be explained in at least two ways. First, our set of 110 PNs may contain a small set of duplicates that went undetected. Because PNs are compared using their responses to three odors only, small amounts of variability across individuals may appear as larger differences than they would if we tested all PNs across many odors. This is the explanation we favor (see Discussion). Second, our assumption that all individuals have the same sets of PNs could be wrong. Although that is possible, all indications from PN structure and responses in other insect species (*Drosophila* in particular, see Discussion) and from locust neurons in general (see Burrows, 1996) are that the same neurons can

generally be found across individuals. While this might not hold true for large populations of neurons involved in learning and memory, such as Kenyon cells in the mushroom body, circuits (including olfactory ones) in insects typically develop under very precise and reliable rules, with little interindividual variability.

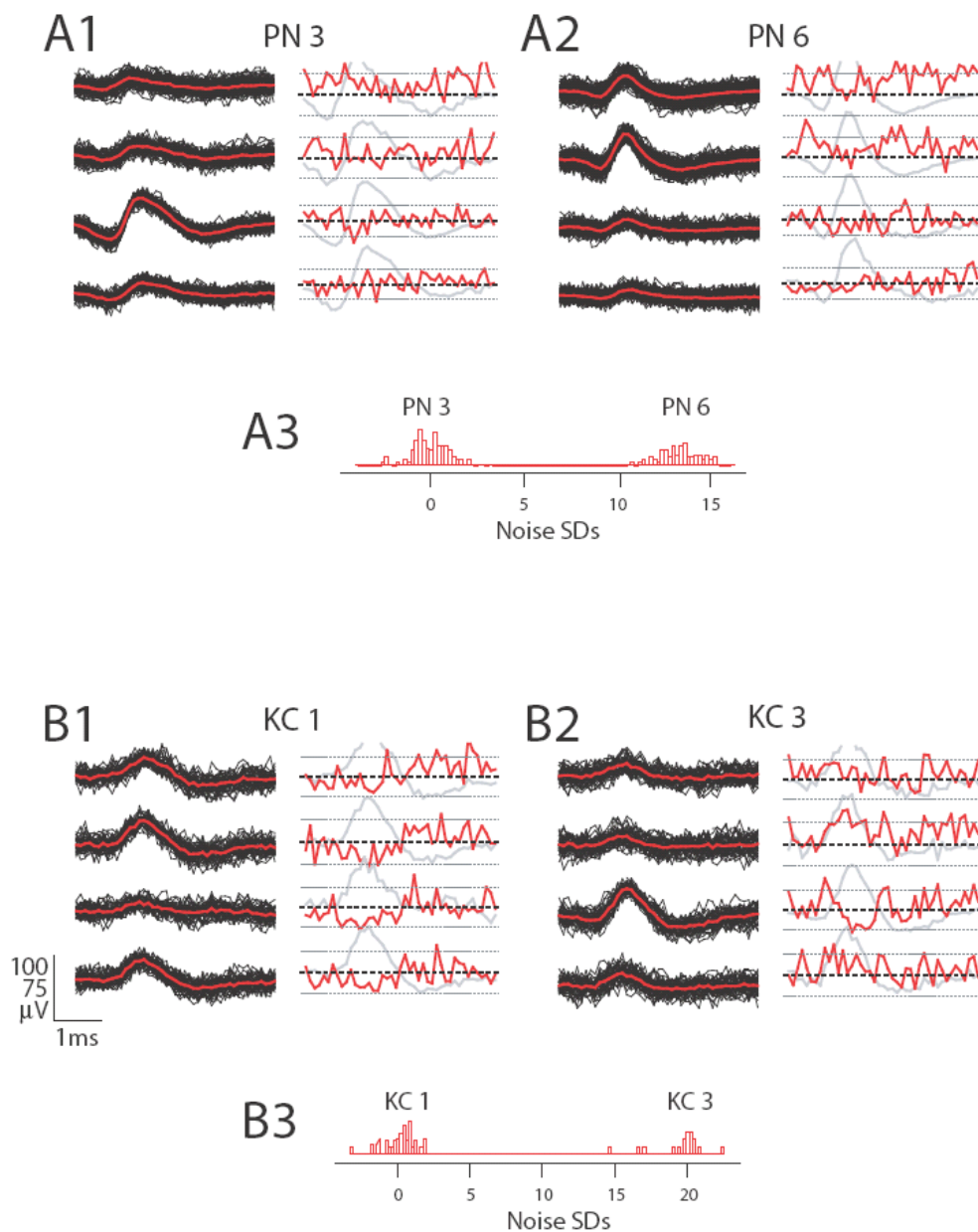


**Figure S4.** Examples of spike sorting. Extracellular records of PNs and KCs were made using tetrodes; thus 4 “views” of each detected spike, together with the noise recorded between spikes, could be analyzed to determine and assign confidence values to spike sources (Pouzat et al., 2002).

(A) PN analysis: example shows PNs 3 and 6 from figure 2C. (A1, A2) Clusters for 2 PNs. Left panels: for each of 4 tetrode channels, all events (black) and their means (red) classified as a unique cluster. Classification was performed using the entire waveforms shown from each channel. Right panels: variance around the mean for each of the 4 channels, together with 95% confidence intervals (based on the interspike noise record). (A3) Clusters are well-separated: each pair of clusters in 180-D space (45 samples/waveform x 4 channels) is projected onto the line connecting the cluster centers. Cluster centers were separated by at least 5 times the noise SD. All extracellular spike sources are evaluated using these and other criteria (Pouzat et al., 2002). (B) KC analysis: same analysis as in S2A, but for KCs 1 and 3 from figure 7A.

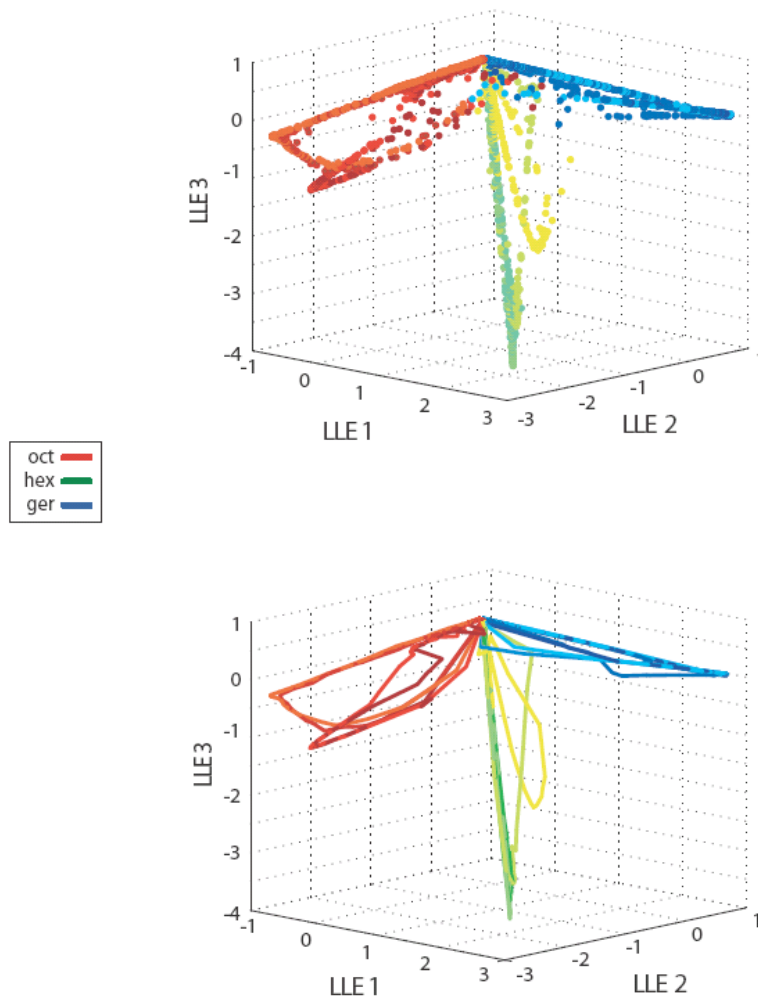


**Figure S5.** Same LLE trajectory plots as in Figure 5 (A-B), here calculated from 50ms bins (averaged over 3 trials, as in Fig 5 (A-B)). The observations made for Figure 5 (A-B) hold true for this temporal resolution as well: the PN ensemble responds with concentration-specific trajectories within odor-specific manifolds.

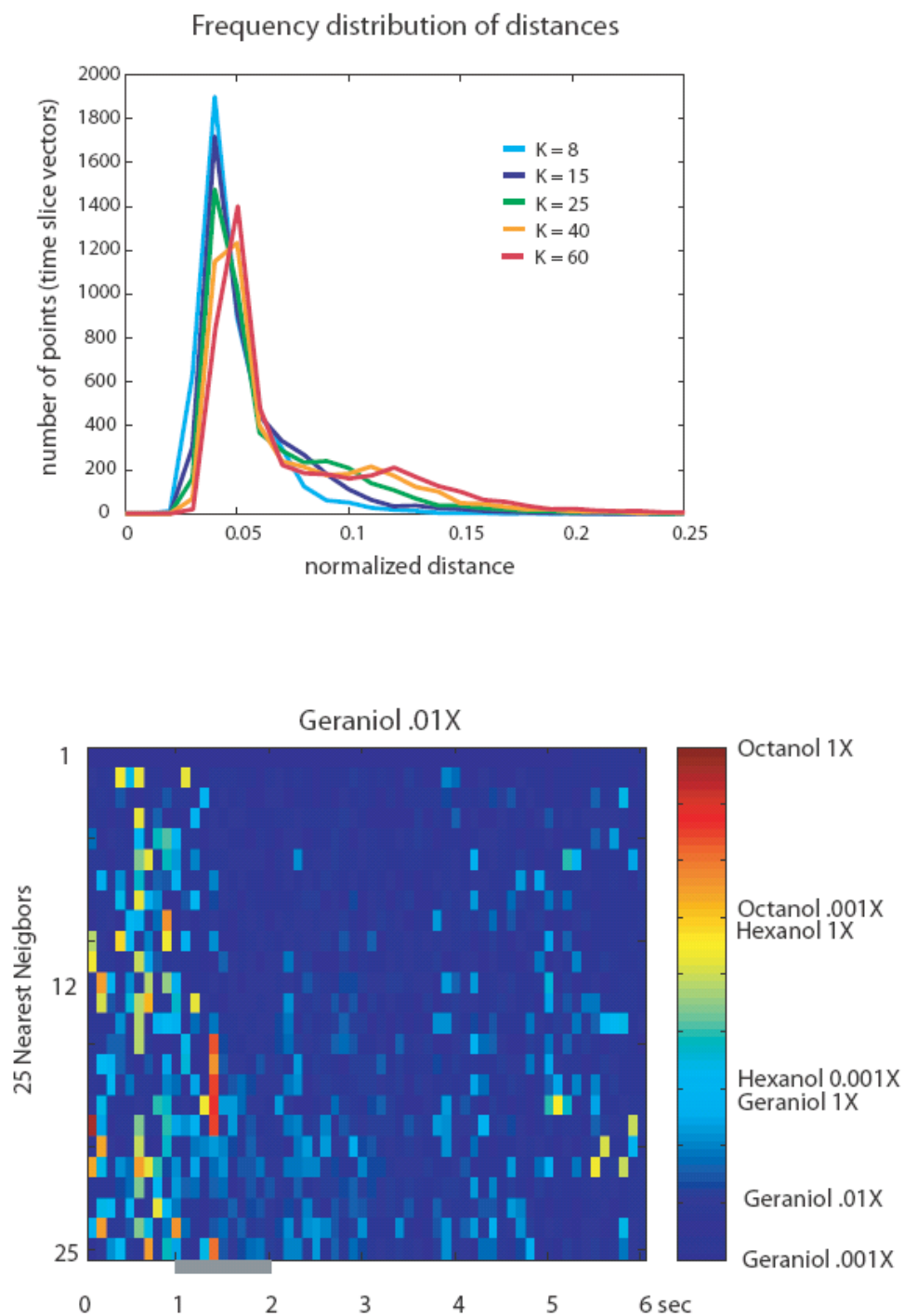


**Figure S6.** Description of the term: “K nearest neighbors” of individual time slices. LLE uses only one user-supplied parameter, K, which is the number of nearest neighbors to consider for locally-linear reconstruction, i.e., for the embedding of a high-dimensional point (or vector) in a lower dimension space, while preserving, for each point, its local neighborhood. The choice of K was

guided by what is known about the average size of the close neighborhood of individual points in the full space.

In our analysis, each point in the full space is a 110-d vector of spike counts across the 110 PNs, measured for each time slice or bin. The distance matrices (Fig 4 E-G) and this figure are used to estimate the sizes of these neighborhoods, and thus provide guidance for the choice of  $K$ .

The top panel shows frequency distributions of distances (normalized to maximum distance in the distance matrix) of all time slice vectors (points) to their (8th, 15th, 25th and 40th) nearest neighbors. For  $K < 15$ , the vast majority of points have very low distances (less than 0.1, i.e., 10% of the maximum) to their  $K$  nearest neighbors, the mean distance is close to the peak at approximately 0.04, and there is little variance around the mode. As  $K$  increases however, the curve begins to develop a second peak at around 0.1-0.12, the first peak and the mean shift to the right and the variance increases. The meaning of "near neighborhood" thus becomes inconsistent and breaks down for a significant number of points as  $K$  increases much beyond 20. This provides bounds on the values of  $K$  to use for the method. We obtained qualitatively similar results for all  $K$  values chosen within those bounds.

The identity of the neighbors helps understand the structure uncovered by LLE. If, for example, several consecutive vectors (at  $\text{bin}_j$  and  $\text{bin}_{j+1}$ ) differ little from one another, we can assume that each point (vector) must have sets of local (here, temporal) neighbors. Further, if as seen in 4 (E-G), time-matched vectors belonging to different concentrations of the same odor differ little from each other, they would also be part of each other's nearest neighborhood and thus closer to each other in the embedding as well.

In the bottom panel, each pixel's color represents the identity (coded: blue = geraniol vectors, yellow and green = hexanol, red = octanol—see color bar at right) of the time-slice vectors that are closest to each individual vector during this geraniol .01X response. (The first row represents identity.) Each column shows the identity of the 25 vectors (ranked by Euclidean distance) nearest to the corresponding time slice vector calculated from the geraniol .01X response. Before response onset, many nearest neighbors come from baseline states of other odors and concentrations. Once the response begins however, the nearest neighbors come exclusively either from preceding or following time slices of the same odor-concentration pair, or from nearby concentrations of geraniol (different shades of blue pixels in columns after 300ms). Near the end of the response, time slice vectors calculated for other odors can be seen once again (e.g., around the 5s point). This is a reflection of what is seen more clearly in the three-dimensional embeddings (Fig 5(A-C) and Fig S2) produced by LLE.

*Chapter 3***ENCODING AND DECODING OF OVERLAPPING ODOR SEQUENCES****Acknowledgements**

Bede M. Broome and I contributed equally to the work in this chapter. Bede performed all the experiments and the spike sorting for the PN and KC tetrode recordings (Figures 1 and 7; Supplementary Figures S5-7). I performed all the other analyses (Figures 2-6 and 8; Supplementary Figures S1-4, S8 and S9).

## Summary

**Odors evoke complex responses in locust antennal lobe projection neurons (PNs)—the mitral cell analogs. These patterns evolve over hundreds of milliseconds and contain information about odor identity and concentration. In nature, animals often encounter many odorants in short temporal succession. We explored the effects of such conditions by presenting two different odors with variable intervening delays. PN-ensemble representations tracked stimulus changes and, in some delay conditions, reached states that corresponded neither to the representation of either odor alone, nor to the binary mixture of the two. We then recorded from Kenyon cells (KCs), the PNs' targets. Their responses were consistent with the PN population's behavior: in some conditions, KCs were recruited that did not fire during single-odor or mixture stimuli. Thus, PN-population dynamics are history dependent, and responses of individual KCs are consistent with piecewise temporal decoding of PN output over large sections of the PN population.**

## Introduction

In nature, animals rarely encounter stimuli in isolation and must often extract meaningful information from complex streams of overlapping signals. In the auditory system, context has well-documented effects on neuronal responses (Bartlett and Wang, 2005) and on sound perception (Wegel and Lane, 1924). For example, the perception of one stimulus can be diminished by the close temporal proximity of another (Wegel and Lane, 1924; Sobel, 1994). Masking, as this phenomenon is called, has also been described in vision (Kahneman, 1968; Macknik and Livingstone, 1998), taste (Vogt and Smith, 1994; Stevens and Traverzo, 1997) and olfaction (Laing et al., 1989; Rouby and Holley, 1995). With odors, stimulus processing is made more difficult by the inherently chaotic—thus often unpredictable—nature of these signals' delivery (Koehl et al., 2001). Understanding how the brain treats such complex stimuli is further complicated by the observation that olfaction is a synthetic sense (Laing and Francis, 1989). That is, with the exception of specialized signals such as pheromones, allomones or kairomones (Mustaparta, 1996;

Vickers et al., 1998; Suh et al., 2004; Lin da et al., 2005), odor segmentation appears to be limited in animals. Similarly, humans can identify individual components in a mixture, but only if less than 3-4 odors are mixed together (Laing and Francis, 1989). Does the presentation of one odor affect the on-going processing of another? How does the brain deal with multiple concurrent odor stimuli that do not co-vary? Does it keep track of each one independently? Does it create a representation of the mixture when there is temporal overlap? Or does it behave differently still?

While the answers to these questions ultimately contain perceptual and behavioral components, we can begin to address them using neurophysiological approaches. These studies should also help us constrain neural coding schemes for odors. Our recent work on insects and fish olfactory systems shows that odors give rise to very different response profiles in two structures separated by only one synapse (Friedrich and Laurent, 2001; Perez-Orive et al., 2002; Mazor and Laurent, 2005). In the locust antennal lobe, odors are represented by distributed assemblies of broadly-tuned principal neurons, whose individual activities evolve deterministically over time, in a PN- and odor-specific manner (Laurent and Naraghi, 1994; Laurent et al., 1996; Wehr and Laurent, 1996; Mazor and Laurent, 2005). In the mushroom body, the direct target of the antennal lobe, odors are represented by very small assemblies of mostly silent and highly specific neurons, called Kenyon cells, or KCs (Laurent and Naraghi, 1994; Perez-Orive et al., 2002). The mechanisms underlying this dramatic transformation of representations are beginning to be understood (Perez-Orive et al., 2002; Perez-Orive et al., 2004): Kenyon cells accomplish a pattern matching between an activity (input) vector—function of the state of the PN population at a given time—and a connectivity vector—the set of PNs that each KC is connected to. With 50,000 KCs, a mushroom body can realize as many connection patterns, and thus, recognize a very large number of PN activity patterns (Jortner et al., 2007). Because each KC contacts about 50% of the PN population, differences between connectivity vectors can be maximized across the population (Jortner et al., 2007); this may in turn explain the sparseness and specificity of the KCs' responses.

For high specificity to arise with such high connectivity, however, pattern matching between input and connectivity vectors must occur over limited time windows: indeed, if KCs were allowed to summate their input over long periods of time, they would eventually reach spike threshold even when stimulated with suboptimal PN activity vectors: sparseness and specificity would disappear. Our present understanding is that the relevant KC integration window corresponds to about one half of one oscillation cycle (about 20 ms) (Wehr and Laurent, 1996; Perez-Orive et al., 2002). Thus, each KC is given one chance to fire during each oscillation cycle, repeatedly for as long as PN output is synchronized; because PN activity vectors change from one oscillation cycle to the next (Laurent et al., 1996; Wehr and Laurent, 1996; Stopfer and Laurent, 1999; Mazor and Laurent, 2005), each KC performs a new pattern matching at each oscillation cycle. In other words, each KC action potential represents a specific instantaneous state of a large percentage of the PN population at that time. If this description is correct, the response of a KC should be sensitive to the instantaneous variations of its input vector (instantaneous state of the PN population). Under conditions of overlapping stimuli, for example, one would predict that a KC that responds to odor *A* at time *t* might not fire if odor *B* were added to *A* a short time before *t*. Conversely, if a KC were found to respond during an overlap between odors *A* and *B*, we predict that its response probability should decline as the relative timing of the *A* and *B* stimuli is changed. The stimulation paradigms we will explore here are, therefore, not only an investigation of how odor mixtures and sequences are processed, but also a means to explore the sensitivity of KCs to the instantaneous state of the PN population.

## **Results**

PNs respond to odors (singular or mixtures) by producing both fast and slow temporally patterned responses. For each PN, these responses are both highly reproducible and odor specific.

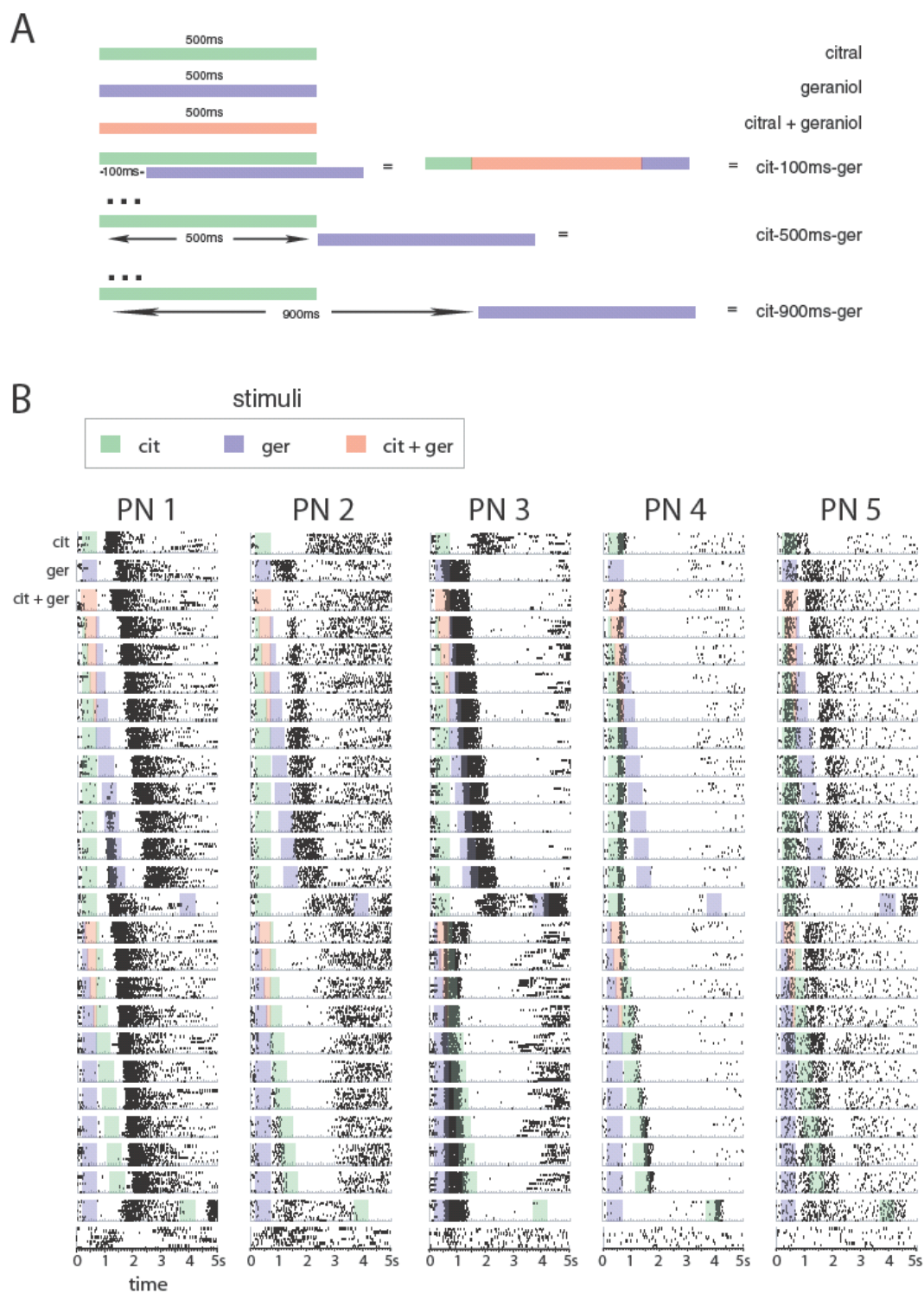


**Figure 1.** Stimulus Description and PN responses to Overlapping Stimuli **A:** Description of stimuli. Two odors, citral (cit) and geraniol (ger), were presented either alone or with staggered onset times. In all cases each odor was presented for 500ms. The start times of the two odors were staggered relative to one another using the notation shown. The separation in odor onset times ranged from 0ms (overlapping presentation, cit+ger) to 1000ms in steps of 100ms. An additional trial with 3.5 s delay between pulse onsets was also included. **B:** Representative PNs displaying olfactory masking.

Raster plots of five odor-responsive PNs (in vivo tetrode recordings). PNs shown here were not recorded simultaneously. Shaded areas correspond to pure, mixed and overlapping odor stimuli indicated in legend as described in A. Fifteen consecutive trials per stimulus condition. Condition order was randomized within a given experiment. See text for detail.

We examine here the responses of PNs in conditions of staggered stimulations with two odors. As previously described (Perez-Orive et al., 2002; Stopfer et al., 2003; Mazor and Laurent, 2005) we performed simultaneous extra-cellular multi-single-unit recordings from groups of PNs ( $n = 87$ , average group size = 9, range = 8 to 25, see Experimental Procedures) in 10 animals while presenting 28 different stimulus conditions (blocks of 15 trials each) composed of 4 pure odor conditions (citral, geraniol, no odor, paraffin oil) and 24 2-odor-pulse stimuli (Fig. 1A), in pseudo-random order. The single-odor conditions (citral and geraniol) were tested twice (at the beginning and at the end of each experiment), to control for stability. All stimuli were presented or mixed in a dry air carrier stream. In all cases, the responses of a given PN to an odor were highly reproducible across a block of 15 trials and across the course of an experiment (Fig. 1B). In locusts, PNs are the only antennal lobe neurons that produce sodium action potentials (Laurent and Davidowitz, 1994). Thus, all spikes reported here can be unambiguously attributed to PNs.

### **Single PN Responses to Overlapping Odor Pulses**

Given the complex nature of PN responses to odors, we first examined whether the firing profiles of individual PNs to overlapping odor pulses could be predicted from the knowledge of their responses to each odor presented alone. Examples of responses to each odor condition are shown for five PNs in Fig. 1B. While these five representative examples show different combinations of response types, the main interactions between overlapping pulses can be described as various forms of masking. When excitation by one of the two odors overlapped with inhibition caused by the other odor, excitation was generally reduced, and sometimes totally suppressed. Consequently, one would predict that the detection of a component within a mixture from PN patterns alone should be compromised. We estimated the predictability of the interactions between firing rates (for each PN) by comparing observed and calculated (summed) firing rate profiles in overlapping stimulus conditions (Fig. 2). These sums were calculated assuming that all cessation of firing, often

caused by inhibition (Leitch and Laurent, 1996; MacLeod and Laurent, 1996), should be represented by the negative of the mean baseline-firing rate (see Experimental Procedures). These comparisons revealed, for example, that the recorded response of a PN could match reasonably well (PN6, Fig. 2), undershoot (PN7, Fig. 2) or exceed (PN8, Fig. 2) the arithmetic sum of the component responses. Many of these more complex interactions could not be explained by an inadequate scoring of inhibition: the excess activity of PN8 or the reduced activity of PN7 (insets, Fig. 2) for example, must be explained by other types of interactions, possibly involving receptor responses to mixtures, local circuit interactions within the antennal lobes, or likely, both.

We then measured the extent of these nonlinear interactions over all the recorded PNs. The distribution of differences between estimated (simple sum) and recorded firing rate profiles during odor overlap conditions varied between 20 and 150%, with a mean of  $\sim 75\%$  (Fig. 3A; also see Experimental Procedures). PN6, PN7 and PN8 were -1.7, -0.9 and 1.55 SDs from the mean respectively (brown labels, Fig. 3A). To confirm that these differences did not result simply from intertrial variability, we computed a control distribution of differences measured between different trials of the same condition (green curve, Fig. 3A for this, we used the first 600 ms of all odor overlap conditions where delays between the onset of each pulse exceeded 600 ms (*i.e.*, cit-600ms-ger/ger-600ms-cit through cit-3.5s-ger/ger-3.5s-cit). For 71 of the 87 PNs, deviations were significantly higher during overlap conditions than in the controls (Wilcoxon signed rank test,  $p < 0.001$ ; see Experimental Procedures and Fig 3A). Large deviations between estimated (by summation) and measured rates occurred at most times during and for some time after the presentation of the second odor (Fig. 3B); they could, in some PNs, be observed as late as 3 s after the second pulse (*e.g.*, yellow and orange pixels at  $t \approx 3.5$ s in cit-100ms-ger, Fig. 3B), and even when both pulses were separated by 3s (*e.g.*,  $t \approx 4$ s in ger-3.5s-cit, Fig. 3B). In conclusion, the responses of individual PNs to overlapping stimuli can generally not be predicted accurately from the knowledge of their responses to those stimuli when presented alone.

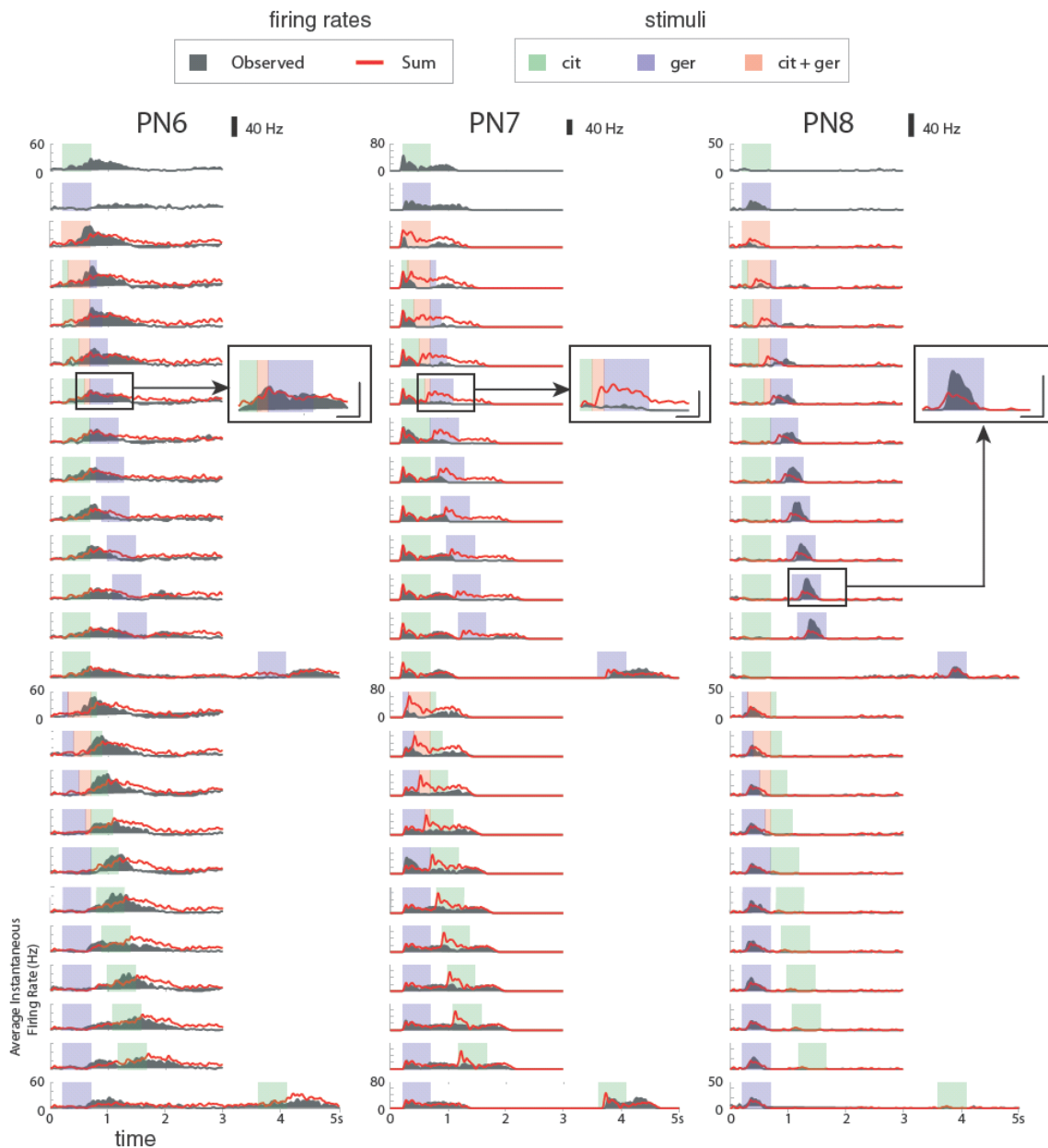


**Figure 2** Comparison of observed and expected PN responses to overlapping stimuli. The (smoothed) instantaneous firing rates (grey histogram) of three PNs (PNs 6-8) in response to all stimulus conditions are compared to those calculated by arithmetic sum (red lines) of their responses to pure odor conditions (top two rows): for this sum, the responses to the odor presented second are shifted by the corresponding delay. Stimulus conditions as defined in Fig. 1A. The computed sum matches PN6's actual response fairly well for most overlap conditions. PN7 responds less to most overlap conditions than might be expected from arithmetic sum of its responses to the pure conditions. PN8 shows unexpectedly strong responses to geraniol when it is presented with a delay after citral (see inset). These observed responses of PN8 to geraniol are significantly stronger than any arithmetic sum of the responses to either odor alone or the mixture; in the cit-900msec-ger condition, for example, the peak response to geraniol is twice as strong as when geraniol is presented by itself (inset). Calibration (inset): 200 ms; 40 spikes/s.

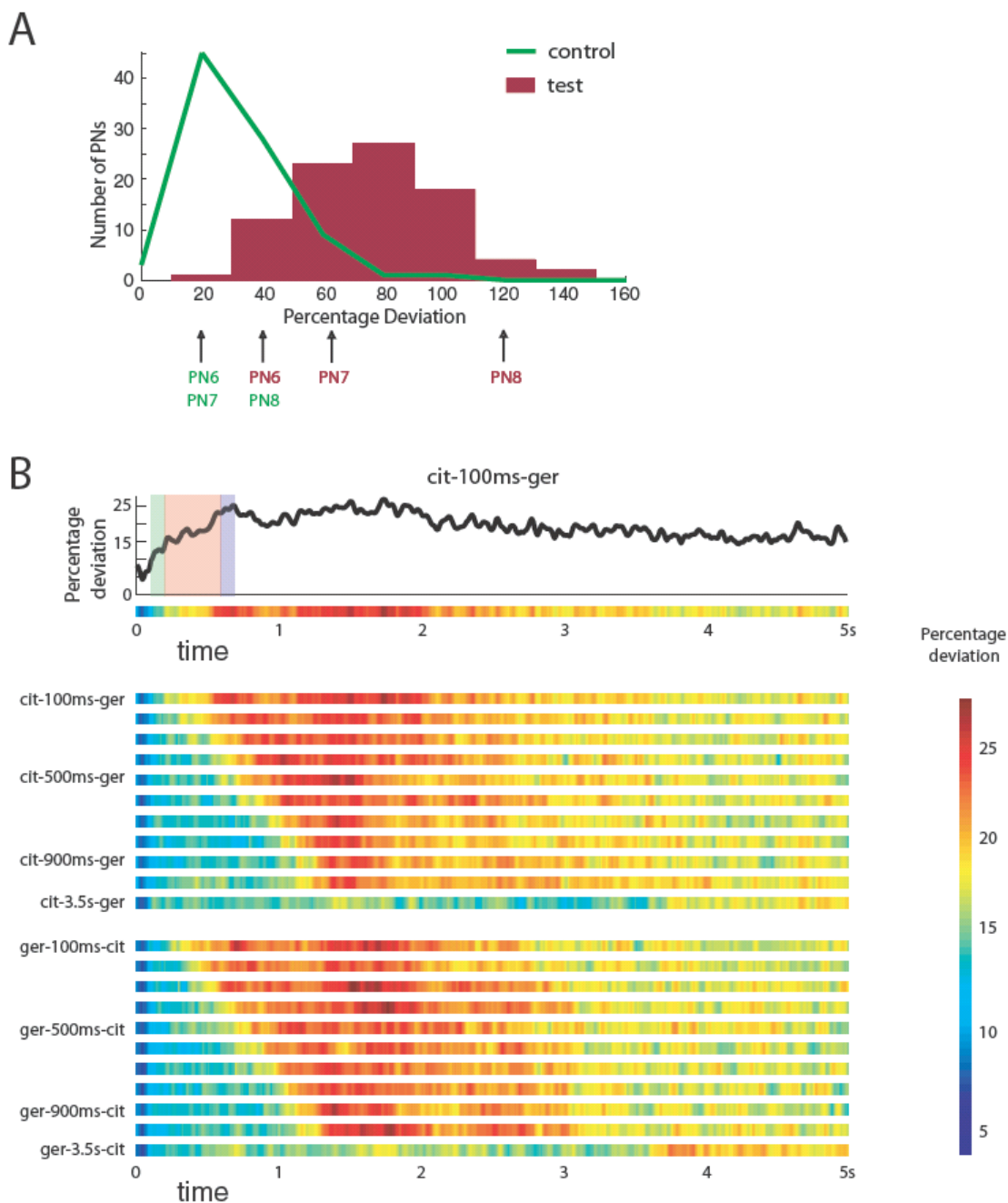


**Figure 3** Quantification of nonlinear interactions during overlapping stimuli. Quantitative analysis of the deviations between observed PN responses and responses calculated by time-delayed arithmetic summation, as shown for three examples in Fig. 2. **A:** Bar plot (test) shows the distribution of deviations (in %) of calculated from observed firing rates (see Experimental Procedures for details) for all 87 recorded PNs (mean = 75%, SD = 22%). The green curve shows the control distribution of deviations expected simply from intertrial variability (mean = 31%, SD = 17%); again, this distribution is calculated for all PNs, using response periods 0-600 msec in conditions with delay  $\geq 600$  ms between pulse onsets; that is, all analyzed raster periods contain only responses to the first odor, and variance is due only to intertrial variability. The test and control

distributions are significantly different (see text). Brown and green labels (arrows) indicate deviation ranges for PNs 6, 7 and 8 for overlap (test) and non-overlap (control) times respectively. **B**: Mean (over all PNs) deviation (in %) for each overlap condition plotted for each time bin (see Experimental Procedures). Each colored bar (bottom) is coded as shown in top panel for the cit-100ms-ger condition, using the color look-up table at right. Times of high deviation from summation-based estimates begin with the presentation of the second odor. Non-zero differences are seen even in the 3.5s-delay conditions, indicating that, in some PNs at least, responses are affected by history going back as far as 3 seconds.

### **PN Population Responses to Overlapping Odor Pulses**

The firing rates of each PN were measured in 50ms bins aligned to the beginning of the trial. We analyzed stimulus representations as time series of PN population vectors (87 PNs, 50-ms resolution, 30-s trials, 15 trials per condition, see schematic in Fig. 4A), as applied previously in a study of the encoding and decoding of odor concentrations (Stopfer et al., 2003).

Figure 4B provides a pictorial representation of this population activity, using Locally Linear Embedding (LLE) (Roweis and Saul, 2000), a nonlinear dimensionality reduction technique well-suited to this kind of data (see Experimental Procedures) (Stopfer et al., 2003). These plots should be read as qualitative indices of PN population states; quantitative analyses, carried out in the original 87-dimensional space, will be shown later. Figure 4B plots the trajectories corresponding to citral (green) and geraniol (cyan), calculated using Euclidian distances in 87-D space and embedded in the space defined by the first 3 LLE dimensions. Baseline (B) represents the state of the population prior to each stimulus (30s interpulse interval). Figures 4C and 4D overlay the trajectories corresponding to three simple stimulus conditions (citral: green; geraniol: cyan; static mixture of the two: red) and one sequence condition (shown in black, different in each panel). In Fig. 4C, citral was presented first; in Fig. 4D, the order was reversed (LLE plots for all stimulus conditions are shown in Figures S3 and S4).

First, we observed that turning on one odor while a pulse with the other odor was already on caused a deviation of the PN trajectory away from that corresponding to the odor presented first. The earlier the second-odor pulse, the earlier the deviation. This is consistent with our earlier observation of masking interactions in single PNs (Figs. 1-3).



each one. The trajectory is then constructed by linking consecutive 87-D vectors (here shown for PNs 1 and 2 only). To visualize 87-D vectors in 3-D, Locally Linear Embedding, a dimensionality reduction technique (see text and Experimental Procedures) is used and vectors are embedded in the space defined by the first three LLE dimensions (B-D). **B**: Three-trial averages (SDs shown at  $t = 0.3s, 0.6s, 0.9s$ ) of trajectories evoked by citral (green) and geraniol (cyan) as analyzed over 87 PNs and plotted in the space of LLE1-3. The two odors evoke different trajectories. The resting state of the PN population at baseline is indicated as B. Arrows indicate direction of motion. **C-D**: Trajectories evoked by overlapping or sequential stimulus pulses (black), superimposed on those corresponding to the single-odor (green, cyan) and static mixture (red) stimuli. Stimuli are shown above each plot; **C**: citral before geraniol; **D**: geraniol before citral. When switching from the first odor to the next, the PN system does not reset (return to baseline); instead, it jumps to a later part of the second odor's response. Ensemble responses to the second odor can be very different based on the overlap conditions (compare ger-100ms-cit sequence with ger-500ms-cit and ger-900ms-cit sequences). Points (3-trial averages) for the overlap sequences were taken from time slices starting at onset of the first pulse and ending 1 second after the end of the second. Correlations between 87-PN (single-time-slice) vectors for these conditions are shown in Figures S1 and S2. For plot of embedded points from which trajectories are traced, see Fig. S9. For LLE plots of all stimulus-overlap conditions, see Figs S3 and S4. For LLE plots of overlap conditions with a different odor pair, see Fig. S8.

The trajectory corresponding to a sequence started like that for the first odor and then moved directly towards the second. The sequence trajectory rejoined the second-odor trajectory in segments corresponding to late phases of the second-odor trajectory as if the second odor had been presented alone.

This result suggests that, at least for epochs corresponding to the slow return to baseline after odor offset, the same PN population states can be reached through different paths or past histories. The cit-500ms-ger trajectory (Fig. 4C, center) provides another illustration of this general observation, as the black and blue trajectories converge at  $t \approx 0.9$  s (for correlation plot, see Fig. S1).

Figure 5 plots the trajectories corresponding to most sequence conditions tested (ten interpulse delays). For clarity, we plotted separately the segments corresponding to (i) divergence (Fig. 5A,C)—when a trajectory moves away from that corresponding to the odor presented first—, (ii) convergence (Fig. 5B,D)—when a trajectory joins that corresponding to the odor presented last—and (iii) transit (Fig. 5E,F)—times at which the trajectory is in between the first- and second-odor trajectories. The plots in Figs. 5A,C show, not surprisingly, that divergence occurred sooner as the second odor was introduced

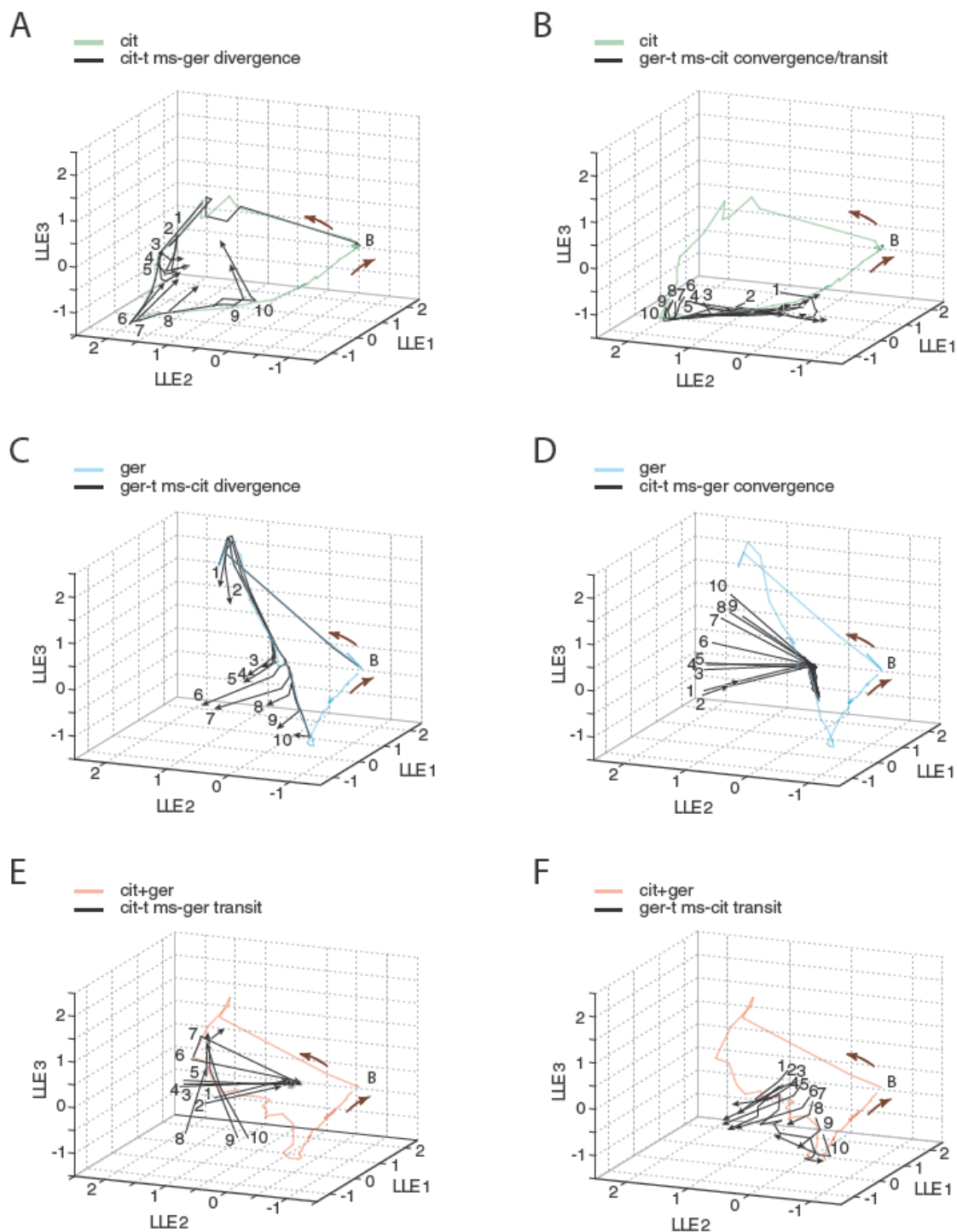


**Figure 5** Divergence, convergence, and transit paths for trajectories corresponding to overlap conditions. **A:** Trajectories for cit-t ms-ger conditions (cit-100ms-ger to cit-1000ms-ger, 100ms steps, numbered 1 to 10) are shown in black from first odor pulse onset until 50ms after divergence from pure citral trajectory. Trajectories diverge away from citral trajectory at later and later points along the pure citral trajectory as interval between citral- and geraniol-pulse onsets increases. Pure citral trajectory shown in green. Direction of motion indicated by arrowheads; B: baseline. **B:** Approach/convergence onto citral orbit of trajectories for ger-t ms-cit conditions (ger-100ms-cit to

ger-1000ms-cit, 100ms steps, numbered 1 to 10, black) from 50ms before convergence until end of second odor pulse. Trajectories approach the pure citral trajectory within a relatively confined region, with limited sensitivity to the preceding overlap duration; for delays  $\geq 600$  ms, they then follow the pure citral trajectory back to baseline. **C**: Diverging trajectories as described in A for overlap conditions ger-tms-cit. **D**: Converging trajectories as described in B for overlap conditions cit-tms-ger. **E**: Segments of trajectories in transit periods: Trajectories for cit-tms-ger conditions (cit-100ms-ger to cit-1000ms-ger, numbered 1 to 10, black) are shown from 50ms after divergence from citral trajectory until 50ms prior to convergence onto pure geraniol trajectory. Contrary to expectations, most trajectories do not follow the mixture trajectory (red) while transiting between the trajectories corresponding to the two single odors. **F**: Transit trajectories as described in E for overlap conditions ger-tms-cit. See also Fig. 6 and Figs. S1, S2.

earlier, and generally, as soon as the second odor has been introduced. Convergence, however, occurred over a narrower range within a trajectory, limited to the return path for the odor presented second (Fig. 5B,D). The transit plots (Fig. 5E,F) suggest that, contrary to initial expectations, most trajectories during overlap did not retrace the mixture trajectory. This was confirmed by odor classification measures done on the PN vectors (below and Fig. 6).

### **Odor Classification**

This population vector analysis proved useful as a potential predictor of Kenyon cell responses. If our present understanding of PN activity decoding by Kenyon cells is correct (Perez-Orive et al., 2002; Stopfer et al., 2003; Mazor and Laurent, 2005), the orbits traced by the PN populations should define a variety of KC response conditions.

For example, if the PN trajectories corresponding to an odor sequence move far away from the trajectories corresponding to either odor alone or to their mixture, we predict that some Kenyon cells should respond only to such sequence conditions, and at particular times corresponding to the structure of these trajectories. This hypothesis will be tested below. To identify these conditions, however, we needed to quantify the qualitative impression generated by LLE in Figs. 4,5. Thus, we examined the PN population in the original 87-D space (using the same time bins and durations), one trial at a time, using multiple-discriminant-analysis (Fig. 6), a technique similar to multivariate analysis of variance (Duda et al., 2000). Our goal was to classify all the trajectories corresponding to overlapping stimuli on the basis of their similarity to the three single-stimulus trajectories

(citral alone, geraniol alone, citral + geraniol). This classification was done piecewise (time bin by time bin), against sixteen templates taken from the single-stimulus conditions (baseline + 3 odors x 5 time bins; Fig 6A, see Experimental Procedures). 87-PN vectors from these sixteen conditions were used to calculate discriminant functions that were subsequently applied to all other PN vectors. For any test trial each PN vector measured at time  $t$  was transformed and then classified on the basis of its similarity to the sixteen templates. Figure 6A plots the results of this classification. We note that, using such measures, very good reconstructions of stimulus histories could be made purely on the basis of the PN population activity. For example, for cit-100ms-ger (fourth row, Fig. 6A) the initial PN vectors were classified as cit-early and cit-mid, the later ones as mix-early, ger-mid, mix-late again, and finally as ger-late (dark blue).

Our approach created linear decoders that maximally separate each of the training template groups, and then applied the decoders to all other PN vectors. By design, the transformed test vectors were classified as “most similar” to one of the templates, although similarly classified vectors probably lay at a range of distances from their templates. To quantify this, we measured the Euclidean distances between each test vector and the template vector to which it had been assigned (Fig. 6B). Those distances were then normalized by the mean intra-cluster distance of the closest training template (Fig. 6B).

We note that, across all conditions, some time bins correspond to vectors that, although often correctly classified, were nevertheless quite different from their template: the darkest pixels represent vectors that are more than twice the average intra-cluster distance from their closest templates. The dark bands they form (Fig. 6B) identify the epochs during which the test trajectories (overlapping conditions) diverged the furthest from the templates. The twenty-five conditions in Figure 6B have been collapsed, offset by the delay to the second odor onset, and averaged over all trials/conditions in Figure 6C, revealing several epochs (horizontal bars) and stimulus conditions when deviations were greatest (see also correlation plots in Fig. S2). Given the degree of PN synchrony measured under these stimulus conditions (Figure S5), we most expected to find Kenyon cell responses specific to overlaps at those times. This hypothesis was tested next.

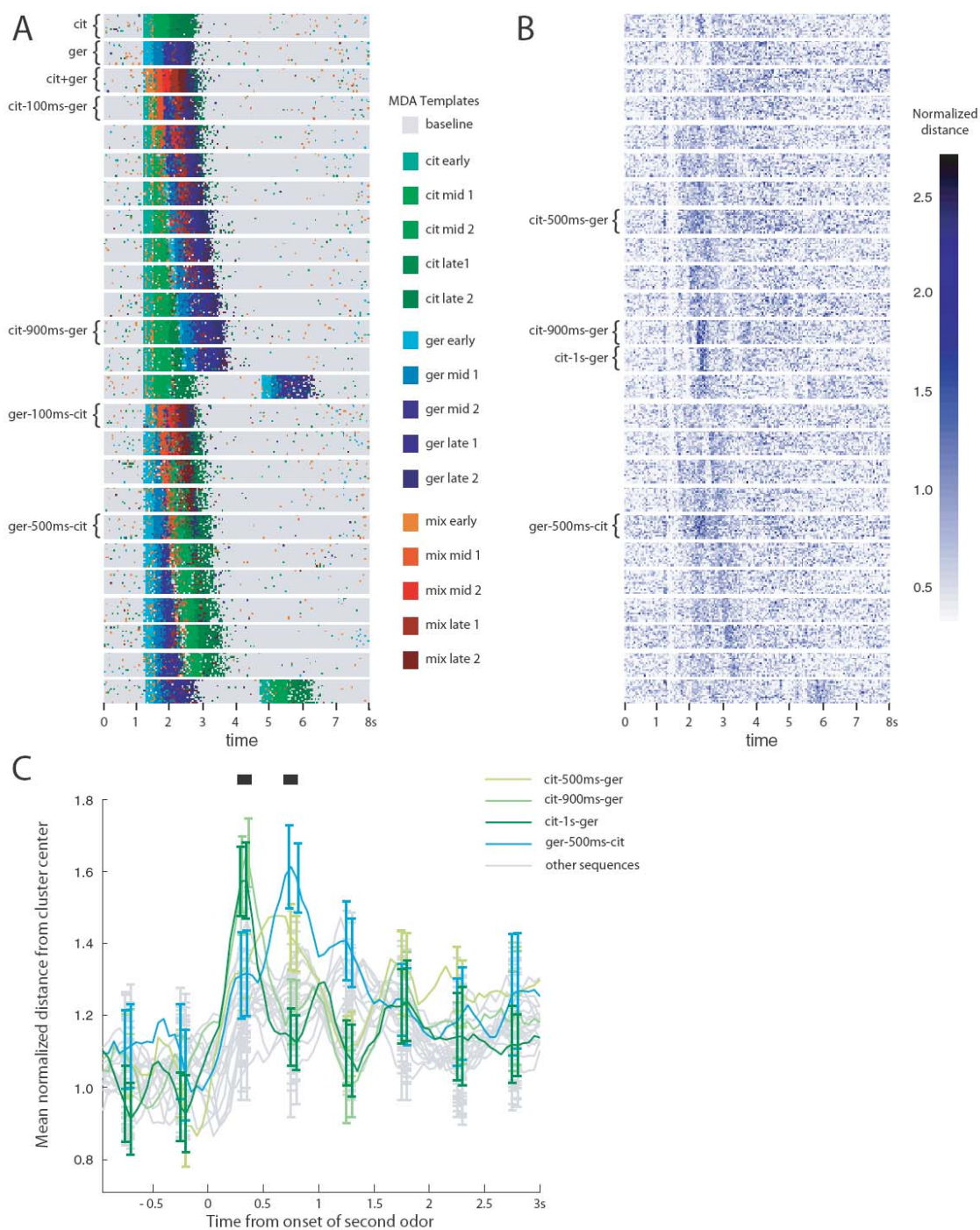


**Figure 6** Prediction of stimulus based on MDA and Euclidean-distance-based classification of PN vectors. **A:** Sixteen groups of 50ms, 87-PN vectors were chosen as templates for baseline (one group) and for the simple odor conditions (five groups for each of citral, geraniol and static mixture conditions, each of the five groups corresponding to a different epoch of the response). Template time bins were chosen based on correlation widths over the course of the responses (see Figure S1 and Experimental Procedures). These 87-D vectors were used for MDA and the 15 discriminant functions calculated (all significant; MANOVA: Wilk's Lambda = 0.0063;  $F = 1.6124 \cdot 10^3$ ) were used on all time slices. The reduced-dimensional time slices for all sequences were then classified

as belonging to one of the clusters defined by the pure condition templates (colors representing the clusters shown at right) using Euclidean distance from cluster centers. **B**: Distance from cluster centers for all time slices normalized by intra-template-cluster distances. Bands of time slices that are distant from their centers (darker blue) occur mainly during times of odor overlap (see, for example, the 4 labeled overlap sequences). **C**: Running 5-time-point averages of mean distances for all overlap conditions (vertical lines at selected vertices indicate S.D.) aligned to the onset of the second odor pulse ( $t = 0$ ). Conditions that feature time slices furthest from the centers of their assigned clusters are shown in color.

### **Kenyon Cell Responses to Simple and Overlapping Stimulus Conditions**

Our results on PN population behavior during overlapping odor stimuli (above) lead to specific predictions about KC responses. If each KC acts as a piecewise classifier of PN patterns (once per oscillation cycle, as PN activity proceeds along its trajectory), deviations of a PN trajectory from a path that normally generates a time-specific response in a KC should suppress that response (masking). Conversely, deviations of a trajectory to new regions of PN phase space (as observed with most overlap conditions, and with three in particular; see Fig. 6C) should generate responses in some KCs that are normally silent when odors are presented separately or as mixtures.

We examined the responses of 203 KCs, recorded over 24 experiments (see Experimental Procedures), using odors, delivery apparatus, and pulse protocols identical to those used with PNs (Fig. 1A). While most PNs exhibit a substantial change in firing rate when challenged with an odor, KCs do not (Perez-Orive et al., 2002). To qualify as “responding”, a KC had to pass the following criteria: respond with a minimum of one spike during the odor presentation or within 500 ms after the odor presentation in at least 5/10 trials excluding the first trial (Stopfer and Laurent, 1999). KCs whose basal firing rate did not remain constant throughout the duration of the experiment were excluded. These criteria are identical to ones used previously to classify KC responses to odors (Perez-Orive et al., 2002). Several response windows were examined, all yielding similar results. (Note: KCs 1-5 in Fig. 7 were classified as responding. KC6, typical of the great majority, was classified as not responding.)

From the 203 KCs recorded, we found 10 that responded only to geraniol, 4 that responded only to citral, 9 that responded equally to both odors. (Note: KC recording sites were

selected on the basis of there being detectable activity upon presentation of these odors. Therefore, these response probabilities are biased towards high values, by experimental design.) We also found 9 KCs that responded specifically to the static binary mixture of the two odors, and 21 that responded both to the static binary mixture and to one of the odors presented by itself. A large fraction of the remaining KCs either did not respond to any odor condition (N=83) or did not respond in a consistent way to either a pure odor or a specific odor pattern. (See Table S1 for a summary of all KC types observed. For KC group selection criteria see Experimental Procedures.)

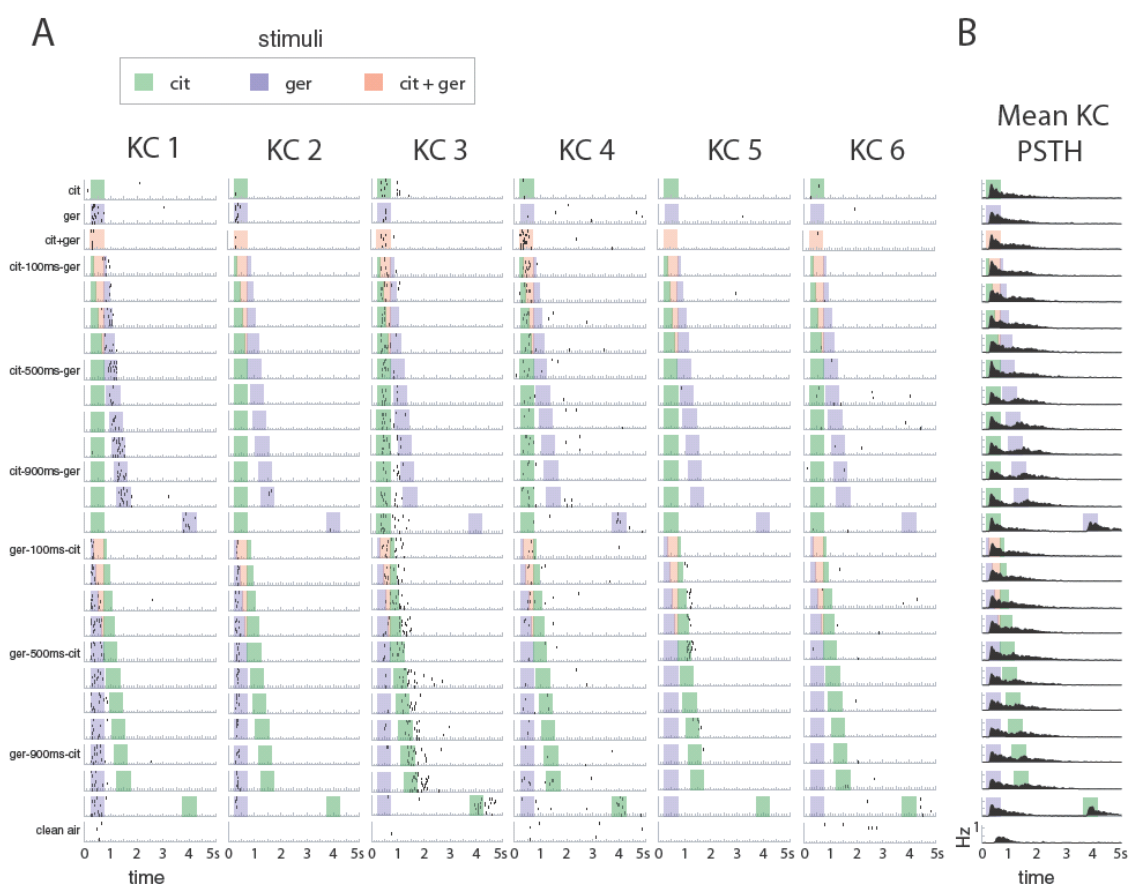


**Figure 7.** KC responses to overlapping stimuli **A:** Representative KCs displaying odor- and condition- specific responses (see text for details of distribution of responses). Raster plots of 6 in vivo tetrode recordings from odor-responsive KCs. KCs shown were not recorded simultaneously. Shaded areas correspond to pure and mixed odors indicated in legend as described in Fig. 1A. Ten consecutive trials per odor condition. Condition order was randomized within a given experiment. **B:** Mean PSTH for all 203 KCs that satisfied inclusion criteria. Plot shows strong response to first odor pulse (all odor conditions), masking of response to second odor and recovery from masking as interpulse interval increases.

KCs that responded specifically to one odor frequently showed masking when the second odor pulse overlapped with the first. This was seen in 54% of single-odor-specific KCs, and is shown for two KCs (KC1 and KC2) in Figure 7A: both were activated by geraniol alone, but this response was suppressed if citral presentations overlapped with or preceded geraniol.

Masking was observed independently of odor pulse order for the odors tested, but one pulse order could have more pronounced effects than the other. KC3 showed a similar (though less pronounced) suppression of its response to citral by the addition of geraniol. KC4 was the counterpart of the preceding three: this KC responded best to the static mixture conditions and responded less and less as the overlap between the two odors was reduced. This was observed in 56% of the KCs selective for the static binary mixture. KC5 (representing 3.5% of KCs) belongs to the most interesting category of KCs encountered in these experiments. KC5 remained silent over most stimulation conditions, except when a citral pulse followed a geraniol pulse onset with some non-zero delay. The most reliable responses occurred for the ger-500ms-cit condition (Fig. 7A). Over all the 203 KCs analyzed, we found 7 KCs with such specific responses, each corresponding to a particular region of PN phase space visited only in specific overlap conditions. Of these 7, 2 responded in the conditions and epochs identified by our PN distance measures (Fig. 6C) and all but one responded in the epochs corresponding to peak distances. Note that such KCs were not looked for at the time of the experiment and all were subsequently confirmed to remain stable throughout the course of the recording (see, for example, Figure S6). Recording sites were chosen simply on the basis of there being some tetrode activity in response to cit, ger, or cit+ger. This explains the numerical bias toward KCs that responded to these particular odor conditions. KCs such as KC5 were discovered upon analyzing the data and their paucity is consistent with the finding that odor representation by KCs is very sparse (Perez-Orive et al., 2004). KC6 was typical of the largest fraction of recorded KCs (41%) and did not respond to any of the stimulus conditions we offered during these experiments. Other examples of KC responses are described in supplementary information (Table S1).

Average KC responses are shown in the mean KC peri-stimulus time histogram (PSTH) in Figure 7B. Most KCs fired in the early part of the response period, as reported previously (Stopfer et al., 2003; Mazor and Laurent, 2005). In overlap conditions, PN ensemble trajectories did not retrace the early path corresponding to the pure responses to the odor that was presented second. Hence, we predicted that KCs with early responses to either odor presented alone—the majority in our sample—would have reduced response probabilities when that odor was presented second. Indeed, peaks in the KC PSTHs corresponding to the second odor were smaller than those corresponding to the first in overlap conditions. Of the 6.5% of KCs that responded specifically to a pure odor, 43% did not fire when their odor came second. Also, for the 4.5% of KCs with responses to both odors (cit+ger), 22% did not fire during the second odor presentation. As the interpulse interval increased, KC responses recovered.

### **Correlations between KC responses and PN population output**

We now examine the correspondence between KC firing and PN trajectories, focusing on the examples of KCs 2 and 5 (Fig 7A). KC2 responded best to the pure geraniol stimulus. The stretch of time over which KC2 produced action potentials (under this condition) is indicated on the geraniol trajectory (magenta, Fig. 8Ai). If citral was superimposed on geraniol with a 100-ms-delay between the two pulse onsets, KC2 responses were reduced (Fig. 8Aii). Under this stimulus condition, the PN trajectory (black) was indeed seen to diverge away from the pure-geraniol trajectory (cyan) about half-way through its KC2-response range (Fig. 8Aii). When stimulus order was reversed, the PN trajectory never approached the region corresponding to KC2 responses (Fig. 8Aiii); correspondingly, KC2 never produced an action potential. These results are consistent with the general model that, to each KC, corresponds a (relatively) small volume of PN state space (defined by PN-KC connectivity); if a stimulus drives the PN population vector through this volume, the KC will fire; if a stimulus condition deviates the PN trajectory from this volume, the KC response will be masked (partially, as in Fig. 8Aii, or totally, as in Fig. 8Aiii), by an amount depending on the extent and timing of the deviation.

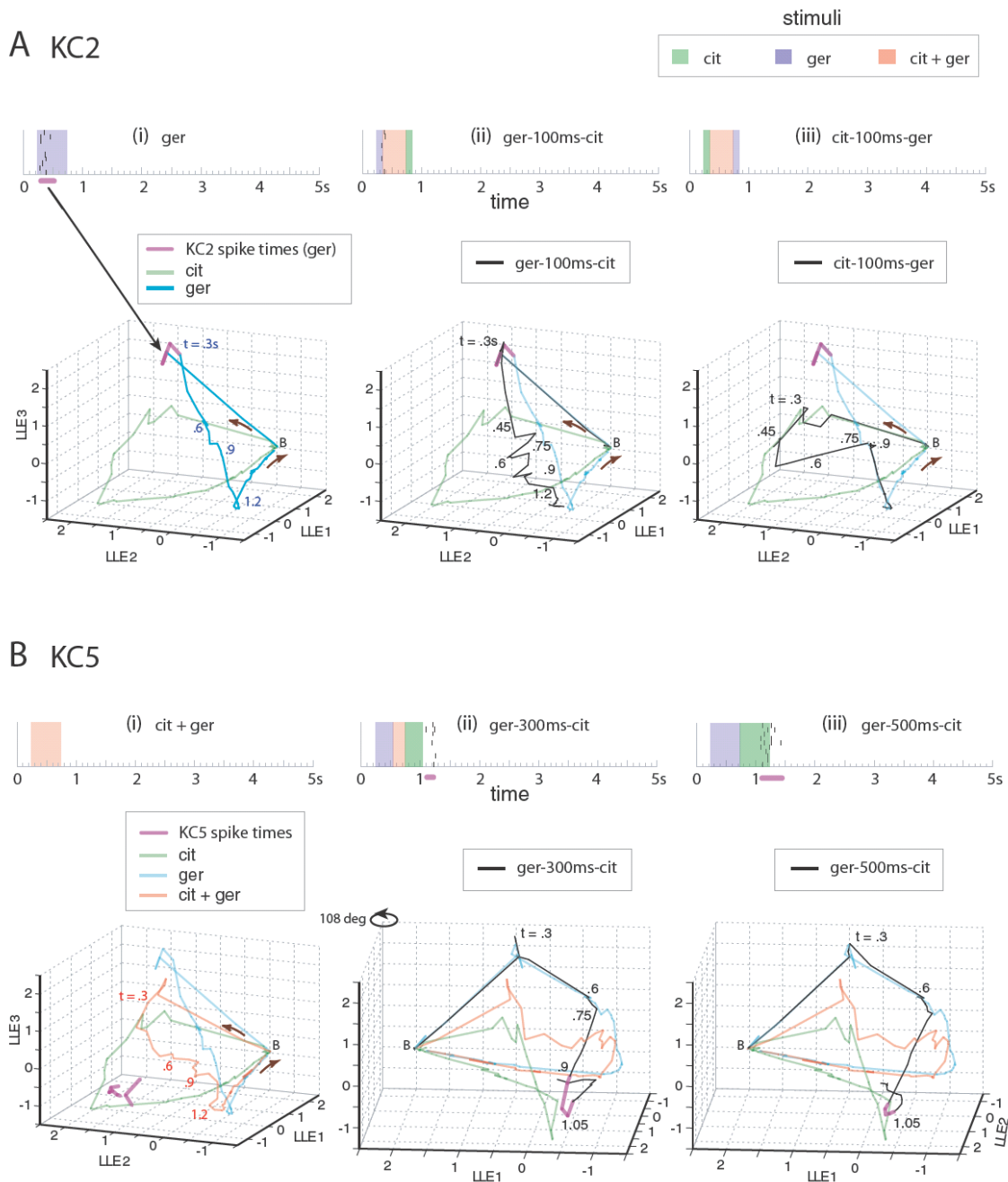


**Figure 8** Correspondence between KC responses and PN trajectories **A**: Spread of KC2 (Fig 7A) spike times in response to geraniol (raster at top) overlaid (magenta) on PN ensemble responses as represented by LLE (bottom, as in Fig. 4). PN ensemble responses are shown for the pure conditions (green, cyan) as well as two overlap conditions (black): (i) geraniol, to which KC2 responds; (ii) ger-100ms-cit, during which the response of KC2 is partly masked; (iii) cit-100ms-ger, during which the response to geraniol is completely masked. The firing times and strengths of KC5 are well matched to the instantaneous state of the PN trajectory. **B**: Spread of KC5 (Fig. 7A) spike times (magenta) in response to the ger-300ms-cit (ii) and ger-500ms-cit (iii) conditions, overlaid on PN trajectories plotted for corresponding overlap (black) and pure (green, cyan, red) conditions. (i) KC5 does not respond to any pure condition. (ii, iii) KC5 responds during a particular period of these overlap conditions, when the PN ensemble trajectories are distant from the

pure-odor conditions and traverse particular regions of PN phase space (shown quantitatively in Fig. 6C). For clarity, axes in ii and iii have been rotated relative to plot in i as indicated in ii.

KC5 illustrates a different case. This neuron never fired in response to citral, geraniol, or the binary mixture of the two (Fig 7A). The (known) regions of PN phase space corresponding to KC5 spiking are shown in Fig. 8Bi (magenta): consistent with this, none of the PN trajectories corresponding to the three simple-odor conditions crossed this volume (the intersection of the magenta and green segments is a 2-d projection artifact; see rotated projections in ii, and correlation plots in Fig. S2). When the stimulus consisted of ger-300ms-cit or ger-500ms-cit, by contrast, the corresponding trajectories moved into the appropriate volume and generated a response in KC5 (Figs. 8bii,iii). Indeed, it is only by systematically varying stimulus conditions that this particular set of delays was found and used to map KC5's response range in PN phase space. From these observations, we conclude that KCs can recognize particular "instantaneous" states of the PN population activity, consistent with the hypothesis that KCs act as piecewise classifiers of PN activity patterns.

## **Discussion**

Our odor stimuli included two single odors, one odor-mixture and multiple pulse-overlap and consecutive-pulse conditions: odor-mixture describes a condition in which both odors were pulsed together from stimulus beginning to end. In all cases, single pulses were 500 ms long. Pulse-overlap describes conditions in which one odor pulse was started before the other odor pulse had ended; during some time, therefore, both odors were present together. We also used consecutive-pulse conditions with intervals up to 3.5s. The rationale for these consecutive pulses is that PN population activity generally outlasts the stimulus that caused it (Laurent et al., 1996); with interpulse delays of up to 3s, overlaps between the responses of the PN population could indeed be seen, even though the stimulus pulses themselves did not overlap. With interpulse intervals greater than 3.5 s, the effects of the two consecutive pulses on PN responses were nearly independent. In other words, consecutive-pulse conditions with intervals between 0 and 3s generated what we will call overlapping responses.

We recorded the responses of eighty-seven PNs (recorded in groups of 8 to 25) to twenty-five odor stimulus conditions (single, mixed, overlapping and consecutive). We examined the responses of the PNs to these stimuli one PN at a time, and analyzed the 87-PN response dataset as time-series of instantaneous vectors of activity across all 87 PNs, as previously described for simpler stimulus conditions (Stopfer et al., 2003; Mazor and Laurent, 2005). This group of 87 PNs represents over 10% of the entire PN population in the locust. PN sampling was broad, in that our tetrodes covered, over all experiments, most regions of the antennal lobe. Our results add to previous results on identity and concentration coding (Stopfer et al., 2003) and single odor pulses (Brown et al., 2005), and suggest that spatio-temporal patterns of PN activity also depend, in ways that we did not predict, on the history of stimulation.

Generally speaking, odor-evoked spatio-temporal patterns of PN activity can be pictured as sequences of instantaneous PN vectors, or trajectories, in PN phase space (see below). We updated each PN vector every 50 ms, a duration corresponding to the average period of the 20-Hz odor-evoked oscillations in this system (Laurent and Naraghi, 1994; Wehr and Laurent, 1996). The relevance of this time scale in locust is determined by the integrative properties of Kenyon cells, the PNs' targets in the mushroom bodies (Laurent and Naraghi, 1994; Perez-Orive et al., 2002). We determined previously that, upon stimulation with a single odor, PN vectors leave a noisy baseline state, defined by uncorrelated, 2-4 spikes/s baseline firing (Perez-Orive et al., 2002; Mazor and Laurent, 2005). Following termination of stimulation, the trajectories return to baseline over several hundreds of milliseconds (Stopfer et al., 2003; Mazor and Laurent, 2005). During stimulation, the trajectories evolve in a stimulus-dependent manner, at a velocity that is highest at onset and decreases monotonically to 0 (thus defining a fixed point) if the stimulus is sustained for 1.5 s or more (Mazor and Laurent, 2005). When the odor pulse is turned off, velocity increases again and progressively returns to 0 as the system relaxes back to baseline in a few hundred ms (Mazor and Laurent, 2005). For 0.5 s long stimuli (as used here) the system never reaches fixed points: the odor-evoked PN patterns we analyzed in this study can thus be described as loops, consisting of one segment (on-transient) away from baseline and a second (off-transient) corresponding to the return to baseline (Stopfer et al., 2003; Mazor

and Laurent, 2005). A recent study examined PN and KC odor representations for a single odor presented in successive 100 ms pulses at different frequencies and suggested that information about individual odors (as measured by classification performance) was not significantly affected by pulse frequency and preceding temporal pattern (Brown et al., 2005). In the present experiments, we examined how odor representations by PNs and by KCs change as different odors coincide within a 3.5 second window.

### **Temporal and spatial scales of analysis**

Our interpretation of high-dimensional, instantaneous PN vectors as a functionally-relevant scale of representation rests on the assumption that the decoding of PN activity by KCs—their targets in the mushroom bodies—follows similar rules: that is, that individual KCs fire or do not fire on the basis of an interpretation of high-dimensional, instantaneous PN vectors of activity. Recent observations from this laboratory indicate that individual KCs sample 50% of all PNs on average (Jortner et al., 2007), and that each oscillation cycle contains spikes from 80-240 PNs over the entire PN population (Mazor and Laurent, 2005). The dimensionality of PN vectors analyzed here (87) is thus less than that of those experienced and decoded by individual KCs (~400); yet, our interpretation of those 87-D vectors and of the trajectories they define is in good agreement with the KC responses we observed. This supports our assumption that interpreting PN population vectors and trajectories, as done here, approximates the decoding conditions for KCs reasonably well. For example, a consistent effect of overlapping odor stimuli was a masking (sometimes complete) of the responses of KCs activated by either odor alone: this observation is in excellent agreement with our synthetic interpretation of PN trajectories. While this result may begin to explain the “binding” nature of odor perception or recognition (Jinks and Laing, 1999), more exhaustive experiments must now be carried out using more complex mixture conditions. This is particularly important because natural odors often contain tens to hundreds of volatile components.

### **Importance of Stimulation History**

We hypothesized that the stimulation of a PN population already activated by one odor with a second odor (odor overlap) might either cause a transient reset of the system—

transient return to baseline followed by the development of the trajectory corresponding to the second odor—or alternatively, cause the first trajectory to deviate from its on-going course to the path corresponding to the mixture of the two odors. Our results rule out the first hypothesis and support the second, with notable differences. When the PN vectors evoked during an overlap condition were compared to those caused by either odor alone or by their binary mixture, distances to the mixture vectors were nearly always shorter. When we measured these distances in absolute terms, however, we observed that they were often large (i.e., that matches with the mixture response were poor). These measures of interPN-vector distances were consistent with the responses of KCs (the PN decoders) to the same stimuli: Kenyon cells that responded to a mixture stimulus did not always respond to an overlap condition, even though the stimuli were, for some time, instantaneously similar; conversely, some KCs responded transiently to a particular overlap condition and yet, did not respond when the two odors were presented as a mixture. These transient-overlap KC responses occurred at times and conditions when the PN-vectors corresponding to the overlap deviated from those corresponding to the mixture (see Experimental Procedures) and when there was significant PN synchrony. To make detailed predictions on overlap-specific KC responses, we will probably need to sample from a greater fraction of the PN population, and better understand the mapping between distances in PN phase space and KC firing probability. Nonetheless, both measures (inter PN-vector distances and KC responses) clearly indicate that odor overlaps cause antennal lobe patterns related to, but not identical to those caused by binary mixture conditions; KCs could thus, by this specificity, encode some aspect of the history of stimulation. Because some overlap conditions create such unique responses—as seen both in the PN population and in single KCs—we predict that these overlaps could also be memorized and/or perceived as different from either odor alone or from their binary mixture. The specificity of these representations may extend to mixtures of particular ratios of these odors. This remains to be tested behaviorally.

Our results may also shed some light on interesting behavioral experiments on odor discrimination with mixtures. Jessica Hopfield and Alan Gelperin examined the ability of the terrestrial mollusk *Limax* to segment a binary odor mixture when classical conditioning

had been done in either of two conditions (Hopfield and Gelperin, 1989): in the first, an *AB* odor mixture was paired with an aversive unconditioned stimulus (US), and animals were later tested with *AB* and either odor (*A* or *B*) alone. In the second, the freely behaving animals were trained in conditions where odors *A* and *B* were located on alternating strips; in this condition, the US could, in principle, be associated by the animal with either odor alone, or with the representation of some (undefined) mixture of them. Again, the animals were tested some time later with odors *A*, *B* and *AB*. With the first training condition, Hopfield and Gelperin (1989) observed that the conditioned response (aversion) was specific to the mixture: the animals failed to show aversion to the mixture components alone. This is consistent with our physiological results: the representation of a binary mixture (assessed as a family of PN vectors) differs from those of the components, and the sets of KCs that responds to a mixture and to its components are not the same. With the second training condition, the behavioral results were different: the animals avoided the mixture but also its components. Assuming that Hopfield and Gelperin's (1989) training paradigm contained stimulus conditions similar to those we used in our study (i.e., periods of partial overlap between the two stimuli or between the responses to these stimuli), these behavioral results are again consistent with our observations: in conditions of stimulus (or response) overlap, some fragments of the PN responses (and correspondingly, the KCs that fire) match those evoked by each odor component alone and sometimes, those evoked by the mixture. What these behavioral experiments do not address, however, is whether conditioned aversion was expressed also towards stimuli that were neither a component, nor the binary mixture, but some particular overlapping sequence of the two components (as we would predict from the physiological results on PNs and KCs). As we indicated above, this remains to be tested.

### **Mechanistic and Functional Implications**

Our results indicate that the antennal lobe is a dynamical system whose responses to stimulation depend, to a significant extent, on initial conditions. For example, the response of the PN population to an odor was usually delayed if that odor pulse followed or overlapped with an earlier one. Also, the path followed by the PN population during an odor overlap condition depended on the precise nature (order, duration) of this overlap.

Hysteresis is well known in the motor system, where for example neuronal activity corresponding to one eye-fixation position depends on preceding saccade history (Aksay et al., 2003). In sensory systems, masking has been studied in vision (Rolls and Tovee, 1994; Macknik and Livingstone, 1998) and audition (Bartlett and Wang, 2005) and its underlying mechanisms are beginning to be understood (Sobel, 1994; Wehr and Zador, 2005).

In the antennal lobe, many mechanisms probably underlie the sensitivity to history. First, the responses of receptor neurons, to the extent that many odorant receptors are broadly tuned (Hallem et al., 2004; Wilson et al., 2004), must depend on past history of stimulation, due to the biophysics of receptor occupancy and to G-protein activation and inactivation kinetics (Kurahashi and Menini, 1997; Zufall and Leinders-Zufall, 1998; Leinders-Zufall et al., 2000). Second, antennal lobe circuits are known to undergo rapid changes under odor stimulation in an odor specific manner (Stopfer and Laurent, 1999). Modeling investigations provide hints that both excitatory and inhibitory synapses should be modulated to reproduce the observed effects (Bazhenov et al., 2005). Third, the locust antennal lobe itself is a recurrent network, with widely branched local inhibitory neurons causing rhythmic negative feedback (MacLeod and Laurent, 1996) as well as slow inhibitory patterning (Laurent et al., 1996). How randomly connected recurrent networks might process time-varying continuous input is the subject of recent theoretical work on “liquid state machines” (Maass et al., 2002). It was suggested that, to perform complex computations on time-varying input, such networks need to operate at the edge of dynamical regimes where behavior becomes chaotic (Bertschinger and Natschlager, 2004). Building on this work, Latham and colleagues have recently investigated the response trajectories of such networks when placed under different initial conditions (Maei and Latham, 2004), but driven by the same input for some time—a situation very similar to our experiments. They examined three cases: convergence, divergence, and neutral. Convergence, after a delay, matches our experimental results for most overlaps and pulse conditions. Divergence is a behavior we did not observe. The ger-100ms-cit condition came closest to what Maei and Latham (2004) call a neutral condition which allows the network to remember input history but is, according to that study, difficult to sustain beyond the time constants of neurons in the network. In a different theoretical study,

Knusel et al. found that, for information encoded over time to be reliably decoded, a reset of the network was desirable (Knusel et al., 2004). This does not match our experimental observations (trajectories moved from one pure condition's trajectory to a later part of the next without going through baseline). While this may place theoretical limits on how much information about an input pattern can be reliably decoded, it may equally indicate that antennal lobe circuits are designed to identify instantaneous odor conditions reliably, rather than recognize particular temporal patterns of odor input. A more complete investigation of the sensitivity of PN ensembles to different odor patterns is the subject of ongoing work (B Broome, M Niemark, M Meister & G Laurent, in prep).

### **Consequences for Natural Odor Plume Conditions**

We observed that trajectories evoked by one odor could be influenced by an earlier pulse of another odor, presented up to 3 s before. Conversely, the return paths to baseline upon the termination of related stimulus conditions (A then B, with different delays between the onsets of A and B) generally converged before (sometimes well before) reaching baseline. These observations identify the interval 0-3s as the time over which different stimuli (of 0.5 s duration) may generally interfere with one another in this system. They also indicate that the degree of interference between odor pulses decreases quite rapidly as the pulse interval increases. Only in limited conditions of close pulse overlap did the PN population response deviate significantly from what could be predicted, knowing the trajectories corresponding to either odor alone or to their binary mixture. For such conditions of close overlap, new KCs were recruited, consistent with large deviations of the PN population vectors. For conditions of limited overlap, masking of KC responses was the main effect. In nature, the distribution of such conditions would depend entirely on the statistics of interpulse intervals and on their temporal correlation. It will be interesting to examine odor learning and recognition in such increasingly complex stimulation conditions.

### **Experimental Procedures**

Two odors were presented in staggered pulses, using 12 different time delays between pulses. We recorded field potential output from olfactory receptor neurons in the antenna, extracellular multi-single-unit activity from groups of up to 25 PNs (74 PNs in pilot

experiments (Figs S7, S8), 87 PNs in reported experiments), the LFP elicited by PNs in the MB and multi-single-unit activity from groups of up to 20 KCs (203 KCs total).

### **Pilot Experiments**

A set of pilot experiments (74 PNs) was carried out first, using geraniol and hexanol as odorants. After data analysis, it appeared that, due to large differences in vapor pressure between the two odors, hexanol (at the concentration used) dominated over geraniol. This can be seen both in EAGs (Fig S7) and in the LLE plots of the odor-evoked trajectories (Fig S8): note for example that the trajectory corresponding to the static mixture matches nearly exactly that for hexanol, indicating its dominance over the array of receptors. (Despite this, the results of these pilot tests show no qualitative difference from those of the final experiments.) To correct for this undesired imbalance, we selected a different pair of odors (below), chosen for their similar vapor pressures and effectiveness on the ORN array, as assayed by EAGs (Fig S7).

### **Odorants**

For all experiments reported here, two odorants (citral and geraniol, Sigma) were diluted 1/100 in mineral oil (J.T. Baker) and stored in separate 60ml scintillation vials. This concentration is comparable to that used in prior studies. Odor vials were prepared fresh each day. The vials were arranged in parallel and 0.5 sec long puffs of desiccated and filtered air (460 ml/min) carried the headspace of each vial into an odor nozzle and then past the antenna. The odor nozzle (1cm diameter, teflon) was placed 1cm in front of the antenna and supplied a constant 900 ml/min carrier stream of desiccated, filtered air. The odors were injected into the carrier stream 6.5 cm from the output end of the odor nozzle to ensure complete mixing by the time the odors exited the tube. A large vacuum hose placed behind the antenna assured the quick removal of odorants from the space surrounding the antenna. Odor puffs were triggered automatically using a custom computer interface (LabView).

### **Electrophysiology**

Experiments were carried out on 34 male locusts (*Schistocerca americana*) raised in a crowded colony. Young adults (prior to reproductive age) were immobilized in a wax cup with their antenna exposed. The cuticle over the brain was removed, the brain was exposed, and later desheathed while the head of the animal was bathed in locust saline, as previously described (Laurent and Naraghi, 1994; Stopfer and Laurent, 1999). PN data were acquired using silicon tetrodes obtained from the Center for Neural Communication Technology (Drake et al., 1988). Our multi-single-unit extracellular recordings only detected events attributable to PNs, for LNs do not produce sodium action potentials (Laurent and Davidowitz, 1994). PNs were recorded from physically distributed areas across the AL. The number of simultaneously sampled PNs varied between 8 and 25. A recording site was chosen if at least some multi-unit activity could be recorded in response to each of the two odors and to a static mixture (coincident pulses) of the two at the beginning of each experiment. Only PNs that exceeded a set of equally applied inclusion criteria (see Experimental Procedures) were selected (n = 87 PNs, from 10 of the 34 animals). In aggregate, this group represents more than 10% of the PN population in the antennal lobe (830 PNs).

KC data were obtained using twisted wire tetrodes obtained from FHC (#CE4B75). Electrodes tips were re-plated with gold prior to each experiment. KCs were recorded in a region containing only KC somata. All KC recordings were performed using wire rather than silicon tetrodes because empirical observations indicate that they yield more and better data. Recording locations were tested randomly across the MB and selected if activity could be elicited by either pure odor or their static mixture. PN and KC spikes were sorted offline using custom designed algorithms (Pouzat et al., 2002) implemented in Igor (WaveMetrics). Clusters were selected for inclusion in the final data set based on their successful completion of several statistical tests. These included: waveform SD variation of  $<0.05$  throughout the length of the stimulus, distance between cluster centers ( $>4$  SD), low numbers ( $<2\%$ ) of spikes with  $<5$ ms interspike-intervals, no significant drop in the SD trace during the spike peak. Identical stimuli were presented at the beginning and end of the experiment to confirm that clusters did not drift significantly over the course of the experiment. Drift was measured qualitatively by determining if a given cell's responses to

pure odors at the beginning of the experiment were similar to the responses of each odor in the cit-3.5s-ger and cit-3.5s-ger trials. cit-3.5s-ger and ger-3.5s-cit were always presented near the end of an experiment.

The KC data was sorted using the first 11 conditions of the experiment (10 trials each) as the basis for the sorting model. The condition that occurs in the middle of the set was used for the noise covariance matrix. The model generated by this method was refined using criteria identical to those used on the PN data. Stability over the course of the experiment was assessed after sorting and was based on a stable baseline-firing rate over the course of the experiment.

### Data analysis

MATLAB and the Statistics Toolbox (The MathWorks, Inc.) were used for data analysis. To test whether a PN's response to an odor overlap was a simple arithmetic sum of its responses to the odors presented individually, we convolved the spikes in each trial with a 20-ms Gaussian, averaged the smoothed spike counts across trials, and subtracted mean baseline spike counts (calculated from time series preceding stimulus onset). Cessation of firing, often caused by inhibition, was represented by the negative of the mean baseline-firing rate. Having no true measure of inhibition (because we recorded extracellularly from the PNs), we considered this assumption to be the simplest one. For each PN,  $p$ , we then compared the response recorded to the overlap condition  $O1-d-O2$  (with  $t_d$  ms delay between presentations of the first and second odors),

$$recorded_{p,O1-d-O2,t} = resp_{p,O1-d-O2,t},$$

with the response to the first odor ( $resp_{p,O1,t}$ ) added to the response to the second odor shifted by the corresponding  $t_d$  ms delay ( $resp_{p,O2,t-t_d}$ ),

$$sum_{p,O1-d-O2,t} = resp_{p,O1,t} + resp_{p,O2,t-t_d}.$$

For each overlap condition,  $O1-d-O2$ , we quantified the deviation of the estimated rate ( $sum$ ) from the recorded rate ( $recorded$ ) as follows: for each PN, condition and time bin,

we calculated the absolute difference (*absdiff*) of *sum* from *recorded* as a percentage of the recorded maximum firing rate of the given PN (across all times and conditions),  $\max FR_p$ :

$$absdiff_{p,O1-d-O2,t} = \frac{|sum_{p,O1-d-O2,t} - recorded_{p,O1-d-O2,t}|}{\max FR_p} \times 100.$$

To identify PNs that showed significantly greater deviation in overlap than in non-overlap conditions, we used a Wilcoxon signed rank test. We compared *absdiffs* for time bins from 0 to 600ms after presentation of the second odor (overlap-pulse conditions: cit/ger-600ms-ger/cit up to cit/ger-1s-ger/cit) with *absdiffs* for time bins with matched delays after presentation of the first odor in the same conditions. For 71 PNs out of the 87 in our sample, the difference between the matched *absdiffs* in the two groups did not come from a distribution whose median is zero ( $p < 0.001$ ). To characterize each PN by a single number representing percentage deviation (distribution shown in Fig. 3A), we used the following procedure:

(i) we defined the percentage difference for a particular condition as:

$$conddiff_{p,O1-d-O2} = \max(absdiff_{p,O1-d-O2,t}, \quad t \in \{t_d, t_d + 1s\}).$$

The percentage deviation for a given PN was then calculated as its mean *conddiff* over all overlap conditions (and, as a control, also for all times of zero-overlap):

$$PNdiff_p = \text{mean}(conddiff_{p,O1-d-O2}, \quad d \in D), \text{ where } D \text{ is the set of all delays.}$$

(ii) We also computed mean percentage differences for each condition and time bin by simply averaging *absdiff* across all PNs. This is shown in Fig. 3B.

$$cond\_time\_diff_{O1-d-O2,t} = \text{mean}(absdiff_{p,O1-d-O2,t}, \quad p \in \{1, 87\})$$

For nonlinear dimensionality reduction with Locally Linear Embedding (Roweis and Saul, 2000), we used code from Sam Roweis (<http://www.cs.toronto.edu/~roweis/lle/>), with Gerard Sleijpen's code for the JDQR eigensolver (<http://www.math.uu.nl/people/vorst/JDQR.html>). In the figures shown for nonlinear dimensionality reduction with LLE, we used as input, 87-D time slices, each 50 ms wide and averaged over 3 trials. Fifteen trials thus generated 5 trajectories per condition. Standard deviations were calculated across these five. For a particular choice of embedding

dimension, LLE requires only one user-specified parameter (K), the number of nearest neighbors to consider in the reconstructions of individual high-dimensional points. We chose values for K such that distances to the K nearest neighbors were, for all points, small (K = 6 for all figures shown, see Fig S9). The results we obtained were qualitatively similar (distinct trajectories for the different odors and the pure mixture; odor sequences with greater delays diverging later from the first odor trajectory and converging earlier on the second) with a wide range of K values (5 to 15).

For multiple discriminant analysis, we used functions from Richard Strauss's MATLAB-based statistics library (<http://www.biol.ttu.edu/Strauss/Matlab/Matlab.htm>). Training data consisted of 16 groups of time slices from single trial responses to pure conditions (5 groups from the citral response, 5 from geraniol, 5 from the citral+geraniol mixture and 1 baseline group). 42 time slices—3 consecutive bins per trial times 14 trials—were used to represent each group. Time slice correlation analysis (Figure S1) and trial-averaged hierarchical clustering were used to guide the choice of groups so as to adequately represent different periods of the evolving population response. We used 672 time slice vectors as training data to compute 15 discriminant functions that were then used to transform the 55,328 sample data vectors. For classification, we used Euclidean distances of individual 15-D points from group centroids (means of the remaining points in a group). Classification with other metrics such as Mahalanobis distance produced similar results. Group centroids were computed using only training data, and distances were normalized by mean intra-cluster distance for training data. -

KCs were grouped into the categories shown in Table S1 based on the following criteria. Condition 1: more than half of all trials with pure odors (*i.e.*, cit, ger, or cit+ger) contain at least one spike during a response window lasting from odor onset to 500ms after odor offset. Condition 2: condition 1 is satisfied for the first odor in a consecutive-pulse trial (*i.e.* cit- $\geq$ 600ms-ger or ger- $\geq$ 600ms-cit). Cells were then classified as follows: Cit, Ger and Mix: satisfy Condition 1 for odors of this type only, and do not satisfy Condition 1 or Condition 2 for any of the other two. Cit+Ger, Cit+Mix, Ger+Mix: satisfy Condition 1 for two odors, and do not satisfy Condition 1 or Condition 2 for the third odor. Pattern-specific: satisfy

Condition 1 during overlap periods when applied to overlap trials, and do not satisfy Condition 1 or Condition 2 for any odor. All Stimuli: do not satisfy Condition 1 or 2 for any pure odor but respond to all stimuli with at least one spike in  $\geq 2$  trials/condition. Paraffin oil/clean air: satisfy Condition 1 for these conditions and do not satisfy Condition 1 or 2 for any other conditions. Respond with Inhibition: no response to the first odor presented regardless of the condition and then response to all conditions  $\geq 500$ ms after odor offset. No Response: do not satisfy Condition 1 or 2 for any stimulus and have no response in  $>75\%$  of conditions.

To construct the KC mean PSTH, we convolved KC spikes with a Gaussian of width 20 ms, and averaged the smoothed spike counts across trials and across cells for each condition.

### **Acknowledgements**

This work was supported by grants from the National Institute for Deafness and Communication Disorders and the National Science Foundation (GL), a pre-doctoral National Research Service Award from the National Institute of Mental Health (BB), and a pre-doctoral fellowship from the Sloan-Swartz Center for Theoretical Neurobiology at Caltech (VJ). We are grateful to Ben Rubin for his valuable suggestions on the visual display of quantitative information and helpful discussions throughout the course of this work, to Ofer Mazor, Stijn Cassenaer and Markus Meister for many useful discussions, and to the Laurent lab and three referees for helpful comments on the manuscript. Multi-channel silicon probes were kindly provided by the University of Michigan Center for Neural Communication Technology, sponsored by NIH NCRR grant P41RR09754.

## BIBLIOGRAPHY

- Aksay, E., Major, G., Goldman, M. S., Baker, R., Seung, H. S., and Tank, D. W. (2003). History dependence of rate covariation between neurons during persistent activity in an oculomotor integrator. *Cereb Cortex* *13*, 1173-1184.
- Bartlett, E. L., and Wang, X. (2005). Long-lasting modulation by stimulus context in primate auditory cortex. *J Neurophysiol* *94*, 83-104.
- Bazhenov, M., Stopfer, M., Sejnowski, T. J., and Laurent, G. (2005). Fast odor learning improves reliability of odor responses in the locust antennal lobe. *Neuron* *46*, 483-492.
- Bertschinger, N., and Natschlager, T. (2004). Real-time computation at the edge of chaos in recurrent neural networks. *Neural Comput* *16*, 1413-1436.
- Brown, S. L., Joseph, J., and Stopfer, M. (2005). Encoding a temporally structured stimulus with a temporally structured neural representation. *Nat Neurosci* *8*, 1568-1576.
- Drake, K. L., Wise, K. D., Farraye, J., Anderson, D. J., and BeMent, S. L. (1988). Performance of planar multisite microprobes in recording extracellular single-unit intracortical activity. *IEEE Trans Biomed Eng* *35*, 719-732.
- Duda, R., Hart, P., and Stork, D. (2000). *Pattern Classification* (New York, Wiley).
- Friedrich, R. W., and Laurent, G. (2001). Dynamic optimization of odor representations by slow temporal patterning of mitral cell activity. *Science* *291*, 889-894.
- Hallem, E. A., Ho, M. G., and Carlson, J. R. (2004). The molecular basis of odor coding in the *Drosophila* antenna. *Cell* *117*, 965-979.
- Hopfield, J., and Gelperin, A. (1989). Differential conditioning to a compound stimulus and its components in the terrestrial mollusc *Limax maximus*. *Behav Neuro* *103*, 329-333.
- Jinks, A., and Laing, D. G. (1999). A limit in the processing of components in odour mixtures. *Perception* *28*, 395-404.
- Kahneman, D. (1968). Method, findings, and theory in studies of visual masking. *Psychol Bull* *70*, 404-425.

- Knusel, P., Wyss, R., Konig, P., and Verschure, P. F. (2004). Decoding a temporal population code. *Neural Comput* 16, 2079-2100.
- Koehl, M. A., Koseff, J. R., Crimaldi, J. P., McCay, M. G., Cooper, T., Wiley, M. B., and Moore, P. A. (2001). Lobster sniffing: antennule design and hydrodynamic filtering of information in an odor plume. *Science* 294, 1948-1951.
- Kurahashi, T., and Menini, A. (1997). Mechanism of odorant adaptation in the olfactory receptor cell. *Nature* 385, 725-729.
- Laing, D. G., and Francis, G. W. (1989). The capacity of humans to identify odors in mixtures. *Physiol Behav* 46, 809-814.
- Laing, D. G., Panhuber, H., and Slotnick, B. M. (1989). Odor masking in the rat. *Physiol Behav* 45, 689-694.
- Laurent, G., and Davidowitz, H. (1994). Encoding of olfactory information with oscillating neural assemblies. *Science* 265, 1872-1875.
- Laurent, G., and Naraghi, M. (1994). Odorant-induced oscillations in the mushroom bodies of the locust. *J Neurosci* 14, 2993-3004.
- Laurent, G., Wehr, M., and Davidowitz, H. (1996). Temporal representations of odors in an olfactory network. *J Neurosci* 16, 3837-3847.
- Leinders-Zufall, T., Lane, A. P., Puche, A. C., Ma, W., Novotny, M. V., Shipley, M. T., and Zufall, F. (2000). Ultrasensitive pheromone detection by mammalian vomeronasal neurons. *Nature* 405, 792-796.
- Leitch, B., and Laurent, G. (1996). GABAergic synapses in the antennal lobe and mushroom body of the locust olfactory system. *J Comp Neurol* 372, 487-514.
- Lin da, Y., Zhang, S. Z., Block, E., and Katz, L. C. (2005). Encoding social signals in the mouse main olfactory bulb. *Nature* 434, 470-477.
- Maass, W., Natschlag, T., and Markram, H. (2002). Real-time computing without stable states: a new framework for neural computation based on perturbations. *Neural Comput* 14, 2531-2560.
- Macknik, S. L., and Livingstone, M. S. (1998). Neuronal correlates of visibility and invisibility in the primate visual system. *Nat Neurosci* 1, 144-149.
- MacLeod, K., and Laurent, G. (1996). Distinct mechanisms for synchronization and temporal patterning of odor-encoding neural assemblies. *Science* 274, 976-979.

- Maei, H., and Latham, P. (2004). How can realistic networks process time-varying signals? . *Society for Neuroscience Abstract 30*, 81.89.
- Mazor, O., and Laurent, G. (2005). Transient Dynamics versus Fixed Points in Odor Representations by Locust Antennal Lobe Projection Neurons. *Neuron 48*, 661-673.
- Mustaparta, H. (1996). Central mechanisms of pheromone information processing. *Chem Senses 21*, 269-275.
- Perez-Orive, J., Bazhenov, M., and Laurent, G. (2004). Intrinsic and circuit properties favor coincidence detection for decoding oscillatory input. *J Neurosci 24*, 6037-6047.
- Perez-Orive, J., Mazor, O., Turner, G., Cassenaer, S., and Laurent, G. (2002). Oscillations and sparsening of odor representations in the mushroom body. *Science 297*, 359-365.
- Pouzat, C., Mazor, O., and Laurent, G. (2002). Using noise signature to optimize spike-sorting and to assess neuronal classification quality. *J Neurosci Methods 122*, 43-57.
- Rolls, E. T., and Tovee, M. J. (1994). Processing speed in the cerebral cortex and the neurophysiology of visual masking. *Proc Biol Sci 257*, 9-15.
- Rouby, C., and Holley, A. (1995). Temporal competition between odorants: effect of different time intervals on the perception of monorhnic and dichorhnic binary mixtures. *Perception 24*, 1083-1097.
- Roweis, S. T., and Saul, L. K. (2000). Nonlinear dimensionality reduction by locally linear embedding. *Science 290*, 2323-2326.
- Sobel, E., and Tank, D. (1994). In Vivo Ca<sup>2+</sup> Dynamics in a cricket auditory neuron: an example of chemical computation. *Science 263*, 823-826.
- Stevens, J. C., and Traverzo, A. (1997). Detection of a target taste in a complex masker. *Chem Senses 22*, 529-534.
- Stopfer, M., Jayaraman, V., and Laurent, G. (2003). Intensity versus identity coding in an olfactory system. *Neuron 39*, 991-1004.
- Stopfer, M., and Laurent, G. (1999). Short-term memory in olfactory network dynamics. *Nature 402*, 664-668.

- Suh, G. S., Wong, A. M., Hergarden, A. C., Wang, J. W., Simon, A. F., Benzer, S., Axel, R., and Anderson, D. J. (2004). A single population of olfactory sensory neurons mediates an innate avoidance behaviour in *Drosophila*. *Nature*.
- Vickers, N. J., Christensen, T. A., and Hildebrand, J. G. (1998). Combinatorial odor discrimination in the brain: attractive and antagonist odor blends are represented in distinct combinations of uniquely identifiable glomeruli. *J Comp Neurol* 400, 35-56.
- Vogt, M. B., and Smith, D. V. (1994). Responses of single hamster parabrachial neurons to binary taste mixtures of NaCl with sucrose or QHCl. *J Neurophysiol* 71, 1373-1380.
- Wegel, R., and Lane, C. (1924). The auditory masking of one pure tone by another and its probable relation to the dynamics of the inner ear. *Physical Review* 23, 266-285.
- Wehr, M., and Laurent, G. (1996). Odor encoding by temporal sequences of firing in oscillating neural assemblies. *Nature* 384, 162-166.
- Wehr, M., and Zador, A. M. (2005). Synaptic mechanisms of forward suppression in rat auditory cortex. *Neuron* 47, 437-445.
- Wilson, R. I., Turner, G. C., and Laurent, G. (2004). Transformation of olfactory representations in the *Drosophila* antennal lobe. *Science* 303, 366-370.
- Zufall, F., and Leinders-Zufall, T. (1998). Role of cyclic GMP in olfactory transduction and adaptation. *Ann N Y Acad Sci* 855, 199-204.

## Supplementary Information

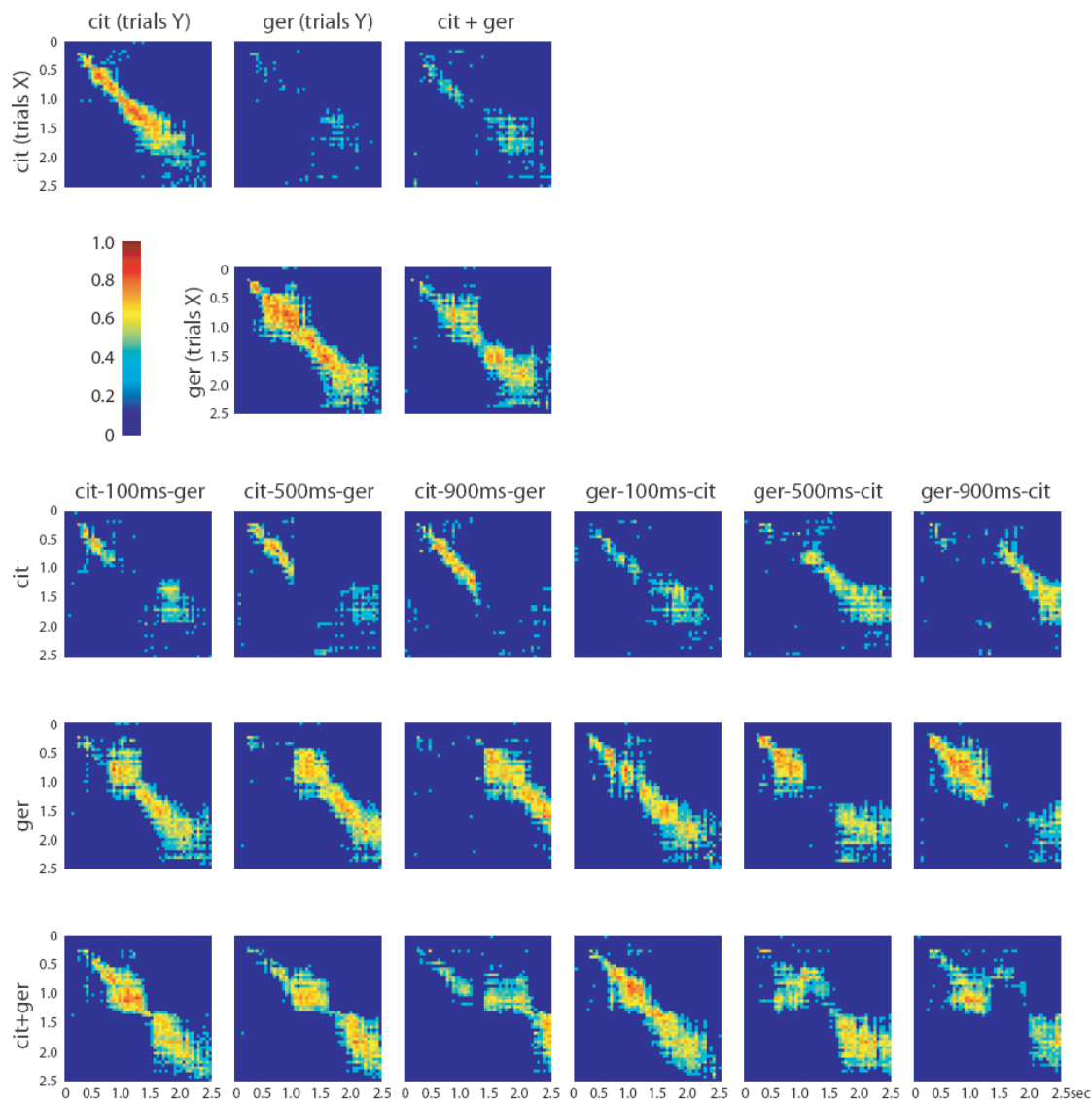


**Figure S1.** Correlation matrices for 87-PN time-slice vectors. Normalized correlation matrices for some of the conditions shown in Figures 4 and 5. The correlation matrices (along with the MDA results shown in Figure 6) provide a quantitative basis for what is seen qualitatively in the LLE plots. Each pixel,  $C_{r,c}$ , represents the correlation of one 3-trial-averaged 87-PN time slice vector,  $\mathbf{r}$ , with another,  $\mathbf{c}$ , from either the same condition (but taken as an average of 3 different trials) or a different condition, as indicated. Thus, a pixel  $C_{1,2}$  represents the correlation of the time slice of trajectory A at time  $t_1$  to the time slice of trajectory B at time  $t_2$ . All correlations shown are significant ( $p < 0.001$ ). In the top two rows, time slices from PN responses to the pure conditions are correlated with each other and with those of the odor mixture. The mixture response is different from both pure odor responses early, and similar to the ger response late. In the lower three rows, time slices from PN responses to these conditions are correlated with some of the conditions shown in Fig. 4A-D and Fig. 5. In agreement with what can be seen in LLE plots (Fig. 4C-D), responses for the overlap conditions are first strongly correlated with the response to the first odor presented; they then switch, with a lag, to being correlated with the response to the second or the mixture.

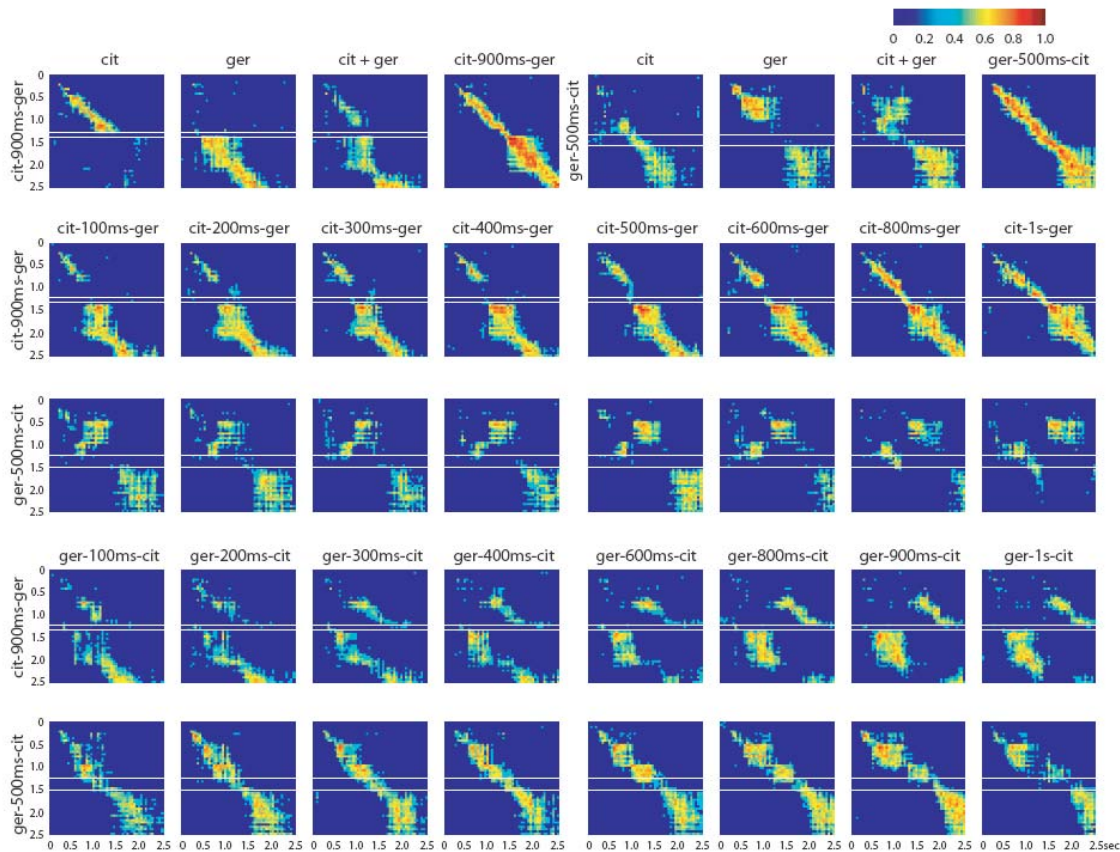


**Figure S2.** Correlation matrices for 87-PN time-slice vectors: correlations between time slices for different overlap responses. White rectangles highlight times when overlap responses show decreased or no correlation with time slices from the pure conditions or the mixture. These times and conditions match those revealed by MDA as being distant from both pure conditions and the mixture, and for which unique KC responses were found. Note that the across-condition correlation levels at these times are not always zero; in some cases (see especially the last row for ger-500ms-cit) they are merely lower than at other times. Whether or not these relatively low correlation levels are significant for the KCs (and ultimately for the animal) depends on the sensitivity of KC firing probability to PN-vector distances and thus, on the synaptic and biophysical mechanisms used by KCs to “decide” whether to fire or not.

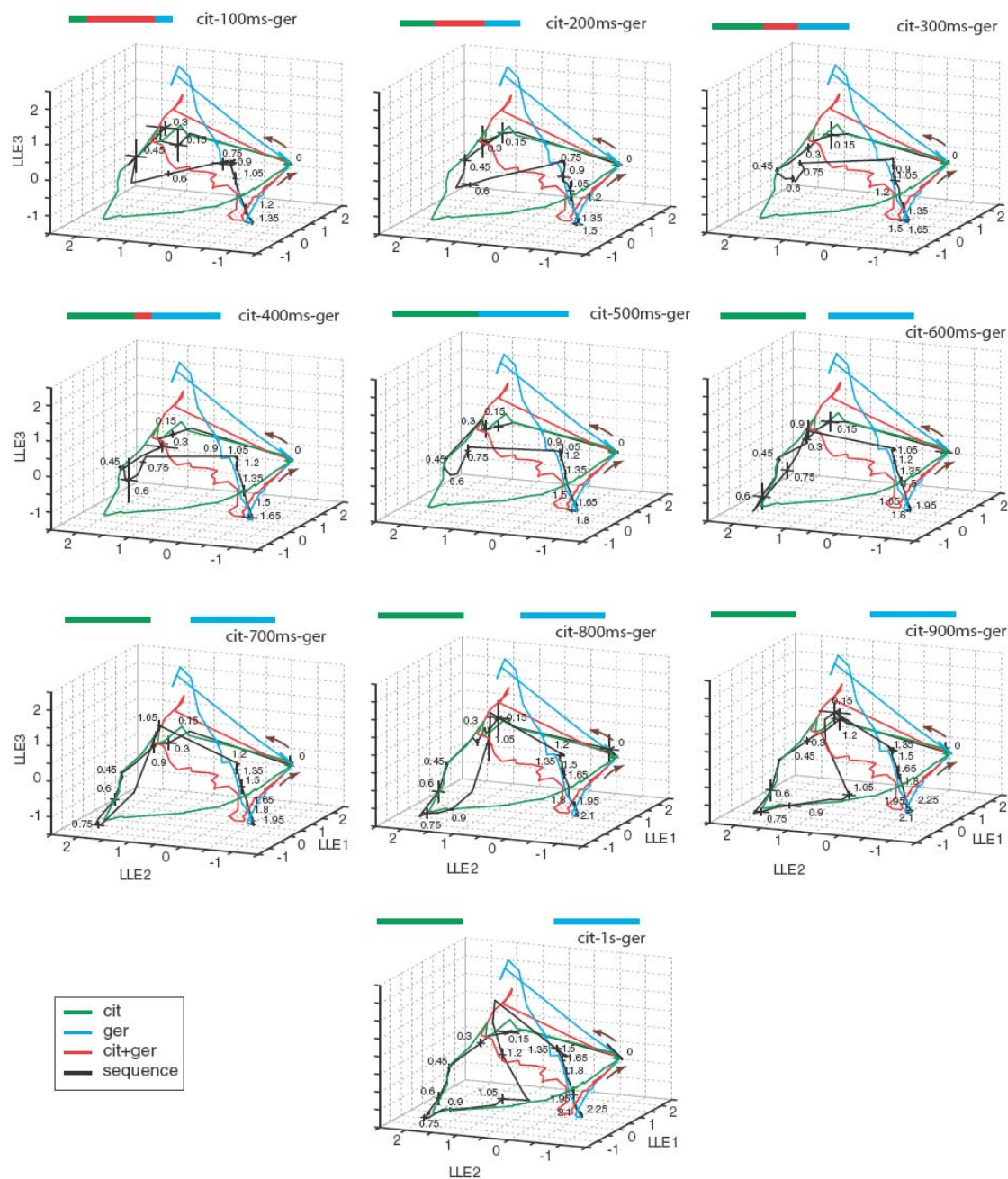


**Figure S3.** PN-ensemble responses for all overlap conditions. LLE plots similar to those in Fig. 4B-D showing PN ensemble responses (trajectories) for all overlap conditions tested. Baseline indicated as origin (O).

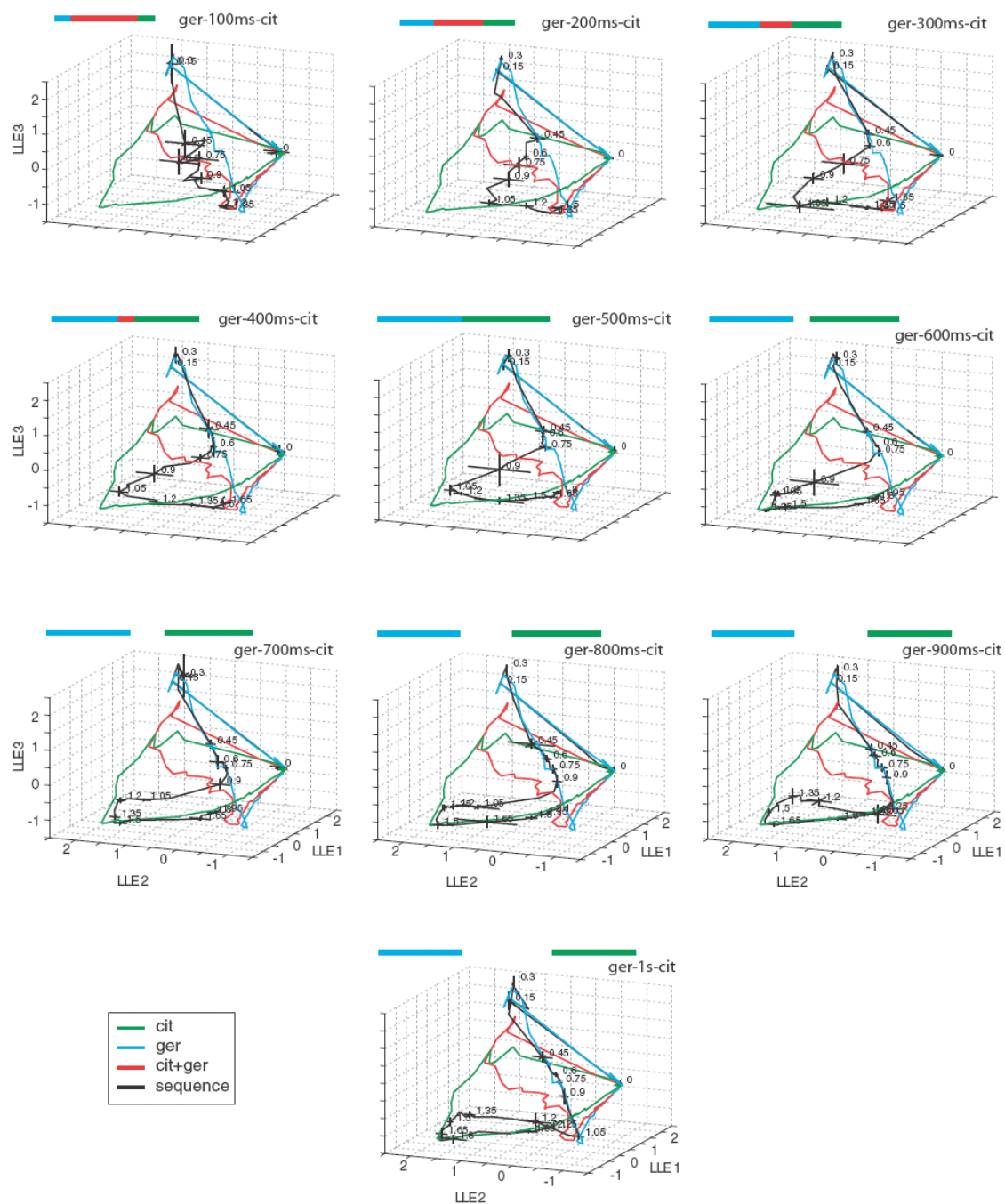


**Figure S4.** PN-ensemble responses for all overlap conditions. LLE plots similar to those in Fig. 4B-D showing PN ensemble responses (trajectories) for all overlap conditions tested. Baseline indicated as origin (O).

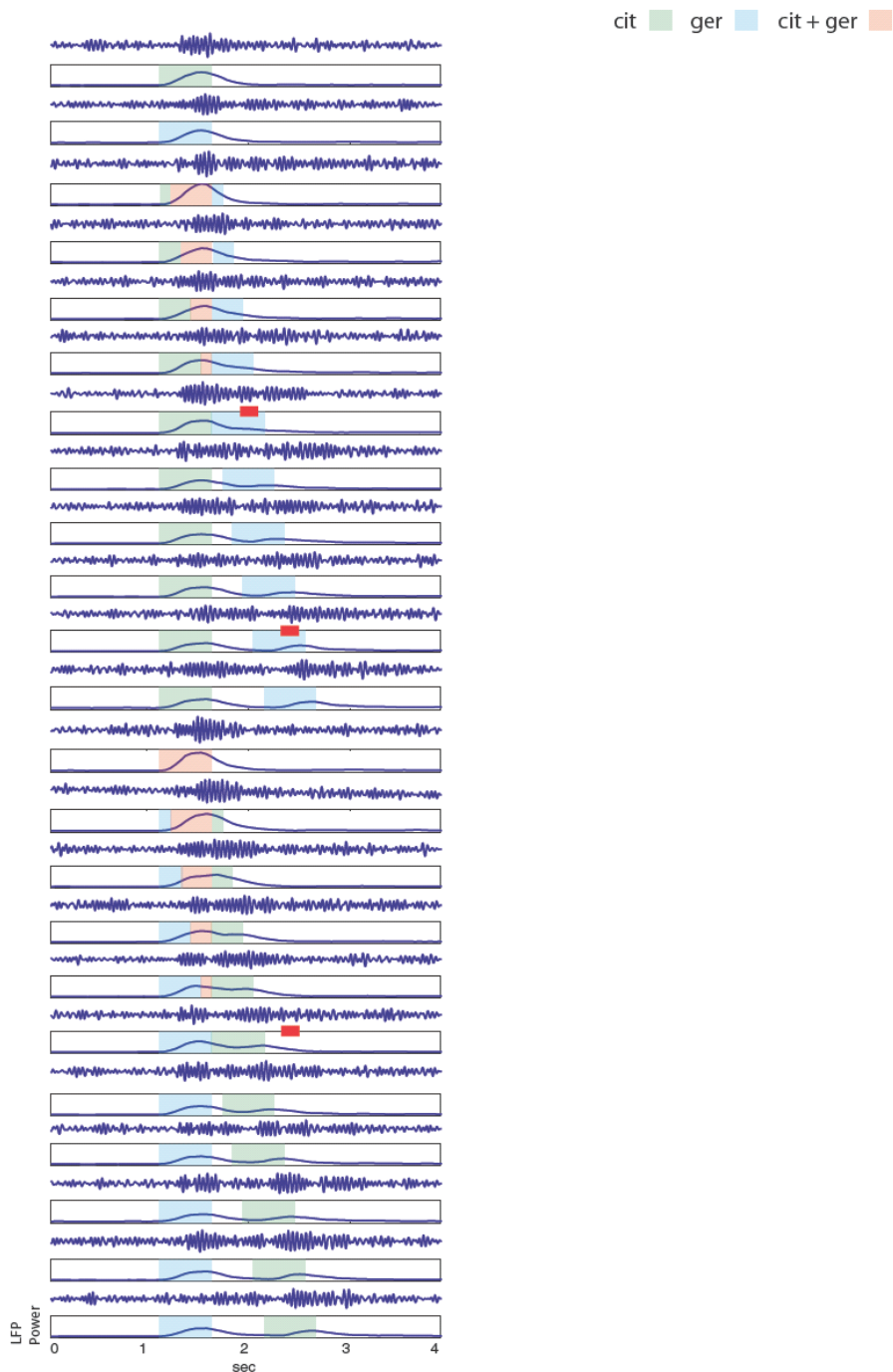


**Figure S5.** PN synchrony during overlapping odor pulses, as measured by local field potential power in the 5-55 Hz band. Shown for all overlap conditions, are sample LFP traces recorded over the course of one experiment, and mean power in the LFP (see Experimental Procedures for details on computation). Shaded areas correspond to pure and mixed odors indicated in legend and described in Fig. 1A. Red lines span times and conditions when PN ensemble trajectories are furthest away from trajectories of the pure conditions. The significant power in the LFP at these times indicates that PNs are synchronized then. KC responses should thus be generated at those times.

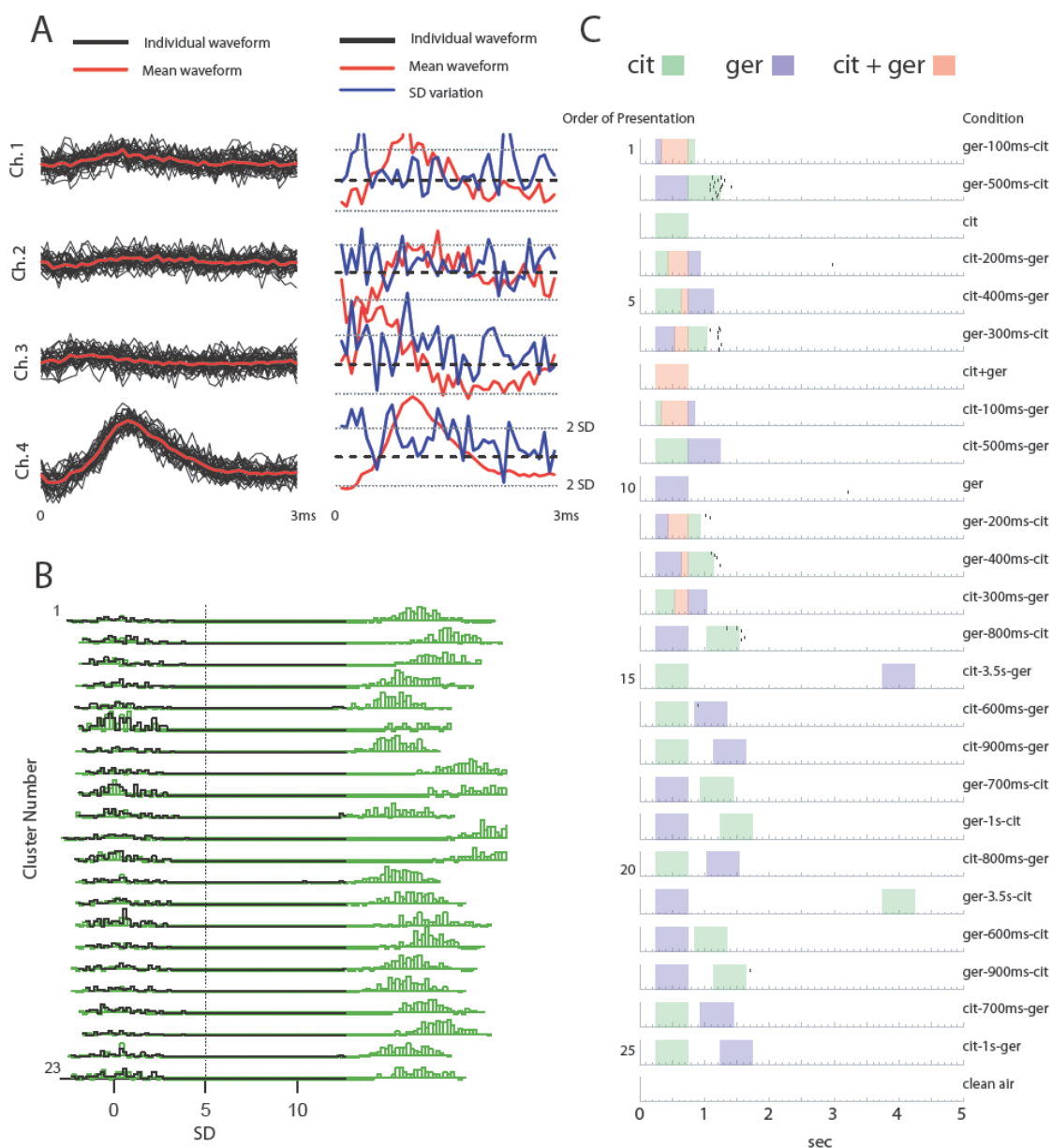


**Figure S6.** KC5 spike sorting. **A.** Example of cluster separation. On the left all of the events (black) that were classified as belonging to KC5 (Fig. 7,8) are shown superimposed, for each channel of the four-channel tetraode. Average waveform is in red. Right: the variance around the mean for each of the four channels (red) with the 95% confidence interval shown for each (dotted lines). The average event waveform is shown again in gray (rescaled). **B.** The projection test for KC5 where each pair of clusters computed for this model in 180-D space is projected onto the axis that connects the centers of those two clusters. This plot shows the large distance ( $>10$  SD) between the cluster attributed to KC5 and all other putative KCs. **C.** Raster plots for KC5 shown in the order in which they were recorded. Shaded areas correspond to pure and mixed odors indicated in legend and described in Fig. 1A.

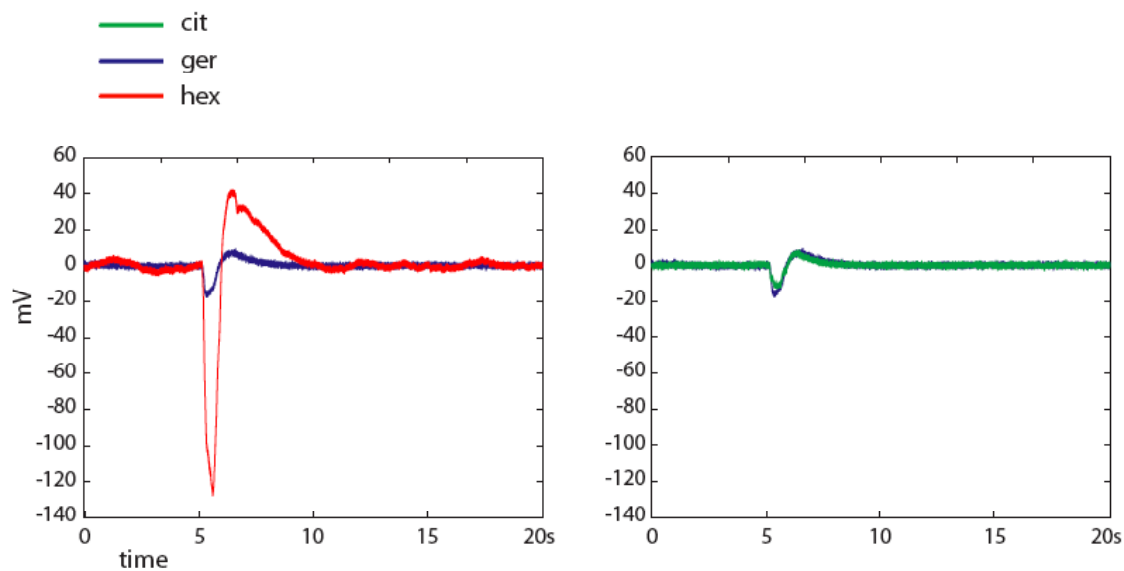


**Figure S7.** Electro-Antennograms. Electro-Antennogram (EAG) recordings from the locust antenna in response to geraniol and hexanol (left: single trial) and citral and geraniol (right: single trial, different antenna from that on left). Pilot PN data were obtained with the ger-hex odor pair first (see Fig S8). Note the large difference in signals for the two odors. The odors were then changed for our main study: citral was chosen (on the basis of its similar vapor pressure to geraniol) to replace hexanol, thus equalizing their effectiveness on the receptor array. *x*- axis: time, in seconds. Methods: an antenna was cut at the proximal and distal ends, metal electrodes were inserted at both ends; the potential difference was measured by differential amplification. An EAG is a field potential, reflecting the combination of receptor and action potentials.

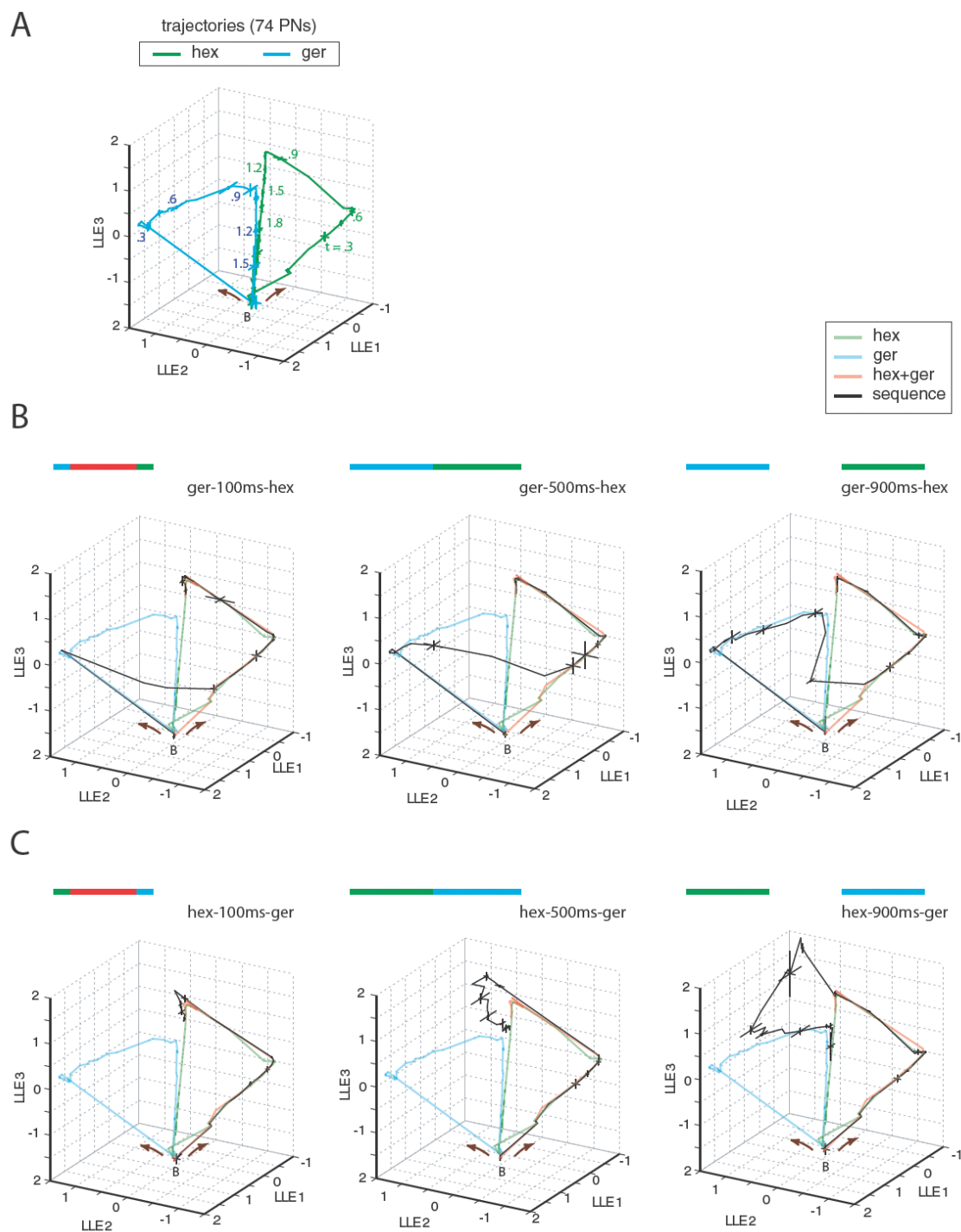


**Figure S8.** LLE projections of PN population responses to hexanol and geraniol. LLE projections of activity in 74 PNs (different from those used in the main paper), in response to the odors hexanol and geraniol (see Fig S7 for EAGs). This set constituted a pilot study, used to better define optimal experimental conditions. The imbalance between the influence of hexanol and geraniol (visible in B) led us to modify our stimulus pair and choose odors of similar vapor pressures. **A.** Projection of PN trajectories in LLE 1-3 dimensions, showing the orbits corresponding to each odor (arrow: direction of motion from baseline, **B**). Three-trial averages, 50-ms time bins. **B,C.** Sequence

conditions, defined as in main paper, but with hexanol (green) and geraniol (cyan). The mixture trajectory is shown in red. Note that the mixture trajectory is nearly identical to that for hexanol alone, consistent with the dominance of this odor, as shown from EAGs in Fig S7. Note, however, that the sequence trajectories (black) show the same qualitative features of divergence as described in the main paper.

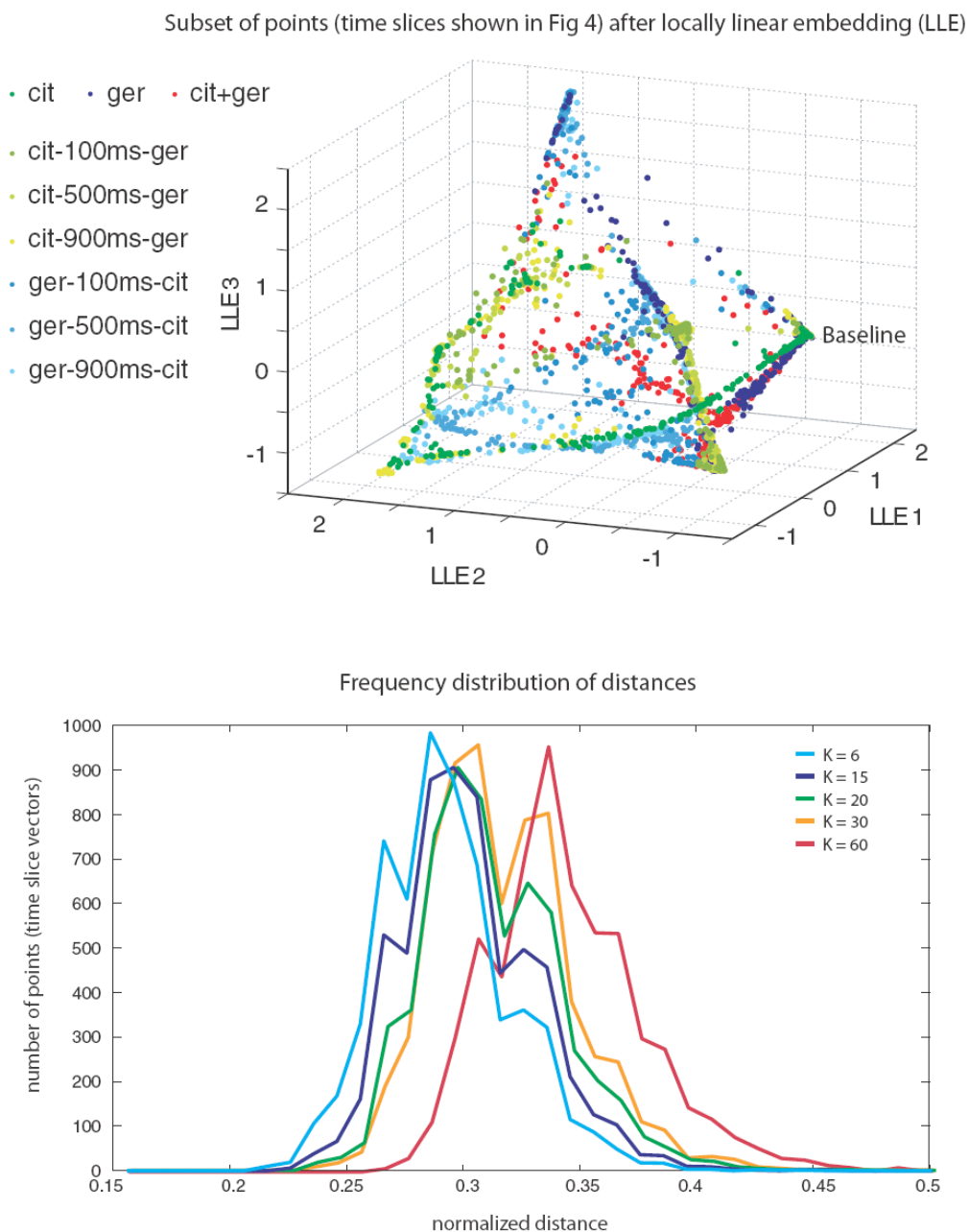


**Figure S9.** Technical details on LLE procedure and choice of K: **Top:** The top panel shows the subset of embedded points (time slice vectors) used to construct the trajectories shown in Figure 4.

Description of the term: “K nearest neighbors” of individual time slices. LLE uses only one user-supplied parameter, K, which is the number of nearest neighbors to consider for locally-linear reconstruction, *i.e.*, for the embedding of a high-dimensional point (or vector) in a lower dimension space, while preserving the local neighborhood of each point. The choice of K was guided by what is known about the average size of the close neighborhood of individual points in the full space.

In our analysis, each point in the full space is a 87-d vector of spike counts across the 87 PNs, measured for each time slice or 50ms-bin. The correlation matrices (Figs S1,S2) and the analysis in the figure below are used to estimate the sizes of these neighborhoods, and thus provide guidance for the choice of K.

**Bottom:** The bottom panel shows frequency distributions of distances (normalized to maximum distance in the distance matrix) of all time slice vectors (points) to their (6th, 15th, 20th, 30th and 60th) nearest neighbors. For  $K < 15$ , the vast majority of points have relatively low distance values (less than 33% of the maximum) to their K nearest neighbors, the mean distance is close to the peaks between 0.28 and 0.30. As K increases, however, the distribution begins to shift to an increasingly prominent second peak at  $\sim 0.34$ , the first peak at 0.30 shrinks and eventually disappears; the mean shifts to the right. The meaning of "near neighborhood" thus becomes inconsistent and breaks down for a significant number of points as K increases much beyond 15. This provides approximate bounds on the values of K to use for the method. We obtained qualitatively similar results for all K values chosen within those bounds, and all plots were constructed with  $K = 6$ .

Response Type	% Recorded KCs
Cit	2.0
Ger	5.0
Mix	4.5
Cit+Ger	4.5
Cit+Mix	3.5
Ger+Mix	7.0
Pattern-specific	3.5
All Stimuli	21.5
Paraffin oil/Clean air	4.5
Respond with Inhibition	2.5
No Response	41.5

**Table S1.** Classes of Recorded KCs. Each one of the two hundred and three recorded Kenyon Cells was assigned to one of eleven classes based on the assignment criteria described in Experimental Procedures.

*Chapter 4***EVALUATING A GENETICALLY ENCODED  
OPTICAL SENSOR OF NEURAL ACTIVITY USING  
ELECTROPHYSIOLOGY IN  
INTACT ADULT FRUIT FLIES****Summary**

Genetically encoded optical indicators hold the promise of enabling non-invasive monitoring of activity in identified neurons in behaving organisms. However, the interpretation of images of brain activity produced using such sensors is not straightforward. Several recent studies of sensory coding used G-CaMP—a calcium sensor—as an indicator of neural activity; some of these studies characterized the imaged neurons as having narrow tuning curves (Wang et al., 2003; Wang et al., 2004; Marella et al., 2006), a conclusion not always supported by parallel electrophysiological studies (Wilson et al., 2004; Olsen et al., 2007). To better understand the possible cause of these conflicting results, we performed simultaneous *in vivo* 2-photon imaging and electrophysiological recording of G-CaMP expressing neurons in the antennal lobe of intact fruit flies. We find that G-CaMP has a relatively high threshold, that its signal often fails to capture spiking response kinetics, and that it can miss even high instantaneous rates of activity if those are not sustained. While G-CaMP can be misleading, it is clearly useful for the identification of promising neural targets: when electrical activity is well above the sensor's detection threshold, its signal is fairly well correlated with mean firing rate and G-CaMP does not appear to alter the responses of neurons that express it significantly. The methods we present should enable any genetically encoded sensor, activator or silencer to be evaluated in an intact neural circuit *in vivo*.

## Introduction

The fruit fly has been a mainstay of behavioral genetics for many decades (Benzer, 1967; Hotta and Benzer, 1970; Quinn et al., 1974). It has not, however, been a model system of choice for systems neuroscience. One reason was the lack of accessibility of its neurons for *in vivo* recordings. Recent developments show, however, that it is possible to record *in vivo* from fly brain neurons with intracellular electrophysiology (Wilson et al., 2004). This approach is direct and has high temporal resolution. Of all the electrophysiological recording methods available, the whole-cell patch-clamp (WCPC) technique (Sakmann and Neher, 1984) may be the most appropriate for small neurons such as *Drosophila's* (Wilson et al., 2004; Wilson and Laurent, 2005). WCPC, however, is invasive: it causes dialysis and can sometimes require direct current injection to hold the neuron at a desired potential when the neuron's normal resting potential is unknown. It is also limited in that only a few neurons can be sampled simultaneously. Alternative techniques use optical reporters of voltage (Cohen and Salzberg, 1978; Cohen et al., 1978; Taylor et al., 2003; Grinvald and Hildesheim, 2004) or intracellular calcium (Grynkiewicz et al., 1985; Tank et al., 1988; Svoboda et al., 1997; Stosiek et al., 2003). Some of these indicators are now genetically encoded (Miyawaki et al., 1997; Persechini et al., 1997; Nakai et al., 2001); using genetic techniques (Brand and Perrimon, 1993), specific cell groups can be targeted selectively (Fiala et al., 2002; Ng et al., 2002; Wang et al., 2003; Schroll et al., 2006), making optical approaches very powerful. Yet, these methods have their own intrinsic limitations. Among them is the interpretability of the signal they produce: natural concerns are about their temporal resolution, sensitivity and correlation to electrical activity (Pologruto et al., 2004; Reiff et al., 2005). These characteristics may vary with cell type and expression level. In

addition, because calcium indicators are modified calcium buffers, their presence in neurons could alter development or function. Thus, it seems important to evaluate the performance of these sensors in the cells of interest before using them as standalone indicators of neural activity.

Combining simultaneous loose-patch-clamp recordings and two-photon calcium imaging (Denk et al., 1990), we performed such direct calibration experiments with G-CaMP-expressing projection neurons (PNs) in the fruit fly antennal lobe (AL). The AL is the first relay in the insect olfactory system and has been the subject of many recent investigations (Wang et al., 2003; Wilson et al., 2004; Yu et al., 2004; Olsen et al., 2007; Shang et al., 2007). Most *Drosophila* PNs each arborize in one glomerulus, where they receive direct afferent input from one olfactory sensory neuron (OSN) type. An issue that has received some attention recently concerns the tuning of PNs to odors: studies based on whole-cell patch-clamp recordings (Wilson et al., 2004; Olsen et al., 2007) report that most PNs respond broadly, and are more broadly tuned than their presynaptic OSNs. By contrast, a study based on two-photon imaging with G-CaMP found sparse PN responses to odors (Wang et al., 2003) suggesting a faithful transfer of representations from OSNs to PNs. Tuning width has consequences on coding efficiency, making this issue one relevant to olfaction in particular and sensory systems in general. The simplest reason for this discrepancy is technical: one set of studies used whole-cell patch-clamp recordings from intact flies, the other G-CaMP imaging from isolated fly heads. The present experiments, because they consist of electrophysiological recordings simultaneously with G-CaMP imaging in intact flies, should help resolve this issue directly.

## Results

### Two-photon Targeted Electrophysiological Recordings

*GCaMP-Gal4*, *UAS-GCaMP* flies (Wang et al., 2003) were used for a series of two-photon targeted electrophysiological recordings from PNs in the fly AL. Approximately half of the PN population is targeted by this line: G-CaMP-expressing PNs showed strong baseline fluorescence, and PNs showed strong and selective changes in fluorescence in response to odors (Fig 1A).

In the first set of experiments, we recorded from G-CaMP-positive PNs using sharp electrodes (n=7; 7 flies). Cells usually began filling with dye immediately upon penetration, and helped us verify that the correct cell was being recorded from (Fig S1A). Recordings were stable only for short periods of time (<20 minutes), and the signal usually degraded over time (Fig S1B). However, synaptic activity and post-spike after-hyperpolarization were clearly visible in most of the recordings. PNs showed significant baseline levels of activity, and responded with both inhibition and excitation to the odors tested (Fig S1B).

Although sharp recordings were informative, they were unsuitable for calibration experiments because of their adverse effect on the imaging signal (G-CaMP baseline fluorescence and G-CaMP odor responses degraded soon after penetration). Thus, for our second set of experiments, we chose to use the loose-patch technique. This minimally invasive technique allowed us to gently seal onto PNs and observe their spiking activity without breaking in (n=8; 7 flies). Cells were targeted using two-channel imaging (Fig 1B,

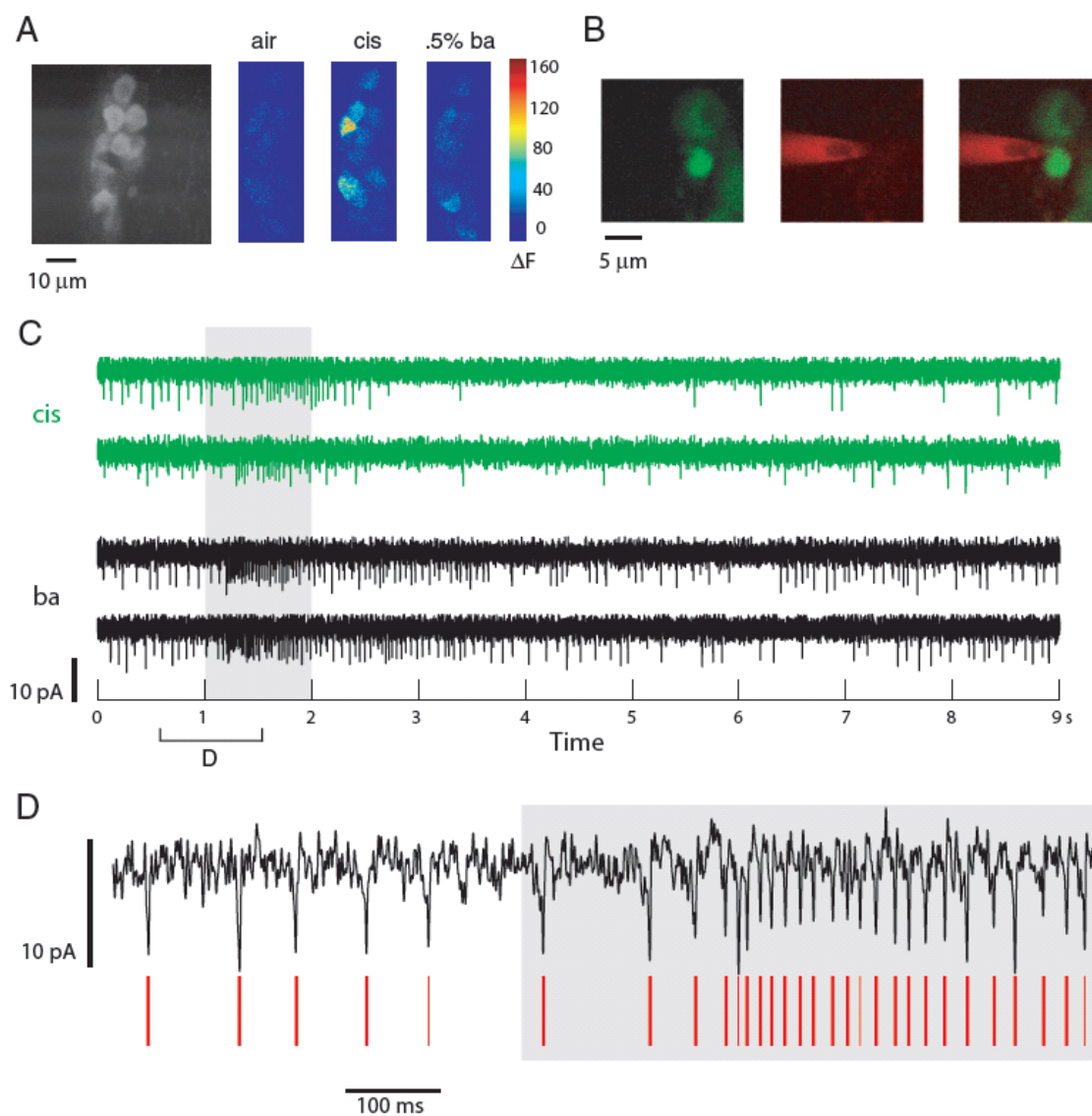


**Figure 1.** Loose-patch recording from identified PNs in *GH146-Gal4,UAS-GCaMP* flies. **A**, Baseline levels of fluorescence (left) of G-CaMP-expressing dorsal PNs, and absolute changes in (8-bit) fluorescence intensity levels in response to air and two odor presentations. **B**, Two-channel imaging showing (from left) images in the green, and red channels; image on right is an image created from merging the two channels. Images verify that cell was not broken into during recording. **C**, Current traces from the PN above. Shown are responses to 2 different odor presentations (2 trials each) (grey bar). **D**, Spikes, although small, can be separated from the noise by a combination of amplitude and fast deflection (see Methods). Red lines indicate spikes detected automatically.

see Methods). Occasionally, we were able to break into the cell at the end of an experiment and confirm cell identity. However, this was usually not possible, and we could only use the two-channel images of the patch pipette near the cell for confirmation of pipette-soma

apposition. The red dye in the pipette was occasionally blown out gently to allow visualization of otherwise non-fluorescent —and therefore invisible— neuropil and non-targeted cells in the neighborhood of the neuron of interest.

Loose-patch recordings, although noisy (because of the low-resistance seals), were fairly stable over sessions lasting up to 40 minutes. PNs responded reliably with excitation and inhibition (visible as a reduction in instantaneous rate relative to baseline) to different odors (Fig 1C). Spike adaptation during bursts of activity meant a local decrease in signal-to-noise, but spikes were still clearly visible based on their amplitude and slope even in periods of high firing during an odor response (Fig 1D).

### **Effect of presence of G-CaMP on normal neuronal function**

The introduction of calcium sensors into a cell can have an impact on the cell's calcium dynamics (Yasuda et al., 2004). If the sensor is present from the birth of the neuron, it is possible that it would change its physiology and even affect network level activity in the targeted population. To investigate this possibility in G-CaMP-positive cells, we performed experiments on identified PNs that project to and receive afferent input from the DL1 glomerulus; these PNs are selectively labeled in the fly line *NP3529-Gal4* (Tanaka et al., 2004). After crossing with a *UAS-eGFP* line, we obtained flies with enhanced-GFP-labelled DL1 PNs. These eGFP flies were used as controls (cytosolic GFP is not considered to have deleterious effects on cell physiology (Su and O'Dowd, 2003)). Comparisons of the physiology of G-CaMP-expressing DL1 PNs (n=6, 5 flies) and GFP-expressing DL1 PNs (n=5, 5 flies) revealed no major differences (Fig 2A-G). Spontaneous firing was limited in

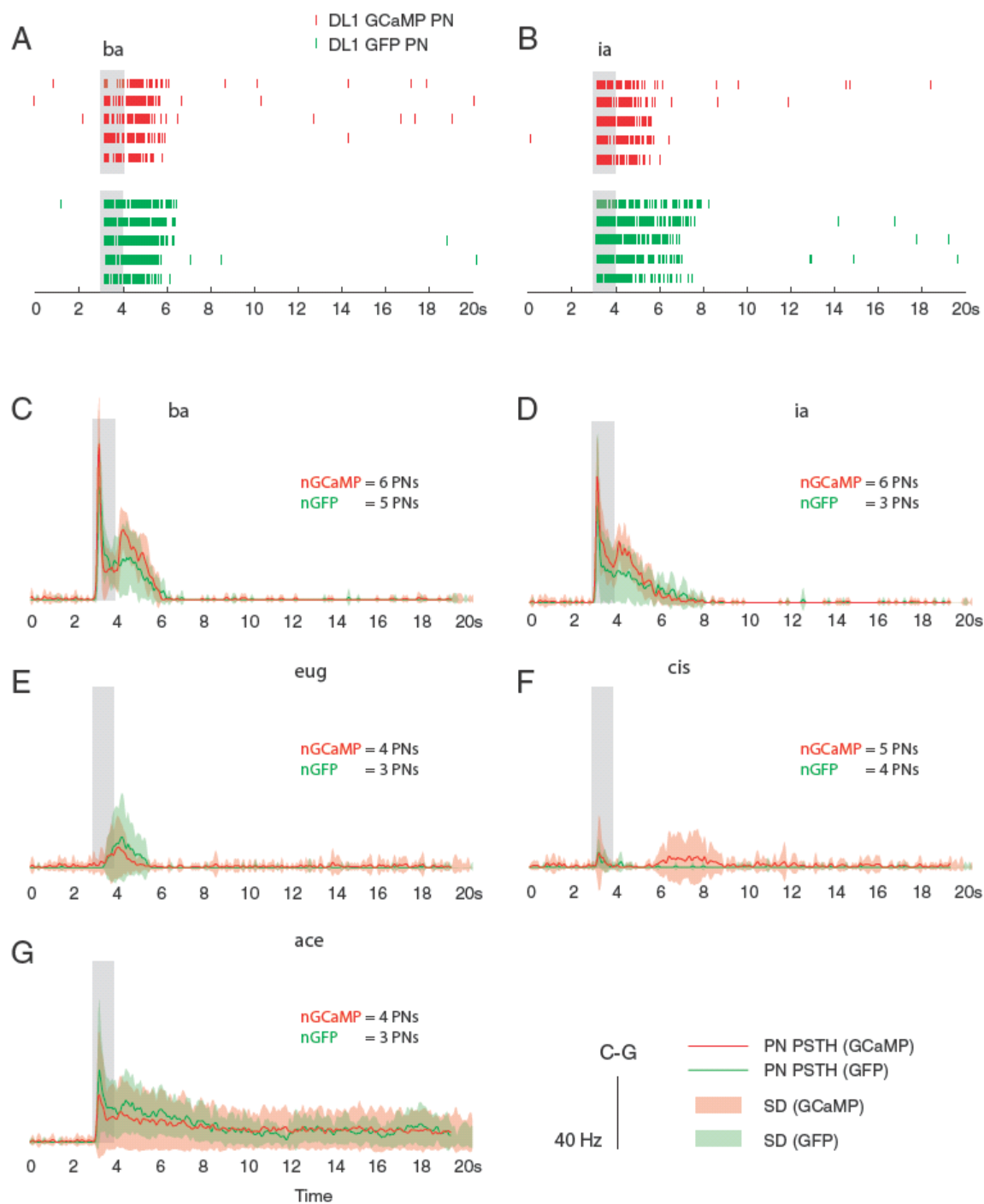


**Figure 2.** G-CaMP-expressing PNs (of the DL1 glomerulus) and their GFP-expressing counterparts do not show significantly different response patterns. **A-B**, Sample responses of two PNs. The first five rows show spike rasters of single trial responses of a G-CaMP-expressing PN (*NP3529-Gal4,UAS-GCaMP*) fly, and the next five show responses of a GFP-expressing PN (*NP3529-Gal4,UAS-eGFP*) to ba and ia respectively. **C-G**, Shown are mean PSTHs for DL1 PN: GFP (in green, with SD in light green) and G-CaMP (in red; SD in pink). PN spiking responses to different odors shown were smoothed (5ms width Gaussian) before trial-averaging to produce

PSTHs. G-CaMP PN responses were almost always within one SD of GFP PN responses (see stats in text).

both cases, with mean baseline firing rates of  $1.33 \text{ Hz} \pm 2.32$  for the G-CaMP PNs and  $0.33 \pm 0.5$  for the GFP PNs (difference of means not significant, two-sample t-test,  $p=0.3556$ ). The PNs also showed similar —albeit not identical— odor response profiles. For example, responses to benzaldehyde (ba) consistently featured two peaks in instantaneous firing rate, one each immediately after odor onset and offset (Fig 2A,C). The same was true, to a lesser extent, for isoamyl acetate (ia) (Fig 2B,D). Responses to acetophenone (ace) showed a similar early increase in firing followed by sustained firing at lower rates for over 20s in both lines (Fig 2G). Inter-individual response variability in PNs of one type (GFP or G-CaMP) was fairly high (see SD of PSTHs in Figs 2) relative to differences between the two types (visible in mean traces in Fig 2). We performed statistical comparisons of mean rate during response (1-sec and 3-sec window immediately after odor onset) for the 5 odors tested on at least 3 PNs of each type. We found no significant differences between the two groups (two-sample t-test:  $p \gg 0.05$  for all comparisons except ia, which had a p-value of 0.09 for a comparison using a 3-sec window for mean rate computation). In conclusion, present indications are that G-CaMP, at the expression level tested, does not have any more significant effects on PN response patterns than GFP.

### **Calibration of G-CaMP using simultaneous electrophysiology and imaging**

To test the effectiveness of G-CaMP as a reporter of neural activity, we combined electrophysiological recording and simultaneous G-CaMP imaging of individual PN responses to odors. We used *GHI46-Gal4*, *UAS-GCaMP* flies for all these experiments

with four copies of G-CaMP (Wang et al., 2003). In all these experiments ( $n=8$ , 7 flies), baseline fluorescence was high, and changes in fluorescence were observed to at least one of the odors tested. This excludes the possibility of problems with the acquisition of the imaging signal.

At the start of each experiment, we identified an “image-positive” PN, that is, one that displayed a detectable G-CaMP response to at least one of the odors tested. We then performed line-scans of the equator of the soma at low laser intensity (sufficient for visible baseline fluorescence) and targeted the same soma with an electrode for loose-patch recording (Fig 3A). The raw fluorescence signal (Fig 3B,C) was boxcar filtered (Fig 3D) before comparisons were made with electrophysiological responses (Fig 3D,E). In this example, we found that G-CaMP was able to detect responses to all three odors, albeit with some lag ( $>500$  msec, measured as the delay between times of firing rate increases of 2.5 SDs above baseline and fluorescence changes of 2.5 SDs over baseline) and with a slow decay (G-CaMP signal returned to baseline up to 5 seconds later than firing rate did).

In a different PN with clear spiking responses to three odors (Fig 3F), G-CaMP signal only reflected a strong response to one odor (cherry). With the odor *ia*, the evoked spiking response had a peak instantaneous rate (measured in 50-ms windows) of 40 spikes/s; this response went undetected with G-CaMP (Fig 3G). This was a consistent trend across all simultaneous recordings, indicating that although G-CaMP is sufficiently sensitive to detect high rates of sustained activity, the sensor has a high threshold and slow kinetics at this

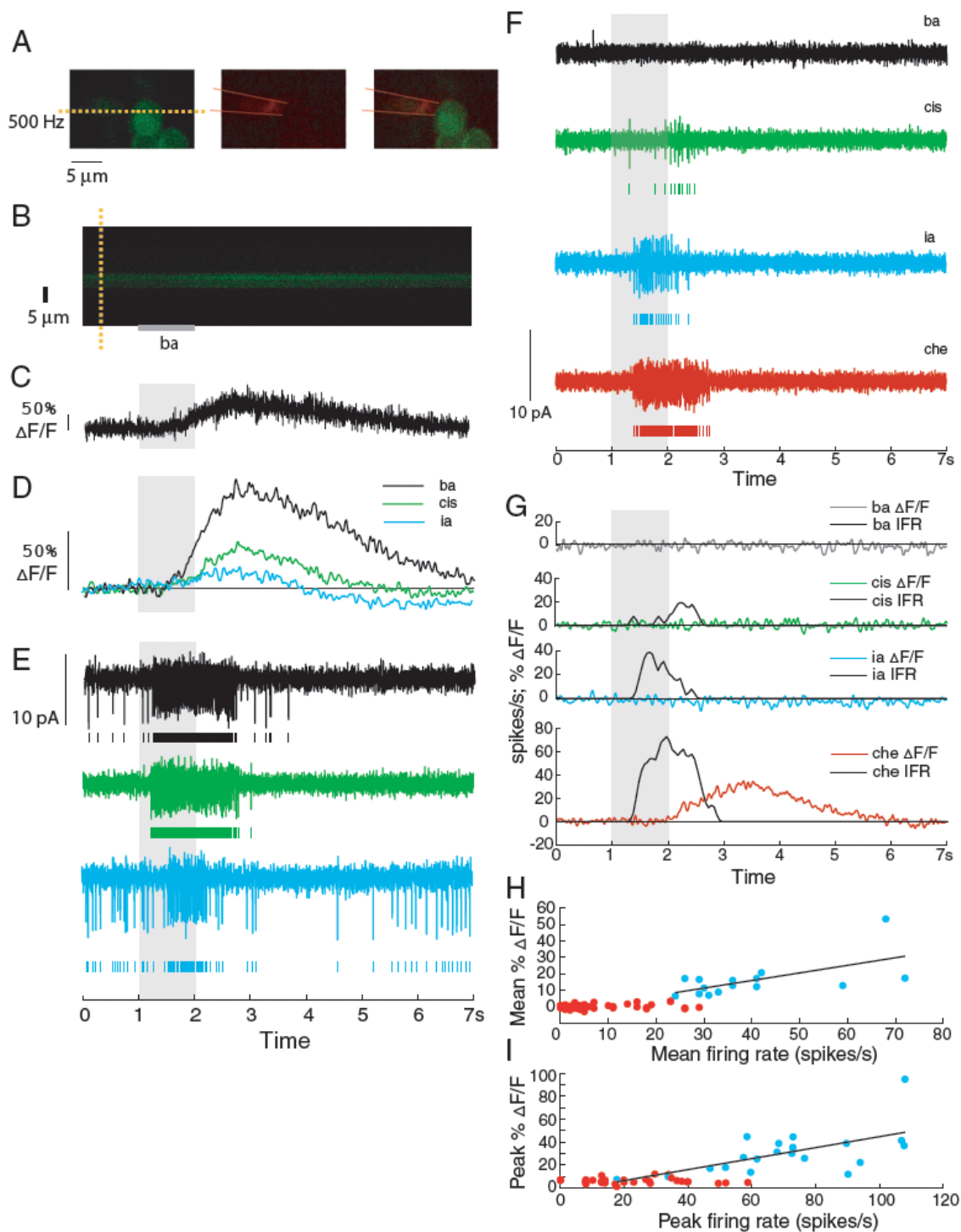


**Figure 3.** Simultaneous electrophysiology and 2-photon G-CaMP imaging of *GH146-Gal4, UAS-GCaMP* PNs. **A**, Shows (from left) G-CaMP-positive PN in green channel, patch electrode in red (outline of approximate electrode position drawn by hand), merge. Yellow dashed line shows line chosen for line scanning in this experiment. **B**, Results of line scan. Shown is the change in intensity levels as the odor is presented. **C**, Raw and unfiltered single trial imaging signal ( $\Delta F/F$ )—based on integrating over the appropriate window in **B**— shows clear response to odor pulse, but

with slow rise time. **D**, Filtered G-CaMP signal shows responses to three odors (ba, cis and ia). Imaging signal in response to ia is just barely detectable. **E**, Simultaneously recorded electrophysiological signal showing PN responses to ba, cis and ia. For each odor response, the first row shows raw signal, second row shows spikes detected. **F**, Electrical recordings of odor responses of a PN from a different fly (also *GHI46-Gal4, UAS-GCaMP*). **G**, Results of simultaneous line scanning of the same PN's soma for the same odors. Shown is the change in fluorescence levels as the odor is presented. Also shown for comparison is the instantaneous firing rate based on simultaneous electrical recordings. G-CaMP signal shows high threshold of activation. Response to ia evoked greater than 40Hz of activity, but did not evoke any G-CaMP signal. **H**, Mean  $\Delta F/F$  following odor presentation is partially correlated with the mean firing rate (during 1s odor period) of various PNs in response to odor presentations. Red dots represent points that fall within 2.5SDs of baseline variation). Best-fit linear regression lines for significant points shown in black. Correlation value for trials with significant  $\Delta F/F$  values: 0.61. Pearson's  $r^2$  is thus .38. **I**, Peak  $\Delta F/F$  following odor presentation is partially correlated with the peak firing rate (during 1s odor period) of various PNs in response to odor presentations. Red dots represent points that fall within range of peak baseline variation). Best-fit linear regression lines for significant points shown in black. Correlation value for trials with significant  $\Delta F/F$  values: 0.51. Pearson's  $r^2$  is thus .26.

expression level. We next measured the correlation between detected G-CaMP signal (defined relative to baseline noise), and spiking activity. This correlation (mean response rate vs. mean fluorescence change) was 0.61 (Pearson's, Fig 3H). The correlation between peak instantaneous rate and peak fluorescence was also significant but not high (0.51; Fig 3I). Other metrics, such as  $\Delta F/F(t)$  time-integral and slope change had similar correlation values. Thus, G-CaMP imaged from PN somata appears to have low sensitivity for spiking activity, but is reasonably correlated with sustained spiking at high firing rates. The poor kinetics and high threshold of the sensor at this expression level meant that computing a transfer function between G-CaMP signal and instantaneous firing rate was not practical.

### **G-CaMP responses in glomeruli**

The response of any calcium sensor depends on the specifics of the compartment being imaged, *e.g.*, the number and types of calcium channels present locally and the existence and nature of intracellular calcium stores (Yasuda et al., 2004). In insects as in most

invertebrates, neuron somata—PNs, included—are unipolar; a primary neurite usually gives rise to “dendritic” and “axonal” compartments. The soma is thus not the integrative bottleneck that it is in most vertebrate neurons. In addition, PN glomerular neurites contain both pre- and post-synaptic specializations (Wilson et al., 2004; Olsen et al., 2007; Shang et al., 2007), and thus, likely have a high concentration of calcium channels. We investigated whether G-CaMP signals sampled from glomeruli are more sensitive than when they are measured from somata.

We compared G-CaMP signals from equally sized areas of the DL1 glomerulus and of the corresponding DL1 PN somata (*NP3529-Gal4, UAS-GCaMP* flies). Those regions were sampled successively in each experiment (3 preparations) for direct comparison. Whereas baseline fluorescence was higher in the soma, response signals ( $\Delta F/F$ ) from the two regions were qualitatively similar and of similar peak amplitude. The main differences concerned response dynamics: response onset in the glomerulus preceded that in the soma by a long interval ( $dt = 400 \pm 226$  ms between crossings of  $+2.5$  SDs of baseline; Fig 4A-D) and response-onset slope was higher (i.e., rise time was faster) in the glomerulus. This may reflect differences between actual  $[Ca^{2+}]$  changes as well as differences in the sensitivity of G-CaMP in the two compartments. First, the glomerular response is the sum of G-CaMP signal from the dendrites of 2 DL1 PNs. Second, G-CaMP expression levels are lower in the glomerulus, reducing the buffering effect of the sensor and improving its observed kinetics (Yasuda et al., 2004). Third, dendritic compartments likely have a different distribution of voltage-dependent calcium channels and different endogenous calcium buffers than the soma (Single and Borst, 2002; Baden and Hedwig, 2007).

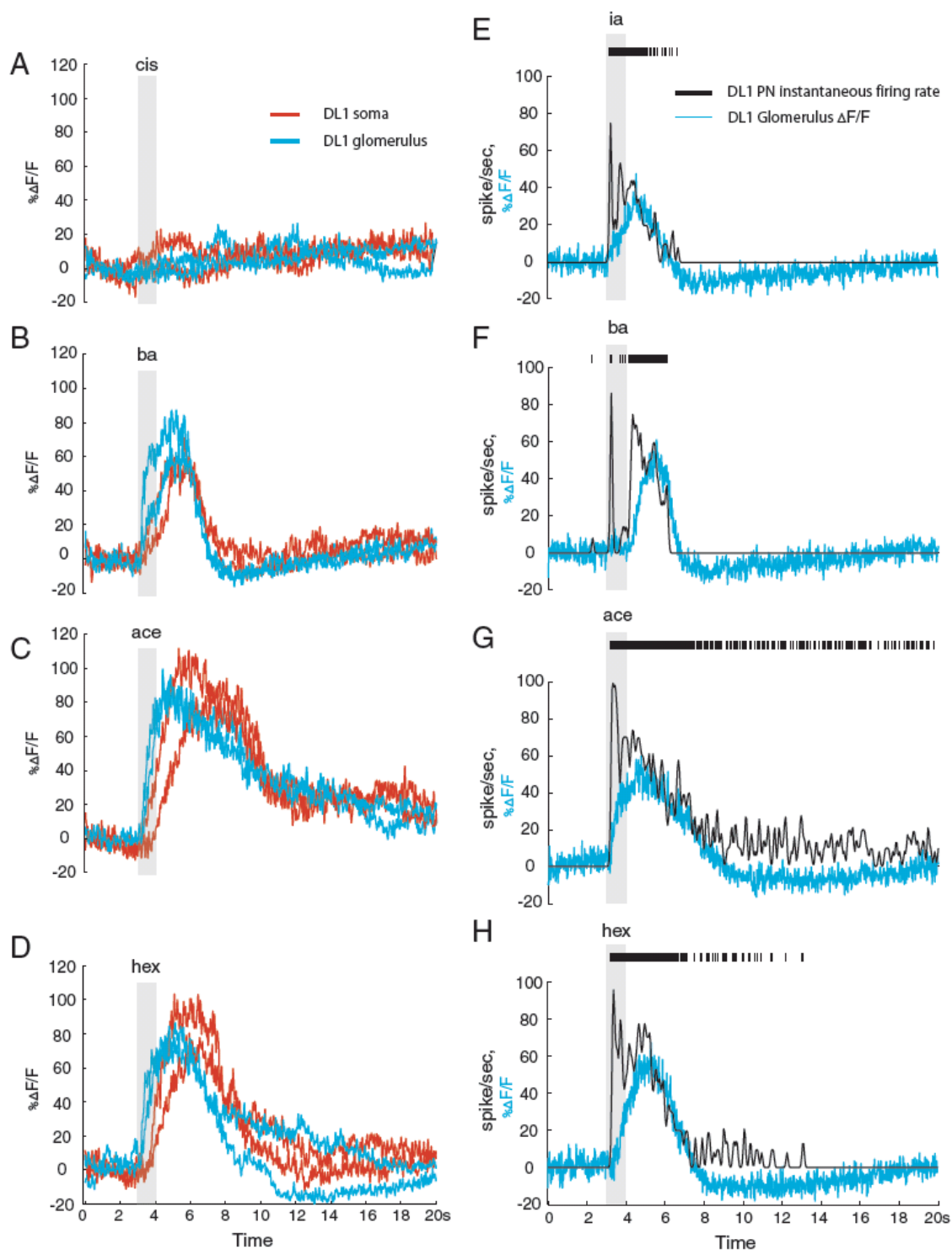


**Figure 4.** G-CaMP signal can be dependent on location imaged. **A**, Glomerular G-CaMP signal versus somatic G-CaMP signal for the same DL1 PN (*NP3529-Gal4,UAS-GCaMP* fly) shows different kinetics. Shown are two trials each of somatic and glomerular line scans (order: soma-glomerulus-soma-glomerulus, all odors tested at each step). Glomerular signal precedes somatic signal by  $400 \pm 226$ ms as measured by odor response signal exceeding 2.5SDs of baseline.

**B**, Comparison of instantaneous firing rate based on somatic electrical recordings and glomerular delta F/F. Although the G-CaMP signals show improved kinetics, they do not accurately capture the dynamics of the response, failing to correctly capture short bursts of intense electrical activity as high as 80Hz. Mean correlation between G-CaMP signal and instantaneous firing rate for these experiments =  $0.71 \pm 0.04$ .

We next combined loose-patch recordings from DL1 PN somata and G-CaMP imaging from the DL1 glomerulus. By tracking the neurites between somata and glomerulus, we could confirm the correspondence between the two recording sites (n=2 preparations). We found that the faster kinetics of the G-CaMP glomerular responses indeed better represented electrical activity in the PNs (Fig 4E-H). Yet, glomerular G-CaMP responses still failed to capture the dynamics of the PN response adequately, to the extent that even high-instantaneous-firing-rates segments of a response could go undetected if those were not sustained (Fig 4E-H). Over all trials in these experiments, G-CaMP failed to report even sustained (> 1s) activity if it was below 30 Hz or to capture fast modulations of instantaneous firing rate, even when those occurred on top of on-going plateaus of activity. For responses with significant ( $p < 0.001$ ) correlation between instantaneous firing rate and G-CaMP signal during the odor response, the average correlation was  $0.51 \pm 0.24$ . (For the experiments shown in 4E-H, the mean correlation was  $0.71 \pm 0.04$ .) Note also that fluorescence response kinetics between the two fly lines were different—the effect, presumably, of unequal promoter strengths and consequently, different levels of G-CaMP expression—lower levels producing faster kinetics (Yasuda et al., 2004; Reiff et al., 2005).

## **Discussion**

We combined *in vivo* loose-patch recordings and two-photon calcium imaging with neurons in the *Drosophila* antennal lobe, to evaluate the correspondence between stimulus-

evoked spike output and G-CaMP signals from soma or dendrites. This approach should be generally useful to evaluate genetically encoded sensors, activators and repressors of neural activity, and to refine the study of neurons first identified genetically in a larger neuron population.

While stable for many minutes, loose-patch recordings usually deteriorated enough over 30 minutes to render the recorded data unusable after this. The principal underlying reasons were electrode-clogging, large increase in seal resistance and accidental break-ins. These experiments thus needed to be performed relatively quickly. We found, however, that the expression of the calcium indicator G-CaMP by DL1 PNs had no more effect on the electrophysiological responses of these PNs than GFP expression. This suggests that G-CaMP *per se*, at the genetic dosages tested here, may have no major deleterious effect on PN spiking activity.

### **Does G-CaMP represent spiking activity faithfully?**

G-CaMP has become a widely used sensor of neural activity in *Drosophila* (Wang et al., 2003; Suh et al., 2004; Wang et al., 2004; Marella et al., 2006; Yu et al., 2006). Some studies have interpreted sparse G-CaMP signals as indicative of sparse neuronal responses in the regions targeted for imaging (Wang et al., 2003; Wang et al., 2004; Marella et al., 2006). Our results, however, indicate that G-CaMP is a low-sensitivity indicator of spiking activity that misses even high instantaneous discharge rates if activity is not sustained. G-CaMP responses show different kinetics and sensitivity when examined in the soma and dendritic compartments, or in different fly lines. This variability might arise because of

spatial differences in the expression levels of G-CaMP, in baseline calcium levels and in the local calcium environment (channels, intracellular stores, buffers). If generally applicable, our findings suggest that conclusions about neural coding based on G-CaMP imaging should be made with caution. In addition to general calibration tests in systems more amenable to electrophysiology (e.g., cultured slices; (Pologruto et al., 2004); *Drosophila* larval neuromuscular junction; (Reiff et al., 2005), careful tests should be carried out in the specific systems of interest. The mismatch we observe also provides one possible explanation for the discrepancy between electrophysiological (Wilson et al., 2004; Olsen et al., 2007) and G-CaMP imaging (Wang et al., 2003) measurements of PN tuning. A high threshold of G-CaMP activation would of course artificially sparsen apparent odor-evoked activity. There may be yet other reasons for the different results: differences in the preparation (whole fly with intact antennae and palps instead of isolated antennae-brain preparations), saline, odor concentrations and odor delivery systems used, holding potentials and consequences of whole-cell recordings (e.g., dialysis) affecting the odor responses seen. More broadly, our findings suggest that, at least at the expression level tested, G-CaMP appears not to have the combination of high signal-to-noise ratio, low threshold of activation and linear (or at least quantifiable) relationship to spiking activity that would make it a suitable substitute for electrophysiological approaches. Expression level is known to have effects on the kinetics and signal-to-noise ratio of calcium sensors (Yasuda et al., 2004; Reiff et al., 2005) and we find that lower levels of expression of G-CaMP might indeed have significantly faster kinetics.

The technique of two-photon targeted loose-patch recordings provides a useful tool for calibration of sensors *in vivo* in neurons of interest in the fly brain. Our results show that calibration is crucial for the correct interpretation of signals from such reporters. The method should also be more broadly useful in studies where imaging can be used to identify loci of interest that can then be targeted for further and more sensitive exploration with an electrode.

The results from testing G-CaMP as a high-resolution reporter of neural activity indicate that this indicator may be ill suited to studies focused on neural coding. However recent reports of the development of new and improved sensors (Reiff et al., 2005; Mank et al., 2006) suggest that there is reason for optimism.

## **Materials and Methods**

*Fly stocks.* Flies were reared on standard cornmeal agar medium. We used the Gal4/UAS-system (Brand and Perrimon, 1993) to direct the expression of the calcium sensor G-CaMP (Nakai et al., 2001) to specific cells. *GHI46-Gal4* flies were a gift from L. Luo (Stanford University, Stanford, CA). *UAS-GCaMP* flies were a gift from R. Axel (Columbia University, New York, NY). *NP3529-Gal4* flies were a gift from K. Ito (The University of Tokyo, Japan). All experimental animals were adult females, 1-2 d after eclosion.

*Fly preparation.* Adult flies were dissected using recently described methods (Wilson et al., 2004). Flies were anesthetized in a glass vial on ice just until movement stopped (~15 sec.) and then gently inserted into a hole in a piece of aluminum foil. Small drops of wax (55°C)

were used to suspend the fly in the hole, with the edge of foil defining a horizontal plane around the head and thorax, from the first antennal segment anteriorly to the scutellum posteriorly. The dorsal side of the foil was bathed in saline, while the ventral side (including antennae and maxillary palps) remained dry and accessible to odors. A window was cut in the dorsal head cuticle between the eyes, extending from the ocelli to the first antennal segment. Fat and air sacs dorsal and anterior to the brain were removed, and the perineural sheath was gently picked away from the antennal lobes. In some preparations, brief exposure to a collagenase solution was used to weaken the sheath; activity in these brains was not noticeably different from brains desheathed mechanically. The proboscis was affixed with a small drop of wax to a strand of human hair to limit brain movement. To further limit brain movement, the pair of small muscles (muscle 16) lying between and ventral to the antennal nerves was also removed. Spontaneous leg movements were typically observed in this preparation for the duration of the recording (1.5-3 hours). The saline composition used in all experiments was (Wang et al., 2003): 108 mM NaCl, 5 mM KCl, 2 mM CaCl<sub>2</sub>, 8.2 mM MgCl<sub>2</sub>, 4 mM NaHCO<sub>3</sub>, 1 mM NaH<sub>2</sub>PO<sub>4</sub>, 5 mM trehalose, 10 mM sucrose, 5 mM HEPES [pH 7.5, 265 mOsm].

*Odor delivery.* Odors (*cis*-3-hexen-1-ol (*cis*), benzaldehyde (*ba*), isoamyl acetate (*ia*), 1-hexanol (*hex*), eugenol (*eug*), acetophenone (*ace*), citral (*cit*), cherry (*che*)) were delivered using a custom-made odor-delivery system and a Teflon nozzle (entry diameter 1 cm, exit ~0.1 cm) directed towards the antennae. Odors were delivered in a constant stream of air (0.4-0.8 l/s) at final concentrations of ca. 0.5% to 50%. The results reported are based on data obtained from 31 PNs in 29 flies. Not all odors could be tested in all animals and the

number of trials of each odor presented varied from 1 to 6, depending on the stability of the recording.

*Electrophysiology: sharp recordings.* Thick (1.0 mm OD, 0.58 mm ID)-walled borosilicate electrodes with filament (Harvard Apparatus, Holliston, MA) were pulled on a Sutter Instruments (Novato, CA) P2000 horizontal laser puller and filled with a solution containing 1 mM sulforhodamine B (Molecular Probes, Eugene, OR) in 1 M potassium acetate (DC resistance: 300-400 M $\Omega$ ). PNs were impaled by targeting their soma (~4  $\mu$ m diameter) under two-channel imaging using the 2-photon microscope (see Fig 1). Useable recordings lasted between 5 and 20 minutes. Data were acquired via an Axoclamp 2B amplifier (Axon Instruments, Union City, CA), a National Instruments A-D card (15 kHz sampling) and LabView software (National Instruments, Austin, TX).

*Electrophysiology: Loose-patch recordings.* Patch-clamp electrodes (4-5 M $\Omega$ ) were pulled on a Sutter Instruments (Novato, CA) P87 horizontal puller and pressure polished before filling with a solution containing 0.1 mM sulforhodamine B (Molecular Probes, Eugene, OR) in saline solution. PNs were approached using two-channel imaging (Margrie et al., 2003) on a two-photon microscope (see Fig 1B). Low resistance (100-300 M $\Omega$ ) seals allowed spikes to be reliably detectable for up to 40 minutes, although some useable recordings lasted only 5 minutes before an increase in seal resistance or spontaneous break-in. Current data were acquired via an Axopatch-1D amplifier (Axon Instruments, Union City, CA), a National Instruments A-D card (15 kHz sampling) and LabView software (National Instruments, Austin, TX).

*Spike detection.* To detect spikes in loose patch recordings, we used a combination of criteria that were kept constant for all traces recorded during an experiment. The current traces were first bandpass filtered (10Hz-1kHz) and then boxcar filtered (~1ms window). We then passed the traces through an amplitude threshold that was held constant for all trials of a given PN. Negative peaks detected in this thresholded trace were considered candidate spikes and were subjected to two further tests. First, we applied a slope threshold by computing the deflection from the negative peak to a point on the trace 2ms later. This threshold—typically twice the amplitude threshold in magnitude, and always held constant for all trials of a given PN—was typically sufficient for clean spike detection (evaluated both manually and by clustering—see Fig 1D). However, for a few noisier recordings, we performed another test by using a template spike. The template spike was chosen by eye. Thresholding the dot product of this waveform with all spike candidates was sufficient to resolve remaining ambiguities.

*Imaging.* A two-photon microscope based on a galvanometric-mirrors-scan-system (Denk et al., 1990) and proximal detection (Radiance 2001; BioRad, Hercules, CA) coupled to an upright microscope (BX51-WI; Olympus, Japan) was used to image calcium signals from PNs. A mode-locked Ti: sapphire laser (Tsunami-10W pump; Spectra Physics, Mountain View, CA) tuned to 920-935 nm was used as excitation light. A whole-field DOT-system used in reflection allowed precise positioning of the brain and electrode, mounted on XY-translation stages. Non pre-chirped excitation pulses were focused onto labeled PNs using a 40x 0.75 NA or 63x 0.90 NA water immersion lens (Leica Microsystems, Germany). The

epi-collected fluorescence was bandpass filtered (Green: HQ515-30, Red: HQ620-100, Chroma Technology, Rockingham, VT) and detected with two photomultiplier tubes (bi-alkali photo cathode; Electron Tubes, UK), one for each channel (red to visualize the electrode and green for the cell, see Fig 1B). Application of up to 50 mW into the sample was sufficient to image somata located at a depth of up to 50  $\mu\text{m}$ . To minimize photodamage, excitation power was adjusted with the depth of the focal plane using a liquid crystal based attenuator (NewPort, Irvine, CA) and kept to a minimum for sufficient S/N ratio. No apparent changes in PN morphology, calcium signal or electrical properties resulted from laser illumination. Twenty-four second-long line scans (512 pixel lines at 500 Hz or 600 Hz) were performed across the width of individual somata in their equatorial plane, and acquired with 16-bit resolution. Imaging and physiological data acquisitions were synchronized with a precision  $<1$  ms from a common pulsed command.

*Data analysis.* Electrophysiological and line-scan data were combined and analyzed off-line using LabView (National Instruments, Austin, TX) and MATLAB (The MathWorks Inc., Natick MA) software. For line-scan data, we excluded the first two seconds of data, and then performed a linear bleach correction using a scale factor calculated using fluorescence levels for one second before the odor stimulus was delivered (4-5s) and one second before the end of the line-scan (23-24s). Consistent with previous results (Reiff et al., 2005), photobleaching appeared to increase with increases in fluorescence intensity, explaining the dips seen in G-CaMP signal immediately after strong responses. Data were box-car filtered (20 ms for all comparisons with electrophysiology and in Fig 4; 40 ms otherwise) before further analysis. In all cases fluorescence changes were calculated

relative to baseline fluorescence levels as determined by averaging over 2s just before odor presentation. To compute first detectable deviations from baselines, we used a threshold of 2.5 SDs. Times reported are when imaging signal first rose above this threshold.

## Acknowledgements

This work was supported by grants from the National Institute for Deafness and Communication Disorders and the National Science Foundation (GL) and a pre-doctoral fellowship from the Sloan-Swartz Center for Theoretical Neurobiology at Caltech (VJ). We would like to thank Glenn Turner for his generous advice throughout the project, and Rachel Wilson for her helpful tutoring on the fly preparation. We would also like to thank Laurent Moreaux for his assistance with two-photon microscopy and for technical advice, Mala Murthy for useful input and *NP3529-Gal4, UAS-eGFP* flies, Stijn Cassenaer, Benjamin Rubin and Anusha Narayan and other members of the Laurent lab for useful technical discussions throughout the course of the project, and Suzuko Yoroza for advice on fly husbandry. Thanks also to Allan Wong for useful discussions.

## References

- Baden T, Hedwig B (2007) Neurite-specific Ca<sup>2+</sup> dynamics underlying sound processing in an auditory interneurone. *Dev Neurobiol* 67:68-80.
- Benzer S (1967) Behavioral mutants of *Drosophila* isolated by countercurrent distribution. *Proc Natl Acad Sci USA* 58:1112-1119.
- Brand AH, Perrimon N (1993) Targeted gene expression as a means of altering cell fates and generating dominant phenotypes. *Development* 118:401-415.
- Cohen LB, Salzberg BM (1978) Optical measurement of membrane potential. *Rev Physiol Biochem Pharmacol* 83:35-88.
- Cohen LB, Salzberg BM, Grinvald A (1978) Optical methods for monitoring neuron activity. *Annu Rev Neurosci* 1:171-182.
- Denk W, Strickler JH, Webb WW (1990) Two-photon laser scanning fluorescence microscopy. *Science* 248:73-76.
- Fiala A, Spall T, Diegelmann S, Eisermann B, Sachse S, Devaud JM, Buchner E, Galizia CG (2002) Genetically expressedameleon in *Drosophila melanogaster* is used to visualize olfactory information in projection neurons. *Curr Biol* 12:1877-1884.

- Grinvald A, Hildesheim R (2004) VSDI: a new era in functional imaging of cortical dynamics. *Nat Rev Neurosci* 5:874-885.
- Grynkiewicz G, Poenie M, Tsien RY (1985) A new generation of Ca<sup>2+</sup> indicators with greatly improved fluorescence properties. *J Biol Chem* 260:3440-3450.
- Hotta Y, Benzer S (1970) Genetic Dissection of Drosophila Nervous System by Means of Mosaics. *Proceedings of the National Academy of Sciences of the United States of America* 67:1156-&.
- Mank M, Reiff DF, Heim N, Friedrich MW, Borst A, Griesbeck O (2006) A FRET-based calcium biosensor with fast signal kinetics and high fluorescence change. *Biophys J* 90:1790-1796.
- Marella S, Fischler W, Kong P, Asgarian S, Rueckert E, Scott K (2006) Imaging taste responses in the fly brain reveals a functional map of taste category and behavior. *Neuron* 49:285-295.
- Margrie TW, Meyer AH, Caputi A, Monyer H, Hasan MT, Schaefer AT, Denk W, Brecht M (2003) Targeted whole-cell recordings in the mammalian brain in vivo. *Neuron* 39:911-918.
- Miyawaki A, Llopis J, Heim R, McCaffery JM, Adams JA, Ikura M, Tsien RY (1997) Fluorescent indicators for Ca<sup>2+</sup> based on green fluorescent proteins and calmodulin. *Nature* 388:882-887.
- Nakai J, Ohkura M, Imoto K (2001) A high signal-to-noise Ca(2+) probe composed of a single green fluorescent protein. *Nat Biotechnol* 19:137-141.
- Ng M, Roorda RD, Lima SQ, Zemelman BV, Morcillo P, Miesenbock G (2002) Transmission of olfactory information between three populations of neurons in the antennal lobe of the fly. *Neuron* 36:463-474.
- Olsen SR, Bhandawat V, Wilson RI (2007) Excitatory Interactions between Olfactory Processing Channels in the Drosophila Antennal Lobe. *Neuron* 54:89-103.
- Persechini A, Lynch JA, Romoser VA (1997) Novel fluorescent indicator proteins for monitoring free intracellular Ca<sup>2+</sup>. *Cell Calcium* 22:209-216.
- Pologruto TA, Yasuda R, Svoboda K (2004) Monitoring neural activity and [Ca<sup>2+</sup>] with genetically encoded Ca<sup>2+</sup> indicators. *J Neurosci* 24:9572-9579.

- Quinn WG, Harris WA, Benzer S (1974) Conditioned behavior in *Drosophila melanogaster*. *Proc Natl Acad Sci U S A* 71:708-712.
- Reiff DF, Ihring A, Guerrero G, Isacoff EY, Joesch M, Nakai J, Borst A (2005) In vivo performance of genetically encoded indicators of neural activity in flies. *J Neurosci* 25:4766-4778.
- Sakmann B, Neher E (1984) Patch clamp techniques for studying ionic channels in excitable membranes. *Annu Rev Physiol* 46:455-472.
- Schroll C, Riemensperger T, Bucher D, Ehmer J, Voller T, Erbguth K, Gerber B, Hendel T, Nagel G, Buchner E, Fiala A (2006) Light-induced activation of distinct modulatory neurons triggers appetitive or aversive learning in *Drosophila* larvae. *Curr Biol* 16:1741-1747.
- Shang Y, Claridge-Chang A, Sjulson L, Pypaert M, Miesenbock G (2007) Excitatory local circuits and their implications for olfactory processing in the fly antennal lobe. *Cell* 128:601-612.
- Single S, Borst A (2002) Different mechanisms of calcium entry within different dendritic compartments. *J Neurophysiol* 87:1616-1624.
- Stosiek C, Garaschuk O, Holthoff K, Konnerth A (2003) In vivo two-photon calcium imaging of neuronal networks. *Proc Natl Acad Sci U S A* 100:7319-7324.
- Su H, O'Dowd DK (2003) Fast synaptic currents in *Drosophila* mushroom body Kenyon cells are mediated by alpha-bungarotoxin-sensitive nicotinic acetylcholine receptors and picrotoxin-sensitive GABA receptors. *J Neurosci* 23:9246-9253.
- Suh GS, Wong AM, Hergarden AC, Wang JW, Simon AF, Benzer S, Axel R, Anderson DJ (2004) A single population of olfactory sensory neurons mediates an innate avoidance behaviour in *Drosophila*. *Nature*.
- Svoboda K, Denk W, Kleinfeld D, Tank DW (1997) In vivo dendritic calcium dynamics in neocortical pyramidal neurons. *Nature* 385:161-165.
- Tanaka NK, Awasaki T, Shimada T, Ito K (2004) Integration of chemosensory pathways in the *Drosophila* second-order olfactory centers. *Curr Biol* 14:449-457.
- Tank DW, Sugimori M, Connor JA, Llinas RR (1988) Spatially resolved calcium dynamics of mammalian Purkinje cells in cerebellar slice. *Science* 242:773-777.

- Taylor AL, Cottrell GW, Kleinfeld D, Kristan WB, Jr. (2003) Imaging reveals synaptic targets of a swim-terminating neuron in the leech CNS. *J Neurosci* 23:11402-11410.
- Wang JW, Wong AM, Flores J, Vosshall LB, Axel R (2003) Two-photon calcium imaging reveals an odor-evoked map of activity in the fly brain. *Cell* 112:271-282.
- Wang Y, Guo HF, Pologruto TA, Hannan F, Hakker I, Svoboda K, Zhong Y (2004) Stereotyped odor-evoked activity in the mushroom body of *Drosophila* revealed by green fluorescent protein-based Ca<sup>2+</sup> imaging. *J Neurosci* 24:6507-6514.
- Wilson RI, Laurent G (2005) Role of GABAergic inhibition in shaping odor-evoked spatiotemporal patterns in the *Drosophila* antennal lobe. *J Neurosci* 25:9069-9079.
- Wilson RI, Turner GC, Laurent G (2004) Transformation of olfactory representations in the *Drosophila* antennal lobe. *Science* 303:366-370.
- Yasuda R, Nimchinsky EA, Scheuss V, Pologruto TA, Oertner TG, Sabatini BL, Svoboda K (2004) Imaging calcium concentration dynamics in small neuronal compartments. *Sci STKE* 2004:pl5.
- Yu D, Ponomarev A, Davis RL (2004) Altered representation of the spatial code for odors after olfactory classical conditioning; memory trace formation by synaptic recruitment. *Neuron* 42:437-449.
- Yu D, Akalal DB, Davis RL (2006) *Drosophila* alpha/beta mushroom body neurons form a branch-specific, long-term cellular memory trace after spaced olfactory conditioning. *Neuron* 52:845-855.

## Supplementary Information

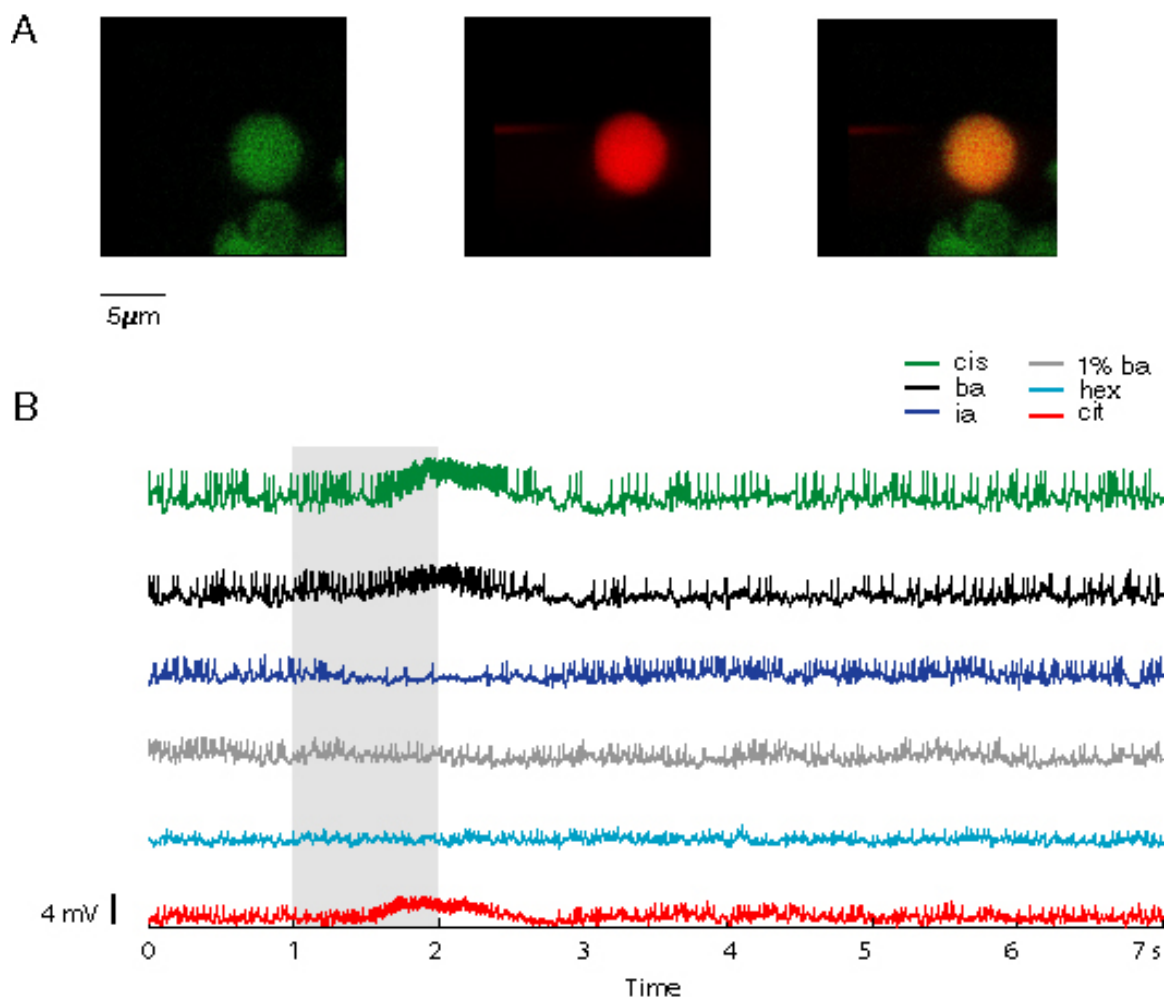


**Figure S1.** Intracellular (sharp) recording from PN in *GH146-Gal4,UAS-GCaMP* fly. **A**, Two-channel imaging showing (from left) images in the green, and red channels; image on right is an image created from merging the two channels. Identity of the cell recorded from is confirmed by filling with sulforhodamine B. **B**, Electrophysiological recordings from the PN above. Shown are voltage traces in response to 6 different odor presentations (grey bar). Deterioration of the quality of the recording is clearly evident in the decreasing amplitude of the spikes.

## *Chapter 5*

### **CONCLUDING REMARKS**

The previous three chapters describe the major results from my thesis research. Below, I summarize my main findings, briefly outline the significance of my results, and suggest where one might go from here.

#### **5.1 Ensemble coding in the locust olfactory system**

##### 5.1.1 Summary of results

The work presented in Chapters 2 and 3 of this thesis focuses on how odors are encoded and decoded across intensities, and under different initial and background (odor) conditions.

Animals can accurately identify odors across a wide range of intensities (Bhagavan and Smith, 1997), but firing patterns of individual olfactory neurons, e.g., locust PNs and rat mitral cells (Harrison and Scott, 1986), can change dramatically with odor intensity. The quantitative analyses in Chapter 2 show that a decoding scheme that is based not on single PNs, but on ensembles of PNs, can resolve the possible confounding of identity and intensity. Ensemble PN responses to an odor presented at different concentrations can be represented as different trajectories on a single odor manifold in PN phase space, with responses to other odors lying on separate manifolds. There is sufficient invariance in the firing patterns of ensembles of PNs for odor identity to be accurately extracted across a range of concentrations. This is reflected in the firing of the population of downstream decoders, the KCs, which can show both concentration specificity and invariance in their responses.

Concentration differences are just one of the many complexities of the odor environment that can confront an animal. Odors in nature are seldom encountered in isolation and identifying odors under noisy odor conditions can be challenging. The work in Chapter 3

uses overlapping odor stimuli to probe how the locust olfactory system deals with the issue of stimulus history. The results, which are based on the application of a combination of linear and nonlinear computational techniques, suggest that the PN ensemble can accurately keep track of an odor under most conditions where it partially overlaps with another. Under some overlap conditions however, the ensemble response to one odor can mask that to a following odor. In some pulse conditions, the ensemble can reach states quite different from those reached in response to both the individual odors and their static binary mixture. Such observations led to predictions for particular types of response patterns in KCs. Actual KC responses bore out these predictions providing support for the ensemble encoding and piecewise, time-slice based decoding model of the AL-MB system.

### 5.1.2 Significance of results

There has been an explosion in studies of neural coding in the past decade. A relatively small number of these studies have attempted to decode information carried by a population of neurons (Wessberg et al., 2000; Hung et al., 2005; Brincat and Connor, 2006). The decoding schemes used, however, do not usually have strong biological justification because the relevant properties of true (neural) recipients of the information are not known. Extensive prior work done in the early locust olfactory system provides us with the rare opportunity to employ decoding schemes that are similar to—albeit not yet the same as—those employed by cells downstream of those being studied.

The studies in Chapters 2 and 3 examine neural coding and decoding under conditions where it is possible to record from a fairly large percentage of encoding neurons (PNs) in a given area (the AL), predict how the ensemble population responses are decoded over time, and then test those predictions by recording from a large number of decoding neurons (KCs in the MB). This enables a more complete understanding of circuit function and allows subtle predictions to be tested. An example is the prediction—based on a quantitative analysis of PN ensemble responses—of the existence of KCs that respond specifically during particular times of certain specific odor-overlap conditions, but do not respond to individual odors or their static binary mixture.

Most prior studies of olfactory coding have examined responses of groups of single neurons to single pulses of odor. This has been partly due to limitations of technology, something that the development of tetrode recording and quantitatively rigorous methods of spike sorting (Buzsaki, 2004) have helped overcome. The work discussed in this thesis goes beyond single-neuron analysis and demonstrates how an ensemble-based view of odor processing offers some novel insights on issues in mixture and concentration coding. There is biological justification for such an approach, because, with exceptions such as those seen in the coding of odors specifically involved in innate behaviors (Suh et al., 2004), a large fraction of neural information processing likely happens at the level of the population.

Finally, this thesis makes a significant contribution in the area of neuronal data visualization and analysis. Many labs now routinely record from large populations of neurons simultaneously (Buzsaki, 2004). The data from such recordings can be challenging to understand, and the identification of appropriate analysis and visualization tools is itself an active area of research (Brown et al., 2004; Kass et al., 2005). In this thesis, I apply LLE, a relatively recent nonlinear dimensionality reduction technique (Roweis and Saul, 2000), to neuronal data for the first time, and employ it to visualize data from up to 110 PNs in 3D. The studies in Chapters 2 and 3 demonstrate the utility of such a tool and its linear counterparts—PCA and MDA, which have been used in neuronal data analysis before (Optican and Richmond, 1987; Nicolelis et al., 1997)—in describing the dynamics of a neuronal ensemble.

### 5.1.3 Future directions

These ensemble coding studies represent only the first steps towards a more biologically accurate analysis of PN data. Although some of the mechanisms underlying how KCs decode their PN ensemble input are known (Laurent, 2002; Perez-Orive et al., 2002; Jortner et al., 2007), a more careful statistical analysis of PN and KC response statistics is necessary to fully understand the relative importance of different factors involved in the process, such as time-scales of across-PN synchrony, PN-KC connectivity, limited integration time windows (coincidence detection) of KCs, and feedforward and feedback inhibition. Such an investigation would be best carried out on a larger dataset than that used

in the present work. Ideally, this study would record responses of large populations of PNs and KCs simultaneously with the LFP. The phase of PN spikes relative to the population could then be used to integrate ensemble responses pooled across experiments.

The methods used here do not yet fully capture the current understanding of how KCs integrate their input. One way forward would be to use simple model KCs to decode ensemble PN activity. The responses of the population of model KCs could then be compared with real KC data. The complexity of the model KCs could be gradually increased to better match real KC data, and the relative importance of different features of the AL-MB system more systematically assessed.

A related issue is how important the sparseness and precision of timing of KC spiking is to the downstream cells in the mushroom body lobes. If their integration time windows are large enough, some of the nuances of PN-KC encoding and decoding may be less relevant to the function of the circuit.

The studies make predictions for both the circuit—something tested by examining KC responses—and the animal. There is currently a huge mismatch between the subtle predictions about odor discrimination and memory made by our experiments and models, and the kinds of behavioral studies that would be required to fully validate them. Closing that gap, whether in locusts or other species more amenable to behavioral experiments, would add significantly to the value of these studies.

Changing the concentration and initial odor conditions are just two stimulus manipulations that are informative about how the locust olfactory circuitry works. There are numerous variations of stimulus conditions—explorations of larger odor sets, mixtures with different numbers of components and background odors, to name a few—that would all help further constrain the working model of the functioning of the circuit as well as improve our understanding of olfactory coding under more naturalistic conditions. Recording PN and KC responses with large odor sets would also enable a thorough exploration of PN phase space and its relation to KC tuning.

The methods used in the studies in this thesis are sufficient to visualize how a few odors are represented in PN phase space. They are, however, inadequate to visualize dynamic representations of tens and hundreds of odors, the olfactory space that the locust is actually confronted by in nature and that the system has presumably evolved to deal with. New and perhaps as yet non-existent analysis and visualization techniques will need to be employed for such purposes. In addition, LLE is not easily interpretable in terms of raw data (ensemble activity of PNs), and, while it is useful as a descriptive tool, distances in LLE-space do not directly map to neural activity because the transformation is non-unique, nonlinear and one-way. Recent developments (Hinton and Salakhutdinov, 2006) may offer solutions that are quantitatively more rigorous.

## **5.2 Simultaneous electrophysiology and imaging of fruit fly neurons**

### 5.2.1 Summary of results

The focus of Chapter 4 is experimental work that represents a significant technical development: electrophysiological recordings from neurons in the adult fruit fly brain that express the genetically expressible calcium sensor G-CaMP (Nakai et al., 2001; Wang et al., 2003) whose signal is being simultaneously monitored optically with a two-photon laser scanning microscope (Denk et al., 1990; Svoboda and Yasuda, 2006).

Genetically expressible sensors allow the activity of particular subsets of identified neurons to be monitored. However, before the signal from such sensors can be interpreted, it is important to verify that they do not affect the behavior of the neurons that they are expressed in, and to understand how their signal relates to spiking activity of the neurons under observation. Imaging fly PNs while simultaneously recording from them enables a quantitative analysis of the abilities of G-CaMP as a sensor of neuronal activity. The results suggest that this version of G-CaMP (G-CaMP 1.3) does not, at the expression levels tested here, affect the spontaneous or response firing properties of neurons it is expressed in. The most important problems with G-CaMP have to do with temporal resolution, consistency and threshold: the sensor lacks the sensitivity to pick up faster dynamics and underreports low firing rate activity, and G-CaMP response may depend to some extent on the strength

of the promoter used to drive its expression. In its present form, it thus has limited utility as a tool to study neural coding. However, it can be useful as a tool to identify cells and areas of possible interest that can then be targeted with an electrode for finer-time-scale examination. The techniques developed and described in Chapter 4 allow for just such explorations. In addition, they provide a means to calibrate future sensors, activators and repressors of neural activity (Mank et al., 2006).

### 5.2.2 Significance of results

The fruit fly has long been the favored organism for behavioral geneticists (Benzer, 1967; Hotta and Benzer, 1970; Quinn et al., 1974). More recently, it has become possible to record the physiology of the small neurons in the fly brain (Wilson et al., 2004). This makes possible the combined use of genetics, physiology and behavior to answer important questions in systems neuroscience. However, the only currently available means to monitor the activity of large numbers of neurons simultaneously is calcium imaging. Recent advances in the design of calcium sensors have allowed for such sensors to be expressed only in genetically identified neurons. Such sensors are very easy to use—unlike synthetic dyes, there is nothing to be injected or loaded, and imaging only requires a small window to be cut out in the cuticle of the fly. As important as such an advance clearly is, there is the danger that the signal from such sensors can be over interpreted. An important step is therefore to understand what the signal actually represents in terms of neuronal firing. The development of techniques to perform such a calibration is therefore of considerable value.

Using the loose-patch technique as opposed to whole-cell patch clamp has the advantage that it leaves the cell and its contents relatively intact. Thus, this technique will be useful in all experiments that require recording only the output of spiking neurons, rather than their subthreshold activity.

Sharp electrode recordings have not previously been reported in fruit fly brain neurons. Although this technique is not ideal for the small cells of the fly brain, it could be very useful for recording from large deep neurons where whole-cell patch clamp recordings are harder to perform. Recording simultaneously using loose-patch electrophysiology and two-

photon imaging from brain neurons of the intact fruit fly is a technical advance that has not previously been reported. A big advantage of the combination of techniques is that cells that are identified to be of interest based on imaging can then be targeted and recorded from with higher resolution. This should be an important tool for circuit exploration.

### 5.2.3 Future directions

The combination of simultaneous two-photon targeted electrophysiology and imaging of fly brain neurons can be applied to a wide range of questions. The combination of these techniques with genetically expressible activators (Boyden et al., 2005; Lima and Miesenbock, 2005; Zhang et al., 2006) of neural activity can be applied to map the functional circuitry of the fly brain. A major advantage of performing these recordings in intact flies is that their behavioral responses can also be monitored simultaneously, opening the possibility of establishing causal links between neural activity patterns and behavior. It is also possible that a different technical strategy may be better for imaging to work in the fly. Hybrid strategies used in different systems to achieve higher temporal resolution include using synthetic extracellular dyes in combination with simple GFP-markers of identified neurons (Yaksi and Friedrich, 2006) and using hybrid systems with a voltage-sensitive component (Chanda et al., 2005), but these have not yet been shown to work in fruit flies.

## BIBLIOGRAPHY

- Abeles M, Bergman, H., Margalit, E., and Vaadia, E. (1993) Spatiotemporal firing patterns in the frontal cortex of behaving monkeys. *J Neurophysiol* 70:1629-1638.
- Adrian E (1942) Olfactory reactions in the brain of a hedgehog. *J Physiol (Lond)* 100:459-473.
- Aksay E, Major G, Goldman MS, Baker R, Seung HS, Tank DW (2003) History dependence of rate covariation between neurons during persistent activity in an oculomotor integrator. *Cereb Cortex* 13:1173-1184.
- Averbeck BB, Latham PE, Pouget A (2006) Neural correlations, population coding and computation. *Nature Reviews Neuroscience* 7:358-366.
- Baden T, Hedwig B (2007) Neurite-specific Ca<sup>2+</sup> dynamics underlying sound processing in an auditory interneurone. *Dev Neurobiol* 67:68-80.
- Bair W (1999) Spike timing in the mammalian visual system. *Curr Opin Neurobiol* 9:447-453.
- Bartlett EL, Wang X (2005) Long-lasting modulation by stimulus context in primate auditory cortex. *J Neurophysiol* 94:83-104.
- Bazhenov M, Stopfer M, Sejnowski TJ, Laurent G (2005) Fast odor learning improves reliability of odor responses in the locust antennal lobe. *Neuron* 46:483-492.
- Bazhenov M, Stopfer M, Rabinovich M, Abarbanel HD, Sejnowski TJ, Laurent G (2001a) Model of cellular and network mechanisms for odor-evoked temporal patterning in the locust antennal lobe. *Neuron* 30:569-581.
- Bazhenov M, Stopfer M, Rabinovich M, Huerta R, Abarbanel HD, Sejnowski TJ, Laurent G (2001b) Model of transient oscillatory synchronization in the locust antennal lobe. *Neuron* 30:553-567.
- Benzer S (1967) Behavioral mutants of *Drosophila* isolated by countercurrent distribution. *Proc Natl Acad Sci USA* 58:1112-1119.
- Bertschinger N, Natschlagler T (2004) Real-time computation at the edge of chaos in recurrent neural networks. *Neural Comput* 16:1413-1436.

- Bhagavan S, Smith BH (1997) Olfactory conditioning in the honey bee, *Apis mellifera*: effects of odor intensity. *Physiol Behav* 61:107-117.
- Boyden ES, Zhang F, Bamberg E, Nagel G, Deisseroth K (2005) Millisecond-timescale, genetically targeted optical control of neural activity. *Nat Neurosci* 8:1263-1268.
- Brand AH, Perrimon N (1993) Targeted gene expression as a means of altering cell fates and generating dominant phenotypes. *Development* 118:401-415.
- Braunig P (1997) The peripheral branching pattern of identified dorsal unpaired median (DUM) neurones of the locust. *Cell Tissue Res* 290:641-654.
- Brincat SL, Connor CE (2006) Dynamic shape synthesis in posterior inferotemporal cortex. *Neuron* 49:17-24.
- Brody CD, Hopfield JJ (2003) Simple networks for spike-timing-based computation, with application to olfactory processing. *Neuron* 37:843-852.
- Broome BM, Jayaraman V, Laurent G (2006) Encoding and decoding of overlapping odor sequences. *Neuron* 51:467-482.
- Brown EN, Kass RE, Mitra PP (2004) Multiple neural spike train data analysis: state-of-the-art and future challenges. *Nat Neurosci* 7:456-461.
- Brown SL, Joseph J, Stopfer M (2005) Encoding a temporally structured stimulus with a temporally structured neural representation. *Nat Neurosci* 8:1568-1576.
- Buck LB, Axel R (1991) A novel multigene family may encode odorant receptors: a molecular basis for odor recognition. *Cell* 65:175-187.
- Buzsaki G (2004) Large-scale recording of neuronal ensembles. *Nat Neurosci* 7:446-451.
- Buzsaki G, Draguhn A (2004) Neuronal oscillations in cortical networks. *Science* 304:1926-1929.
- Chalfie M, Tu Y, Euskirchen G, Ward WW, Prasher DC (1994) Green fluorescent protein as a marker for gene expression. *Science* 263:802-805.
- Chanda B, Blunck R, Faria LC, Schweizer FE, Mody I, Bezanilla F (2005) A hybrid approach to measuring electrical activity in genetically specified neurons. *Nat Neurosci* 8:1619-1626.
- Chapman R (1998) *The Insects: Structure and Function*, 4th Edition. Cambridge: Cambridge University Press.

- Clyne PJ, Warr CG, Freeman MRLD, Kim J, Carlson JR (1999) A novel family of divergent seven-transmembrane proteins: Candidate odorant receptors in *Drosophila*. *Neuron* 22:327-338.
- Cohen LB, Salzberg BM (1978) Optical measurement of membrane potential. *Rev Physiol Biochem Pharmacol* 83:35-88.
- Cohen LB, Salzberg BM, Grinvald A (1978) Optical methods for monitoring neuron activity. *Annu Rev Neurosci* 1:171-182.
- Csicsvari J, Henze DA, Jamieson B, Harris KD, Sirota A, Bartho P, Wise KD, Buzsaki G (2003) Massively parallel recording of unit and local field potentials with silicon-based electrodes. *J Neurophysiol* 90:1314-1323.
- Davis RL (1993) Mushroom bodies and *Drosophila* learning. *Neuron* 11:1-14.
- Dayan P, Abbott L (2001) *Theoretical Neuroscience: Computational and Mathematical Modeling of Neural Systems*. Cambridge: MIT Press.
- de Bruyne M, Foster K, Carlson JR (2001) Odor coding in the *Drosophila* antenna. *Neuron* 30:537-552.
- Denk W, Strickler JH, Webb WW (1990) Two-photon laser scanning fluorescence microscopy. *Science* 248:73-76.
- Drake KL, Wise KD, Farraye J, Anderson DJ, BeMent SL (1988) Performance of planar multisite microprobes in recording extracellular single-unit intracortical activity. *IEEE Trans Biomed Eng* 35:719-732.
- Duda R, Hart P, Stork D (2000) *Pattern Classification*. New York: Wiley.
- Engel AK, Fries P, Singer W (2001) Dynamic predictions: oscillations and synchrony in top-down processing. *Nat Rev Neurosci* 2:704-716.
- Ernst K, Boeckh J, Boeckh V (1977) A neuroanatomical study on the organization of the central antennal pathways in insects. *Cell Tissue Res* 176:285-308.
- Farivar SS (2005) *Cytoarchitecture of the locust olfactory system*. In: *Biology*. Pasadena: PhD thesis, California Institute of Technology.
- Fiala A, Spall T, Diegelmann S, Eisermann B, Sachse S, Devaud JM, Buchner E, Galizia CG (2002) Genetically expressed cameleon in *Drosophila melanogaster* is used to visualize olfactory information in projection neurons. *Curr Biol* 12:1877-1884.

- Fiete IR, Hahnloser RH, Fee MS, Seung HS (2004) Temporal sparseness of the premotor drive is important for rapid learning in a neural network model of birdsong. *J Neurophysiol* 92:2274-2282.
- Freeman WJ (1959) Distribution in time and space of prepyriform electrical activity. *J Neurophysiol* 22:644-665.
- Friedrich RW, Laurent G (2001) Dynamic optimization of odor representations by slow temporal patterning of mitral cell activity. *Science* 291:889-894.
- Fries P, Reynolds JH, Rorie AE, Desimone R (2000) Modulation of oscillatory neuronal synchronization by selective visual attention. *Science* 291:1560-1563.
- Frye MA, Dickinson MH (2001) Fly flight. A model for the neural control of complex behavior. *Neuron* 32:385-388.
- Gao Q, Yuan B, Chess A (2000) Convergent projections of *Drosophila* olfactory neurons to specific glomeruli in the antennal lobe. *Nat Neurosci* 3:780-785.
- Gelperin A (2006) Olfactory computations and network oscillation. *J Neurosci* 26:1663-1668.
- Gelperin A, Tank D (1990) Odour-modulated collective network oscillations of olfactory interneurons in a terrestrial mollusc. *Nature* 345:437-440.
- Grinvald A, Hildesheim R (2004) VSDI: a new era in functional imaging of cortical dynamics. *Nat Rev Neurosci* 5:874-885.
- Grynkiewicz G, Poenie M, Tsien RY (1985) A new generation of Ca<sup>2+</sup> indicators with greatly improved fluorescence properties. *J Biol Chem* 260:3440-3450.
- Hahnloser RH, Kozhevnikov AA, Fee MS (2002) An ultra-sparse code underlies the generation of neural sequences in a songbird. *Nature* 419:65-70.
- Hallem EA, Carlson JR (2006) Coding of odors by a receptor repertoire. *Cell* 125:143-160.
- Hallem EA, Ho MG, Carlson JR (2004) The molecular basis of odor coding in the *Drosophila* antenna. *Cell* 117:965-979.
- Hammer M (1993) An identified neuron mediates the unconditioned stimulus in associative olfactory learning in honeybees. *Nature* 366:59-63.
- Hansson BS, Anton S (2000) Function and morphology of the antennal lobe: new developments. *Annu Rev Entomol* 45:203-231.

- Harrison TA, Scott JW (1986) Olfactory bulb responses to odor stimulation: analysis of response pattern and intensity relationships. *J Neurophysiol* 56:1571-1589.
- Heimbeck G, Bugnon V, Gendre N, Keller A, Stocker RF (2001) A central neural circuit for experience-independent olfactory and courtship behavior in *Drosophila melanogaster*. *Proc Natl Acad Sci U S A* 98:15336-15341.
- Heisenberg M, Borst A, Wagner S, Byers D (1985) *Drosophila* mushroom body mutants are deficient in olfactory learning. *J Neurogenet* 2:1-30.
- Hinton GE, Salakhutdinov RR (2006) Reducing the dimensionality of data with neural networks. *Science* 313:504-507.
- Hopfield J, Gelperin A (1989) Differential conditioning to a compound stimulus and its components in the terrestrial mollusc *Limax maximus*. *Behav Neuro* 103:329-333.
- Hotta Y, Benzer S (1970) Genetic Dissection of *Drosophila* Nervous System by Means of Mosaics. *Proceedings of the National Academy of Sciences of the United States of America* 67:1156-&.
- Hung CP, Kreiman G, Poggio T, DiCarlo JJ (2005) Fast readout of object identity from macaque inferior temporal cortex. *Science* 310:863-866.
- Jinks A, Laing DG (1999) A limit in the processing of components in odour mixtures. *Perception* 28:395-404.
- Jortner RA, Farivar SS, Laurent G (2007) A simple connectivity scheme for sparse coding in an olfactory system. *J Neurosci* 27:1659-1669.
- Kahneman D (1968) Method, findings, and theory in studies of visual masking. *Psychol Bull* 70:404-425.
- Kanerva P (1988) *Sparse Distributed Memory*. Cambridge, MA: MIT Press.
- Kass RE, Ventura V, Brown EN (2005) Statistical issues in the analysis of neuronal data. *J Neurophysiol* 94:8-25.
- Kido A, Ito K (2002) Mushroom bodies are not required for courtship behavior by normal and sexually mosaic *Drosophila*. *J Neurobiol* 52:302-311.
- Kitamoto T (2002) Conditional disruption of synaptic transmission induces male-male courtship behavior in *Drosophila*. *Proc Natl Acad Sci U S A* 99:13232-13237.
- Knusel P, Wyss R, Konig P, Verschure PF (2004) Decoding a temporal population code. *Neural Comput* 16:2079-2100.

- Koehl MA, Koseff JR, Crimaldi JP, McCay MG, Cooper T, Wiley MB, Moore PA (2001) Lobster sniffing: antennule design and hydrodynamic filtering of information in an odor plume. *Science* 294:1948-1951.
- König P, Engel AK, Singer W (1996) Integrator of coincidence detector? The role of the cortical neuron revisited. *Trends Neurosci* 19:130-137.
- Konopka RJ, Benzer S (1971) Clock Mutants of *Drosophila-Melanogaster*. *Proceedings of the National Academy of Sciences of the United States of America* 68:2112-2116.
- Kurahashi T, Menini A (1997) Mechanism of odorant adaptation in the olfactory receptor cell. *Nature* 385:725-729.
- Laing DG, Francis GW (1989) The capacity of humans to identify odors in mixtures. *Physiol Behav* 46:809-814.
- Laing DG, Panhuber H, Slotnick BM (1989) Odor masking in the rat. *Physiol Behav* 45:689-694.
- Laissue PP, Reiter C, Hiesinger PR, Halter S, Fischbach KF, Stocker RF (1999) Three-dimensional reconstruction of the antennal lobe in *Drosophila melanogaster*. *J Comp Neurol* 405:543-552.
- Laurent G (1996) Dynamical representation of odors by oscillating and evolving neural assemblies. *Trends Neurosci* 19:489-496.
- Laurent G (2002) Olfactory network dynamics and the coding of multidimensional signals. *Nat Rev Neurosci* 3:884-895.
- Laurent G, Naraghi M (1994) Odorant-induced oscillations in the mushroom bodies of the locust. *J Neurosci* 14:2993-3004.
- Laurent G, Davidowitz H (1994) Encoding of olfactory information with oscillating neural assemblies. *Science* 265:1872-1875.
- Laurent G, Wehr M, Davidowitz H (1996) Temporal representations of odors in an olfactory network. *J Neurosci* 16:3837-3847.
- Leinders-Zufall T, Lane AP, Puche AC, Ma W, Novotny MV, Shipley MT, Zufall F (2000) Ultrasensitive pheromone detection by mammalian vomeronasal neurons. *Nature* 405:792-796.
- Leitch B, Laurent G (1996) GABAergic synapses in the antennal lobe and mushroom body of the locust olfactory system. *J Comp Neurol* 372:487-514.

- Leonardo A (2005) Degenerate coding in neural systems. *J Comp Physiol A Neuroethol Sens Neural Behav Physiol* 191:995-1010.
- Lima SQ, Miesenbock G (2005) Remote control of behavior through genetically targeted photostimulation of neurons. *Cell* 121:141-152.
- Lin da Y, Zhang SZ, Block E, Katz LC (2005) Encoding social signals in the mouse main olfactory bulb. *Nature* 434:470-477.
- Maass W, Natschlagier T, Markram H (2002) Real-time computing without stable states: a new framework for neural computation based on perturbations. *Neural Comput* 14:2531-2560.
- Macknik SL, Livingstone MS (1998) Neuronal correlates of visibility and invisibility in the primate visual system. *Nat Neurosci* 1:144-149.
- MacLeod K, Laurent G (1996) Distinct mechanisms for synchronization and temporal patterning of odor-encoding neural assemblies. *Science* 274:976-979.
- MacLeod K, Backer A, Laurent G (1998) Who reads temporal information contained across synchronized and oscillatory spike trains? *Nature* 395:693-698.
- Maei H, Latham P (2004) How can realistic networks process time-varying signals? . *Society for Neuroscience Abstract* 30:81.89.
- Mank M, Reiff DF, Heim N, Friedrich MW, Borst A, Griesbeck O (2006) A FRET-based calcium biosensor with fast signal kinetics and high fluorescence change. *Biophys J* 90:1790-1796.
- Marella S, Fischler W, Kong P, Asgarian S, Rueckert E, Scott K (2006) Imaging taste responses in the fly brain reveals a functional map of taste category and behavior. *Neuron* 49:285-295.
- Margrie TW, Meyer AH, Caputi A, Monyer H, Hasan MT, Schaefer AT, Denk W, Brecht M (2003) Targeted whole-cell recordings in the mammalian brain in vivo. *Neuron* 39:911-918.
- Marin EC, Jefferis GS, Komiyama T, Zhu H, Luo L (2002) Representation of the glomerular olfactory map in the *Drosophila* brain. *Cell* 109:243-255.
- Marr D (1969) A theory of cerebellar cortex. *J Physiol* 202:437-470.
- Masson C, Mustaparta H (1990) Chemical information processing in the olfactory system of insects. *Physiol Rev* 70:199-245.

- May RM (1988) How Many Species Are There on Earth. *Science* 241:1441-1449.
- Mazor O, Laurent G (2005) Transient Dynamics versus Fixed Points in Odor Representations by Locust Antennal Lobe Projection Neurons. *Neuron* 48:661-673.
- Menzel R, U. Müller (1987) Memory traces in honeybees. In: *Neurobiology and behavior of honeybees* (Menzel R, A. Mercer, ed), pp 310-325. Berlin: Springer.
- Miesenbock G, Kevrekidis IG (2005) Optical imaging and control of genetically designated neurons in functioning circuits. *Annu Rev Neurosci* 28:533-563.
- Miyawaki A, Llopis J, Heim R, McCaffery JM, Adams JA, Ikura M, Tsien RY (1997) Fluorescent indicators for Ca<sup>2+</sup> based on green fluorescent proteins and calmodulin. *Nature* 388:882-887.
- Mombaerts P (1996) Targeting olfaction. *Curr Opin Neurobiol* 6:481-486.
- Mustaparta H (1996) Central mechanisms of pheromone information processing. *Chem Senses* 21:269-275.
- Nakai J, Ohkura M, Imoto K (2001) A high signal-to-noise Ca(2+) probe composed of a single green fluorescent protein. *Nat Biotechnol* 19:137-141.
- Ng M, Roorda RD, Lima SQ, Zemelman BV, Morcillo P, Miesenbock G (2002) Transmission of olfactory information between three populations of neurons in the antennal lobe of the fly. *Neuron* 36:463-474.
- Nicolelis MA, Lin RC, Chapin JK (1997) Neonatal whisker removal reduces the discrimination of tactile stimuli by thalamic ensembles in adult rats. *J Neurophysiol* 78:1691-1706.
- Nitabach MN, Blau J, Holmes TC (2002) Electrical silencing of *Drosophila* pacemaker neurons stops the free-running circadian clock. *Cell* 109:485-495.
- Ohki K, Chung S, Ch'ng YH, Kara P, Reid RC (2005) Functional imaging with cellular resolution reveals precise micro-architecture in visual cortex. *Nature* 433:597-603.
- Ohki K, Chung S, Kara P, Hubener M, Bonhoeffer T, Reid RC (2006) Highly ordered arrangement of single neurons in orientation pinwheels. *Nature* 442:925-928.
- Oleskevich S (1999) Cholinergic synaptic transmission in insect mushroom bodies in vitro. *J Neurophysiol* 82:1091-1096.
- Olsen SR, Bhandawat V, Wilson RI (2007) Excitatory Interactions between Olfactory Processing Channels in the *Drosophila* Antennal Lobe. *Neuron* 54:89-103.

- Olshausen BA, Field DJ (2004) Sparse coding of sensory inputs. *Curr Opin Neurobiol* 14:481-487.
- Optican LM, Richmond BJ (1987) Temporal encoding of two-dimensional patterns by single units in primate inferior temporal cortex. III. Information theoretic analysis. *J Neurophysiol* 57:162-178.
- Perez-Orive J, Bazhenov M, Laurent G (2004) Intrinsic and circuit properties favor coincidence detection for decoding oscillatory input. *J Neurosci* 24:6037-6047.
- Perez-Orive J, Mazor O, Turner G, Cassenaer S, Laurent G (2002) Oscillations and sparsening of odor representations in the mushroom body. *Science* 297:359-365.
- Persechini A, Lynch JA, Romoser VA (1997) Novel fluorescent indicator proteins for monitoring free intracellular Ca<sup>2+</sup>. *Cell Calcium* 22:209-216.
- Pesaran B, Pezaris JS, Sahani M, Mitra PP, Andersen RA (2002) Temporal structure in neuronal activity during working memory in macaque parietal cortex. *Nat Neurosci* 5:805-811.
- Pologruto TA, Yasuda R, Svoboda K (2004) Monitoring neural activity and [Ca<sup>2+</sup>] with genetically encoded Ca<sup>2+</sup> indicators. *J Neurosci* 24:9572-9579.
- Pouget A, Dayan P, Zemel R (2000) Information processing with population codes. *Nat Rev Neurosci* 1:125-132.
- Pouzat C, Mazor O, Laurent G (2002) Using noise signature to optimize spike-sorting and to assess neuronal classification quality. *J Neurosci Methods* 122:43-57.
- Python F, Stocker RF (2002) Immunoreactivity against choline acetyltransferase, gamma-aminobutyric acid, histamine, octopamine, and serotonin in the larval chemosensory system of *Drosophila melanogaster*. *J Comp Neurol* 453:157-167.
- Quian Quiroga R, Reddy L, Kreiman G, Koch C, Fried I (2005) Invariant visual representation by single-neurons in the human brain. *Nature* In Press.
- Quinn WG, Harris WA, Benzer S (1974) Conditioned behavior in *Drosophila melanogaster*. *Proc Natl Acad Sci U S A* 71:708-712.
- Reiff DF, Ihring A, Guerrero G, Isacoff EY, Joesch M, Nakai J, Borst A (2005) In vivo performance of genetically encoded indicators of neural activity in flies. *J Neurosci* 25:4766-4778.

- Rieke F, Warland D, de Ruyter van Steneninck R, Bialek W (1997) *Spikes*. Cambridge: MIT Press.
- Rinberg D, Koulakov A, Gelperin A (2006) Sparse odor coding in awake behaving mice. *J Neurosci* 26:8857-8865.
- Rolls ET, Tovee MJ (1994) Processing speed in the cerebral cortex and the neurophysiology of visual masking. *Proc Biol Sci* 257:9-15.
- Rouby C, Holley A (1995) Temporal competition between odorants: effect of different time intervals on the perception of monorhnic and dichorhnic binary mixtures. *Perception* 24:1083-1097.
- Roweis ST, Saul LK (2000) Nonlinear dimensionality reduction by locally linear embedding. *Science* 290:2323-2326.
- Sakmann B, Neher E (1984) Patch clamp techniques for studying ionic channels in excitable membranes. *Annu Rev Physiol* 46:455-472.
- Schaefer AT, Angelo K, Spors H, Margrie TW (2006) Neuronal oscillations enhance stimulus discrimination by ensuring action potential precision. *PLoS Biol* 4:e163.
- Schneidman E, Bialek W, Berry MJ (2003) Synergy, redundancy, and independence in population codes. *Journal of Neuroscience* 23:11539-11553.
- Schroll C, Riemensperger T, Bucher D, Ehmer J, Voller T, Erbguth K, Gerber B, Hendel T, Nagel G, Buchner E, Fiala A (2006) Light-induced activation of distinct modulatory neurons triggers appetitive or aversive learning in *Drosophila* larvae. *Curr Biol* 16:1741-1747.
- Sederberg PB, Schulze-Bonhage A, Madsen JR, Bromfield EB, McCarthy DC, Brandt A, Tully MS, Kahana MJ (2006) Hippocampal and Neocortical Gamma Oscillations Predict Memory Formation in Humans. *Cereb Cortex*.
- Shadlen MN, Movshon JA (1999) Synchrony unbound: A critical evaluation of the temporal binding hypothesis. *Neuron* 24:67-77.
- Shang Y, Claridge-Chang A, Sjulson L, Pypaert M, Miesenbock G (2007) Excitatory local circuits and their implications for olfactory processing in the fly antennal lobe. *Cell* 128:601-612.
- Siapas AG, Wilson MA (1998) Coordinated interactions between hippocampal ripples and cortical spindles during slow-wave sleep. *Neuron* 21:1123-1128.

- Singer W, and Gray, C. (1995) Visual feature integration and the temporal correlation hypothesis. *Annu Rev Neurosci* 18:555-586.
- Single S, Borst A (2002) Different mechanisms of calcium entry within different dendritic compartments. *J Neurophysiol* 87:1616-1624.
- Sobel E, D. W. Tank (1994) In Vivo Ca<sup>2+</sup> Dynamics in a cricket auditory neuron: an example of chemical computation. *Science* 263:823-826.
- Steriade M, Timofeev I (2003) Neuronal plasticity in thalamocortical networks during sleep and waking oscillations. *Neuron* 37:563-576.
- Steriade M, McCormick DA, Sejnowski TJ (1993) Thalamocortical oscillations in the sleeping and aroused brain. *Science* 262:679-685.
- Stevens JC, Traverzo A (1997) Detection of a target taste in a complex masker. *Chem Senses* 22:529-534.
- Stocker RF (1994) The organization of the chemosensory system in *Drosophila melanogaster*: a review. *Cell Tissue Res* 275:3-26.
- Stocker RF, Singh RN, Schorderet M, Siddiqi O (1983) Projection patterns of different types of antennal sensilla in the antennal glomeruli of *Drosophila melanogaster*. *Cell Tissue Res* 232:237-248.
- Stocker RF, Lienhard MC, Borst A, Fischbach KF (1990) Neuronal architecture of the antennal lobe in *Drosophila melanogaster*. *Cell Tissue Res* 262:9-34.
- Stopfer M, Laurent G (1999) Short-term memory in olfactory network dynamics. *Nature* 402:664-668.
- Stopfer M, Jayaraman V, Laurent G (2003) Intensity versus identity coding in an olfactory system. *Neuron* 39:991-1004.
- Stopfer M, Bhagavan S, Smith BH, Laurent G (1997) Impaired odour discrimination on desynchronization of odour-encoding neural assemblies. *Nature* 390:70-74.
- Stosiek C, Garaschuk O, Holthoff K, Konnerth A (2003) In vivo two-photon calcium imaging of neuronal networks. *Proc Natl Acad Sci U S A* 100:7319-7324.
- Strausfeld NJ (2002) Organization of the honey bee mushroom body: representation of the calyx within the vertical and gamma lobes. *J Comp Neurol* 450:4-33.
- Strausfeld NJ, Hildebrand JG (1999) Olfactory systems: common design, uncommon origins? *Curr Opin Neurobiol* 9:634-639.

- Strausfeld NJ, Sinakevitch I, Vilinsky I (2003) The mushroom bodies of *Drosophila melanogaster*: an immunocytological and golgi study of Kenyon cell organization in the calyces and lobes. *Microsc Res Tech* 62:151-169.
- Su H, O'Dowd DK (2003) Fast synaptic currents in *Drosophila* mushroom body Kenyon cells are mediated by alpha-bungarotoxin-sensitive nicotinic acetylcholine receptors and picrotoxin-sensitive GABA receptors. *J Neurosci* 23:9246-9253.
- Suh GS, Wong AM, Hergarden AC, Wang JW, Simon AF, Benzer S, Axel R, Anderson DJ (2004) A single population of olfactory sensory neurons mediates an innate avoidance behaviour in *Drosophila*. *Nature*.
- Sullivan MR, Nimmerjahn A, Sarkisov DV, Helmchen F, Wang SS (2005) In vivo calcium imaging of circuit activity in cerebellar cortex. *J Neurophysiol* 94:1636-1644.
- Svoboda K, Yasuda R (2006) Principles of two-photon excitation microscopy and its applications to neuroscience. *Neuron* 50:823-839.
- Svoboda K, Denk W, Kleinfeld D, Tank DW (1997) In vivo dendritic calcium dynamics in neocortical pyramidal neurons. *Nature* 385:161-165.
- Tanaka NK, Awasaki T, Shimada T, Ito K (2004) Integration of chemosensory pathways in the *Drosophila* second-order olfactory centers. *Curr Biol* 14:449-457.
- Tang S, Guo A (2001) Choice behavior of *Drosophila* facing contradictory visual cues. *Science* 294:1543-1547.
- Tank DW, Sugimori M, Connor JA, Llinas RR (1988) Spatially resolved calcium dynamics of mammalian Purkinje cells in cerebellar slice. *Science* 242:773-777.
- Taylor AL, Cottrell GW, Kleinfeld D, Kristan WB, Jr. (2003) Imaging reveals synaptic targets of a swim-terminating neuron in the leech CNS. *J Neurosci* 23:11402-11410.
- Teyke T, and Gelperin, A. (1999) Olfactory oscillations augment odor discrimination, not odor identification in *Limax* CNS. *NeuroReport* 10:1-8.
- Vaadia E, Haalman I, Abeles M, Bergman H, Prut Y, Slovin H, Aertsen A (1995) Dynamics of neuronal interactions in monkey cortex in relation to behavioural events. *Nature* 373:515-518.

- Vickers NJ, Christensen TA, Hildebrand JG (1998) Combinatorial odor discrimination in the brain: attractive and antagonist odor blends are represented in distinct combinations of uniquely identifiable glomeruli. *J Comp Neurol* 400:35-56.
- Vogt MB, Smith DV (1994) Responses of single hamster parabrachial neurons to binary taste mixtures of NaCl with sucrose or QHCl. *J Neurophysiol* 71:1373-1380.
- Vosshall LB (2000) Olfaction in *Drosophila*. *Curr Opin Neurobiol* 10:498-503.
- Vosshall LB, Amrein H, Morozov PS, Rzhetsky A, Axel R (1999) A spatial map of olfactory receptor expression in the *Drosophila* antenna. *Cell* 96:725-736.
- Wang JW, Wong AM, Flores J, Vosshall LB, Axel R (2003) Two-photon calcium imaging reveals an odor-evoked map of activity in the fly brain. *Cell* 112:271-282.
- Wang Y, Guo HF, Pologruto TA, Hannan F, Hakker I, Svoboda K, Zhong Y (2004) Stereotyped odor-evoked activity in the mushroom body of *Drosophila* revealed by green fluorescent protein-based Ca<sup>2+</sup> imaging. *J Neurosci* 24:6507-6514.
- Watson AH, Schurmann FW (2002) Synaptic structure, distribution, and circuitry in the central nervous system of the locust and related insects. *Microsc Res Tech* 56:210-226.
- Wegel R, Lane C (1924) The auditory masking of one pure tone by another and its probable relation to the dynamics of the inner ear. *Physical Review* 23:266-285.
- Wehr M, Laurent G (1996) Odor encoding by temporal sequences of firing in oscillating neural assemblies. *Nature* 384:162-166.
- Wehr M, Zador AM (2005) Synaptic mechanisms of forward suppression in rat auditory cortex. *Neuron* 47:437-445.
- Wessberg J, Stambaugh CR, Kralik JD, Beck PD, Laubach M, Chapin JK, Kim J, Biggs SJ, Srinivasan MA, Nicolelis MA (2000) Real-time prediction of hand trajectory by ensembles of cortical neurons in primates. *Nature* 408:361-365.
- Wilson RI, Laurent G (2005) Role of GABAergic inhibition in shaping odor-evoked spatiotemporal patterns in the *Drosophila* antennal lobe. *J Neurosci* 25:9069-9079.
- Wilson RI, Turner GC, Laurent G (2004) Transformation of olfactory representations in the *Drosophila* antennal lobe. *Science* 303:366-370.
- Wong AM, Wang JW, Axel R (2002) Spatial representation of the glomerular map in the *Drosophila* protocerebrum. *Cell* 109:229-241.

- Yaksi E, Friedrich RW (2006) Reconstruction of firing rate changes across neuronal populations by temporally deconvolved Ca<sup>2+</sup> imaging. *Nat Methods* 3:377-383.
- Yasuda R, Nimchinsky EA, Scheuss V, Pologruto TA, Oertner TG, Sabatini BL, Svoboda K (2004) Imaging calcium concentration dynamics in small neuronal compartments. *Sci STKE* 2004:pl5.
- Yasuyama K, Meinertzhagen IA, Schurmann FW (2003) Synaptic connections of cholinergic antennal lobe relay neurons innervating the lateral horn neuropile in the brain of *Drosophila melanogaster*. *Journal of Comparative Neurology* 466:299-315.
- Yu D, Ponomarev A, Davis RL (2004) Altered representation of the spatial code for odors after olfactory classical conditioning; memory trace formation by synaptic recruitment. *Neuron* 42:437-449.
- Yu D, Akalal DB, Davis RL (2006) *Drosophila* alpha/beta mushroom body neurons form a branch-specific, long-term cellular memory trace after spaced olfactory conditioning. *Neuron* 52:845-855.
- Zhang F, Wang LP, Boyden ES, Deisseroth K (2006) Channelrhodopsin-2 and optical control of excitable cells. *Nat Methods* 3:785-792.
- Zhu S, Chiang AS, Lee T (2003) Development of the *Drosophila* mushroom bodies: elaboration, remodeling and spatial organization of dendrites in the calyx. *Development* 130:2603-2610.
- Zufall F, Leinders-Zufall T (1998) Role of cyclic GMP in olfactory transduction and adaptation. *Ann N Y Acad Sci* 855:199-204.